



UNIL | Université de Lausanne

Unicentre

CH-1015 Lausanne

<http://serval.unil.ch>

Year : 2018

GAMMA KNIFE RADIOSURGERY OF THE VIM: FROM THE LESION AL EFFECT TOWARDS NEUROMODULATION

Tuleasca Constantin

Tuleasca Constantin, 2018, GAMMA KNIFE RADIOSURGERY OF THE VIM: FROM THE
LESION AL EFFECT TOWARDS NEUROMODULATION

Originally published at : Thesis, University of Lausanne

Posted at the University of Lausanne Open Archive <http://serval.unil.ch>

Document URN : urn:nbn:ch:serval-BIB_70ADEF95A6464

Droits d'auteur

L'Université de Lausanne attire expressément l'attention des utilisateurs sur le fait que tous les documents publiés dans l'Archive SERVAL sont protégés par le droit d'auteur, conformément à la loi fédérale sur le droit d'auteur et les droits voisins (LDA). A ce titre, il est indispensable d'obtenir le consentement préalable de l'auteur et/ou de l'éditeur avant toute utilisation d'une oeuvre ou d'une partie d'une oeuvre ne relevant pas d'une utilisation à des fins personnelles au sens de la LDA (art. 19, al. 1 lettre a). A défaut, tout contrevenant s'expose aux sanctions prévues par cette loi. Nous déclinons toute responsabilité en la matière.

Copyright

The University of Lausanne expressly draws the attention of users to the fact that all documents published in the SERVAL Archive are protected by copyright in accordance with federal law on copyright and similar rights (LDA). Accordingly it is indispensable to obtain prior consent from the author and/or publisher before any use of a work or part of a work for purposes other than personal use within the meaning of LDA (art. 19, para. 1 letter a). Failure to do so will expose offenders to the sanctions laid down by this law. We accept no liability in this respect.



UNIL | Université de Lausanne

Faculté de biologie
et de médecine

**Département de Neurosciences Cliniques,
Service de Neurochirurgie et Centre Gamma Knife**

**GAMMA KNIFE RADIOSURGERY OF THE VIM: FROM THE
LESIONAL EFFECT TOWARDS NEUROMODULATION**

Thèse de doctorat en médecine et ès sciences

MD-PhD

Présentée à la

Faculté de biologie et de médecine
de l'Université de Lausanne

par

Constantin TULEASCA

Médecin diplômé de la Roumanie

Jury

Prof. Jean-Philippe Thiran, président et répondant MD-PhD

Prof. Marc Levivier, directeur de thèse

MER, PD Meritxell Bach Cuadra, co-directrice de thèse

Prof. Jean Régis, co-directeur de thèse

Prof. Serge Blond, expert

Prof. Philippe Maeder, expert

Lausanne 2018



UNIL | Université de Lausanne

Ecole doctorale

Ecole Doctorale

Doctorat MD-PhD

Imprimatur

Vu le rapport présenté par le jury d'examen, composé de

Président·e	Monsieur Prof. Jean-Philippe Thiran
Directeur·trice de thèse	Monsieur Prof. Marc Levivier
Co-Directeur·trice de thèse	Madame Dre Meritxell Bach Cuadra
Co-Directeur·trice de thèse	Monsieur Prof. Jean Régis
Répondant·e	Monsieur Prof. Jean-Philippe Thiran
Expert·es	Monsieur Prof. Philippe Maeder Monsieur Prof. Serge Blond

le Conseil de Faculté autorise l'impression de la thèse de

Monsieur Constantin TULEASCA

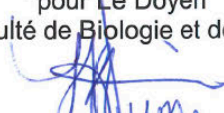
Docteur en Médecine Université de Iasi, Roumanie

intitulée

**Gamma Knife radiosurgery of the Vim: from the lesional effect
towards neuromodulation**

Lausanne, le 12 septembre 2018

pour Le Doyen
de la Faculté de Biologie et de Médecine


Prof. Jean-Philippe Thiran

To my wife, Ana and to my son, Eric-Constantin, all my love, tenderness and affection

*To my grandmother, Ecaterina, to my mother, Melba, and to my sister, Alexandra
To my mother, sister and father-in-law, Livia, Diana and Constantin*

*To my grandfather, Constantin, who unfortunately left us much too early,
for teaching me so many wonderful things about life, for his precious love and affection,
as he will always be in my heart and in my spirit*

*To Mariana and Viorel, as you have surrounded me and Ana, and further Eric
with much unconditional love and support*

*To Vasco, for a precious friendship and paternal feelings and attitude,
and so many memories of nice and difficult moments we shared together*

To Mioara and Mihai, for their friendship

*To all people, who are not listed here, who understood my passion for neurosurgery,
and supported me to follow my Path in many crucial moments of my life, all my gratitude*

Acknowledgements and personal thoughts

To Professor Marc Levivier, for his continuous support for entering and continuing the beautiful Path of *Neurosurgery*; for helping me to enroll the MD-PhD program of the University of Lausanne; for developing together the Gamma Knife activity in Lausanne. For his friendship and attention, I am mostly grateful.

To Professor Jean-Philippe Thiran, for sustaining me to enroll the MD-PhD program; for welcoming me in his laboratory, LTS-5; for the simple and nice interactions and the richness of our continuous exchanges; for his friendship. I am mostly grateful.

To Professor Jean Régis, as he taught me functional neurosurgery and Gamma Knife, which I was already impassioned as early as the second year of my training. He encouraged and sustained my career, surrounded me with friendship and attention. I am mostly grateful.

To Meritxell Bach Cuadra, for welcoming me to Medical Image Analysis Laboratory and for the research work we did together with regards to the segmentation of the thalamus. For the positive interaction and help.

To Professor Phillipe Maeder, for being a part of my thesis committee and for a constructive and goodwill attitude.

To Professor Serge Blond, I was mostly honored to have you as a member of my thesis committee. You remain a model for me, as you combined clinic, electrophysiology, surgery and radiosurgery during your career, as I would love to do in the future.

To Professor Dimitri Van de Ville, a mentor and I dare to say a friend. Although you were not part of my thesis committee, you have so much contributed to my academic profile. You have taught me the pure science, which I was searching for in the MD-PhD program. You tempered my impatience and created positive paths, so as to be able to achieve my goals.

To Elena Najdenovska, who was my scientific binome, and who became a true friend. You introduced me to the beautiful world of research, in which I felt home, grace to you. I don't think that writing these lines would ever compensate for the time you spent to explain, teach or collaborate with me. The same applied when I needed personal advices, and that is priceless. If I showed you the big picture, as you say, you have showed me your patience and your unconditional help in the projects I wanted to make.

To the next steps of my medical career. By the time I wrote these lines, little remains till I will go back to the operative theater, which I also love and missed during this period. I loved and enjoyed the MD-PhD program, in each step. Research and Gamma Knife radio-neurosurgery are and will be a natural part of my medical life. They have been my priorities for the past 8 years. Microsurgery will soon complete my training. *The Path is always the Path and we should always remember what's driving us, as for me the motivation is something we should never lose. "Real knowledge is to know the extent of one's ignorance" (Confucius)*

Table of content (brief overview)	3-8
Abstract (in English)	9
Abstract (in French)	10
Abbreviation list	11
Peer-reviewed papers	12-13
1. Introduction	14-37
1.1. Clinical context	
1.1.1. Gamma Knife radiosurgery	14-15
1.1.2. The ventro-intermediate nucleus, as part of the thalamic nuclei	15-18
1.1.3. Essential tremor	18-20
1.1.4. The eye-hand coordination, a link with the visual system	20-22
1.1.5. Surgical targets for drug-resistant essential tremor: brief overview	22-23
1.1.6. Surgical therapeutic approaches for drug-resistant essential tremor	23-25
1.1.7. Limitations of Vim radiosurgery for tremor	25-29
1.1.8. Addressing Vim's radiosurgery limitations in the present thesis	29
1.2. Neuroimaging context	
1.2.1. Ultra high field 7 T MTRI for thalamic nuclei visualization	30-31

1.2.2. 3T MRI for exploring the radiobiology of radiosurgery	31
1.2.2.1. Voxel-based morphometry	32
1.2.2.1.1. General aspects	32
1.2.2.1.2. VBM in essential tremor	33
1.2.2.2. Resting-state functional MRI	33
1.2.2.2.1. General aspects	33-34
1.2.2.2.2. Resting-state fMRI studies in ET	35-36
1.10.2.3. Resting-state fMRI processing (pipeline)	36
1.10.2.4. The general linear model	36-37
2. Thesis objectives	38
3. Address the limitation of indirect targeting	39-53
Publications related to this chapter	39
3.1. indirect landmarks: radiation prelemniscalis	40-42
3.2. The Vim through multimodal imaging at 3 and 7 T	42-43

3.2.1. Materials and methods	43-45
3.2.2. Methods of Vim identification	45
3.2.2.1. The quadrilatre of Guiot	45
3.2.2.2. Manual Vim delineation on 7T SWI	45-46
3.2.2.3. The automated 3T dMRI-based segmentation	46
3.2.2.4. Multi-atlas segmentation	46
3.2.3. Quantitative analysis	46-47
3.2.4. Qualitative analysis	47
3.2.5. Results	47
3.2.5.1. The points from the quadrilatre of Guiot	47-48
3.2.5.2. Manual Vim delineation on 7 T SWI	48-49
3.2.5.3. Correlation between the manual delineation and the Guiot's points	49
3.2.5.4. Comparison with the automated methods	49-50
3.2.5.4.1. Automated 3T dMRI-based segmentation	49
3.2.5.4.2. Multi-atlas segmentation	49-51
3.2.6. Discussion	51-53

4. Understanding the radiobiology of radiosurgery: structural changes 54-63

Publications related to this chapter	54
4.1. General aspects	55
4.2. Main hypothesis	55
4.3. Voxel-based morphometry analysis	56
4.3.1. Relationship between clinical improvement and GMD changes between pretherapeutic and 1 year after Vim GKR state	56
4.3.1.1. Methodological aspects	56-57
4.3.1.2. Results: changes in GMD between R and NR, <i>during time</i>	57-58
4.3.1.3. Summary of findings and anatomical relevance	58
4.3.2. Correlation between pretherapeutic GMD and 1-year tremor improvement after Vim GKR	59
4.3.2.1. Methodological aspects	59-60
4.3.2.2. Results: right visual association area (Brodmann area 18, V2)	60-61
4.3.2.3. Summary of findings and anatomical relevance	61
4.3.3. Preliminary hypothesis with regard to the present VBM studies	61-62
4.3.4. Strengths of both VBM projects	62-63
4.3.5. Limitations	63

5. Understanding the radiobiology of radiosurgery: resting-state functional MRI changes 64-94

Publications related to this chapter 64-65

5.1. Important methodological aspects: general processing and scrubbing 66

5.2. Patient population 67

5.3. Radiological answer: MR signature volume 1 year after Vim GKR 67

5.4. Motion scrubbing (see previous pre-processing steps) 68

5.5. Statistical analysis 68

5.5.1. Independent component analysis 68

5.5.1.1. Only using baseline, pretherapeutic data (n=17) 68-74

5.5.1.2. Both on pre- and posttherapeutic data, as single patient group (n=17 subjects x 2 time-points, n=34) 74-79

5.5.2. Seed based approaches 79

5.5.2.1. General concept 79

5.5.2.2. Main hypothesis 79

5.5.2.3 Methodological aspects and VLV extraction from diffusion MR data 79-81

4.4.5.2.4. Results 81-85

4.4.5.2.5. Summary and anatomical relevance 85-87

5.5.3. Methodological perspectives: connectivity activation patterns 87

5.5.3.1. General concept 87

5.5.3.2. Materials and methods 87

5.5.3.2.1. Subjects	88
5.5.3.2.2. Co-activation pattern mapping: brief description	88-89
5.5.3.2.3. Results	89-90
5.5.4. General discussion of radiobiology of Vim GKR in ET	91-93
5.5.5. Strengths and limitations	93-95
6. Conclusion and perspectives	94-98
6.1. Summary of MD-PHD thesis contribution	94-96
6.2. Overall limitations	97
6.3. General perspectives	97-98
Annexes (including published peer-reviewed papers)	

Gamma Knife radiosurgery (GKR) is a neurosurgical stereotactic procedure, combining image guidance, with high-precision convergence of multiple gamma rays, currently emitted by 192 sources of Cobalt-60 (Leksell Gamma Knife ICON®, Elekta Instruments, AB, Sweden). The intimate mechanisms of action are not all very well understood and vary according to the treated pathological condition. In functional disorders, GKR is used either to target a specific anatomical point [e.g. thalamus- ventro-intermediate nucleus (Vim) for tremor] or to target a larger zone, such as an epileptic focus.

The present thesis focuses on Vim GKR for drug-resistant essential tremor (ET). Essential tremor is the most common movement disorder, with the predominant clinical finding being kinetic tremor of the arms. Radiosurgery (RS) has several limitations in this indication: (1) indirect targeting (Vim is not visible on current MR acquisitions), with (2) no intraoperative confirmation of the target, (3) delayed clinical effect, (4) inability to predict the radiological response and a (5) lack of understanding of its radiobiological effect. Moreover, despite a standard radiosurgical procedure, there is a variability of clinical effect, with a lower efficacy rate as compared to standard deep-brain stimulation, the reference technique. Gamma Knife radiosurgery has no access to tissue analysis, and targeting and follow-up evaluation are based only on neuroimaging. We addressed the limitation of the indirect targeting by using high-field 7 Tesla (T) MRI, and combining multimodal imaging for Vim definition, at both 3 and 7 T. The central core of this thesis was the understanding of radiobiology of RS for tremor, using both structural [e.g. T1 weighted (T1-w), voxel-based morphometry (VBM)] and functional resting-state functional MRI (rs-fMRI).

We aimed for a direct Vim visualization using ultra-high field 7 T. The former allows an increased signal to noise ratio, an improved spatial resolution, as well as a superior sensitivity to magnetic susceptibility engendered contrast. Susceptibility-weighted images (SWI) might be an important step to allow a direct visualization of thalamic subparts (including the Vim). We explored 7T SWI advantages, which were done in a qualitative manner. We combined several different methodologies for Vim definition (in healthy subjects of different ages): manual delineation on 7T, quadrilatre of Guiot used in common clinical practice and automated segmentation based on diffusion weighted imaging and atlases (last two performed by and in collaboration with Dr Najdenovska). We concluded that although 7T SWI, alone or in combination with other neuroimaging modalities, is useful, several limitations need to be overcome yet, precluding a standardization of a direct Vim visualization, with the current state-of-the art.

The T1-w and rs-fMRI based studies analyzed the radiobiology effects of Vim GKR for intractable tremor and led to several important contributions. The most relevant and novel was the presence of a visually-sensitive structural and functional network, involved in tremor generation and further arrest after Vim GKR. The patients with this network more integrated pretherapeutically benefited more from RS. The candidate had shaped the term “cerebello-thalamo-cortical” into the “cerebello-thalamo-visuo-motor” network, as a step forward in the understanding of essential tremor’s pathophysiology. Two structures were proposed as main calibrators of this network, in the light of the present thesis: the cerebellum (as the most probable) versus the thalamus itself. Moreover, a more classical basal ganglia network, interconnected with a salience one, as well as a cerebellar, interconnected with the motor and visual one, were reported. Other longitudinal changes involved dorsal attention, insular or supplementary motor area circuitries. Particular phenotypes of ET, including patients with head tremor, were analyzed and discussed. As a perspective and future work, in progress, the dynamics of the extrastriate cortex was further analyzed, using co-activation patterns.

La radio-neurochirurgie par Gamma Knife (GK) est une procédure de neurochirurgie stéréotaxique, combinant l'utilisation d'une imagerie multimodale, avec la convergence de multiples rayons Gamma émis par 192 sources of Cobalt-60 (Leksell Gamma Knife ICON®, Elekta Instruments, AB, Suède). Ses mécanismes pathophysiologiques ne sont pas complètement élucidés et varient selon la condition traitée. Lors des procédures fonctionnelles, le GK est utilisé pour irradier avec une haute précision, soit un point précis (par exemple, le noyau ventro-intermédiaire, Vim, du thalamus pour le tremblement), soit une zone plus large, comme un foyer d'épilepsie.

La présente thèse a comme sujet principal la radiochirurgie du Vim (RC du Vim) pour le tremblement essentiel (TE). Le TE est un des mouvements anormaux le plus commun, manifesté principalement avec un tremblement d'action de la main. Toutefois, la RC du Vim a plusieurs limitations: (1) le ciblage est indirect (le Vim n'est pas visible sur les séquences IRM classiques), (2) elle ne permet pas la confirmation électrophysiologique de la cible, (3) l'effet clinique est délayé dans le temps, (4) la réponse radiologique est difficile à prédire et, (5) il manque une compréhension claire de son effet radiobiologique. De plus, malgré le fait que la procédure soit standardisée, il y a une variabilité de son effet clinique. La RC ne permet pas d'analyser le tissu et, le ciblage ainsi que le suivi, sont réalisés uniquement sur la base de la neuroimagerie. Nous avons analysé la limitation du ciblage indirect en utilisant l'IRM à haut champs [7 Tesla (T)] et en la combinant avec une imagerie multimodale, incluant des séquences 3T et 7T, pour la définition du Vim. La partie centrale de la thèse se focalise sur la compréhension de l'effet radiobiologique de la RC du Vim dans le TE. Cette partie se base tant de l'analyse de l'imagerie structurale (séquence classique T1) que sur l'imagerie fonctionnelle (IRM de repos).

Le but de la première partie de la thèse est la visualisation directe du Vim en utilisant l'IRM 7T, qui a plusieurs avantages par rapport à l'IRM 3T, y compris une meilleure résolution spatiale. Notamment, la séquence SWI a un intérêt particulier, mais elle n'avait encore jamais été explorée que de manière quantitative au niveau du thalamus (qui contient le Vim). Nous avons combinée plusieurs modalités pour définir le Vim (chez des sujets sains de différents âges): visualisation directe sur la 7T, quadrilatère de Guiot tel qu'utilisé en pratique clinique courante, ainsi que segmentation automatique en imagerie de diffusion ou par des atlas (ces dernières deux approches ont été réalisées par, et en collaboration avec, Dr Najdenovska). Nous avons conclu que la séquence 7T SWI, malgré certains avantages, et utilisée seule ou combinée avec d'autres modalités, présente certaines limitations qui ne permettent pas, à l'heure actuelle, de l'utiliser d'une manière standardisée, tant chez les sujets sains que chez les patients atteints de TE.

Dans la deuxième partie, l'étude de la radiobiologie de la radiochirurgie pour le TE a permis d'apporter plusieurs contributions. La plus importante est la mise en évidence d'un « réseau visuel » structurel et fonctionnel, impliqué dans la genèse du tremblement et dans son amélioration après une RC du Vim. Les patients dont ce réseau est mieux intégré avant la procédure ont de meilleures chances d'amélioration clinique du TE. Dans ce contexte, nous avons proposé d'adapter le terme classique d'« axe cérébello-thalamo-moteur » en le modifiant en « axe cérébello-thalamo-visuo-moteur », ce qui pourrait aider à une meilleure compréhension de la pathophysiologie du TE. Nous proposons également que deux structures puissent jouer le rôle de neuromodulateur de ce réseau, le cervelet et le thalamus. Une autre contribution est la description de l'interconnexion entre le réseau classique impliquant les noyaux de la base et celui l'attention, ainsi que de l'interconnexion entre le réseau cérébelleux et celui des cortex moteur primaire et visuel associatif. Des phénotypes particuliers du tremblement ont été analysés, incluant par exemple des tremblements du chef. Des travaux en cours incluent l'étude de la dynamique du cortex extra-strié en utilisant de nouvelles approches, comme les patterns de co-activation.

Abbreviation list

- AC: anterior commissure
- ADL: activities of daily living
- ALFF: amplitude of low-frequency fluctuations
- BA: Brodman area
- BOLD: blood-oxygen-level-dependent
- DBS: deep-brain stimulation
- DTI: diffusion tensor imaging
- EMG: electromyography
- ES: elderly subjects (considered healthy)
- ET: essential tremor
- FA: fractional anisotropy (from diffusion tensor imaging)
- fMRI: functional magnetic resonance imaging
- FC: functional connectivity
- HC: healthy controls
- HIFU: high intensity focused ultrasound
- GLM: general linear model
- GM: gray matter
- GMD: gray matter density
- GK: Gamma Knife
- GKR: Gamma Knife radiosurgery
- MR: magnetic resonance
- MRI: magnetic resonance imaging
- MS: multiple sclerosis
- NEJM: New England Journal of Medicine
- IC: interconnectivity
- ICA: independent component analysis
- ION: inferior olivary nucleus
- PD: Parkinson's disease
- PC: posterior commissure
- PET: positron emission tomography
- PPN: pedunclopontine nucleus
- PSA: posterior subthalamic area
- Pu: pulvinar
- QSM: quantitative susceptibility mapping
- RAPRL: radiation prelemniscalis
- ReHo: regional homogeneity
- RF-T: radiofrequency thalamotomy
- RS: radiosurgery
- Rs-fMRI: resting-state functional MRI
- STN: subthalamic nucleus
- SWI: Susceptibility Weighted Imaging
- T: Tesla
- TETRAS: tremor research group essential tremor rating assessment
- TSTH: tremor score on the treated hand
- Vc: ventral caudalis
- VBM: voxel-based morphometry
- Vim: ventro-intermediate nucleus of the thalamus
- YS: young subjects (considered healthy)
- ZI: zona incerta

Peer-reviewed papers

1. Imaging of the Ventral Intermediate Thalamic Nucleus at 7T"

Journal of Scientific Reports, Nature (under review)

E. Najdenovska, C. Tuleasca (equally contributor as first author), J. Jorge, P. Maeder, J. P. Marques, T. Roine, D. Gallichan, J.-Ph. Thiran, M. Levivier and M. Bach Cuadra

2. "Towards an automated segmentation of the ventro-intermediate thalamic nucleus"

E. Najdenovska, C. Tuleasca, J. Jorge, P. Maeder, J.-Ph. Thiran, M. Levivier and M. Bach Cuadra; proceedings of the CLIP workshop on the 20th International Conference on Medical Image Computing and Computer Assesed Intervention (MICAAI)

3. "Assessing the clinical outcome of Vim radiosurgery with voxel-based morphometry: visual areas are linked with tremor arrest!", Acta Neurochirurgica

Constantin Tuleasca, Tatiana Witjas, Elena Najdenovska, Antoine Verger, Nadine Girard, Jerome Champoudry, Jean-Philippe Thiran, Dimitri van de Ville, Meritxell Bach Cuadra, Marc Levivier, Eric Guedj, Jean Régis (DOI 10.1007/s00701-017-3317)

4. "Right Brodman area 18 predicts tremor arrest after Vim radiosurgery for tremor", Acta Neurochirurgica (DOI 10.1007/s00701-017-3391-x)

Constantin Tuleasca, Tatiana Witjas, Dimitri van de Ville, Elena Najdenovska, Antoine Verger, Nadine Girard, Jerome Champoudry, Jean-Philippe Thiran, Meritxell Bach Cuadra, Marc Levivier, Eric Guedj, Jean Régis

5. "Pretherapeutic functional neuroimaging predicts tremor arrest after thalamotomy", Acta Neurologica Scandinavica- one of our illustrations gave the cover page (DOI 10.1111/ane.12891)

Constantin Tuleasca, Elena Najdenovska, Jean Régis, Tatiana Witjas, Nadine Girard, Jerome Champoudry, Jean-Philippe Thiran, Meritxell Bach Cuadra, Marc Levivier, Dimitri van de Ville

6 "Clinical response to Vim's thalamic stereotactic radiosurgery for essential tremor is associated with distinctive functional connectivity patterns", Acta Neurochirurgica- one of our illustrations gave the cover page (DOI 10.1007/s00701-017-3456-x)

Constantin Tuleasca, Elena Najdenovska, Jean Régis, Tatiana Witjas, Nadine Girard, Jerome Champoudry, Jean-Philippe Thiran, Meritxell Bach Cuadra, Marc Levivier, Dimitri Van de Ville

7. "Pretherapeutic functional imaging allows prediction of head tremor arrest after thalamotomy for essential tremor: the role of altered interconnectivity between thalamolimbic and supplementary motor circuits", World Neurosurgery (DOI 10.1016/j.wneu.2018.01.063)

Constantin Tuleasca, Jean Régis, Elena Najdenovska, Tatiana Witjas, Nadine Girard, Jerome Champoudry, Jean-Philippe Thiran, Meritxell Bach Cuadra, Marc Levivier, Dimitri van de Ville

8. "Ventro-lateral motor thalamus abnormal connectivity in essential tremor before and after thalamotomy", World Neurosurgery (DOI 10.1016/j.wneu.2018.02.055)

Constantin Tuleasca, Elena Najdenovska, Jean Régis, Tatiana Witjas, Nadine Girard, Jerome Champoudry, Faouzi Mohamed, Jean-Philippe Thiran, Meritxell Bach Cuadra, Marc Levivier, Dimitri Van de Ville

9. "Visually-sensitive networks in essential tremor: evidence from structural and functional imaging", Brain (DOI 10.1093/brain/awy094)

Constantin Tuleasca, Jean Régis, Elena Najdenovska, Tatiana Witjas, Nadine Girard, Jean-Philippe Thiran, Meritxell Bach Cuadra, Marc Levivier, Dimitri van de Ville

10. "Pretherapeutic motor thalamus resting-state functional connectivity with visual areas predicts tremor arrest after thalamotomy for essential tremor: tracing the cerebello-thalamo-visuo-motor network",

World Neurosurgery (10.1016/j.wneu.2018.06.049)

Constantin Tuleasca, Jean Régis, Elena Najdenovska, Tatiana Witjas, Nadine Girard, Jean-Philippe Thiran, Meritxell Bach Cuadra, Marc Levivier, Dimitri van de Ville

11. "Pretherapeutic resting-state fMRI profiles are associated with MR signature volumes after stereotactic radiosurgical thalamotomy for essential tremor" (accepted for publication, Journal of Neurosurgery)

Constantin Tuleasca, Jean Régis, Elena Najdenovska, Tatiana Witjas, Nadine Girard, Thomas Bolton, Francois Delaire, Marion Vincent, Mohamed Faouzi, Jean-Philippe Thiran, Meritxell Bach Cuadra, Marc Levivier, Dimitri van de Ville

12. "Treating essential tremor with radiosurgery", New England Journal of Medicine
Constantin Tuleasca, Jean Régis, Marc Levivier

13. "Letter: Deep Brain Stimulation of the Pedunculopontine Nucleus Area in Parkinson Disease: MRI-Based Anatomoclinical Correlations and Optimal Target", Neurosurgery
(accepted for publication, in press)

Constantin Tuleasca, Jean Régis, Elena Najdenovska, Tatiana Witjas, Nadine Girard, Jean-Philippe Thiran, Meritxell Bach Cuadra, Marc Levivier, Dimitri van de Ville

Introduction

1.1. Clinical context

1.1.1. Gamma Knife radiosurgery

Radiosurgery (RS) was invented by the Swedish neurosurgeon Lars Leksell at the beginning of the 1950s¹ and defined as the “delivery of a single, high dose of ionizing radiation to a small and critically located intracranial volume through the intact skull”¹. Originally, Leksell conceived RS as a primary tool for functional disorders^{1,2}. In fact, as early as 1951, he treated a trigeminal neuralgia sufferer using a prototype guiding-device linked to a dental X-ray machine¹. The word “stereotactic”, frequently employed as “stereotactic radiosurgery”, refers to a three-dimensional coordinate system, which enables accurate correlation of a virtual target, seen in patient’s therapeutic images, with the actual target position in the patient. The principle of this device was to irradiate an intracranial target with narrow beams of radiation from multiple directions. The beam paths converge in the target volume, delivering a desired cumulative dose of radiation there, while limiting the dose to the adjacent healthy tissue, to obtain a radiobiological effect. Ten years later, significant progress had been made, due also in considerable measure to the contribution of the physicists Kurt Liden and Börje Larsson³. At that time, stereotactic proton beams had replaced the X-rays⁴. However, the synchrocyclotron was too clumsy. Leksell was thinking about a simple tool, which could be handled easily by the surgeon himself.

In the 1968, Leksell created the Gamma Knife (GK), a tool for RS using multiple focusing cobalt-60 sources². Gamma Knife radiosurgery (GKR) is a neurosurgical stereotactic procedure, combining image guidance with high-precision convergence of multiple gamma rays, currently emitted by 192 sources of Cobalt-60 (Leksell Gamma Knife ICON®, Elekta Instruments, AB, Sweden)⁵. Nowadays, the clinical applications of GKR include benign and malignant tumors of the brain and skull-base, vascular malformations, functional and psychiatric disorders^{6,7}. The intimate mechanisms of action are not all very well understood. In fact, they may differ according to the treated condition and the targeting strategy. In the case of tumors, apoptosis may be the major mechanism of cell death⁸⁻¹⁰; in vascular malformations, RS induces vessels obliteration by thrombotic endothelial proliferation¹¹⁻¹³; in functional disorders, GKR is used either to target a specific anatomical point in an anatomical structure (e.g. thalamus^{14,15}, anterior limb of the internal capsule¹⁶, trigeminal nerve¹⁷⁻¹⁹) or to target a larger zone, such as an epileptic focus^{20,21}, and the mechanism of action may differ.

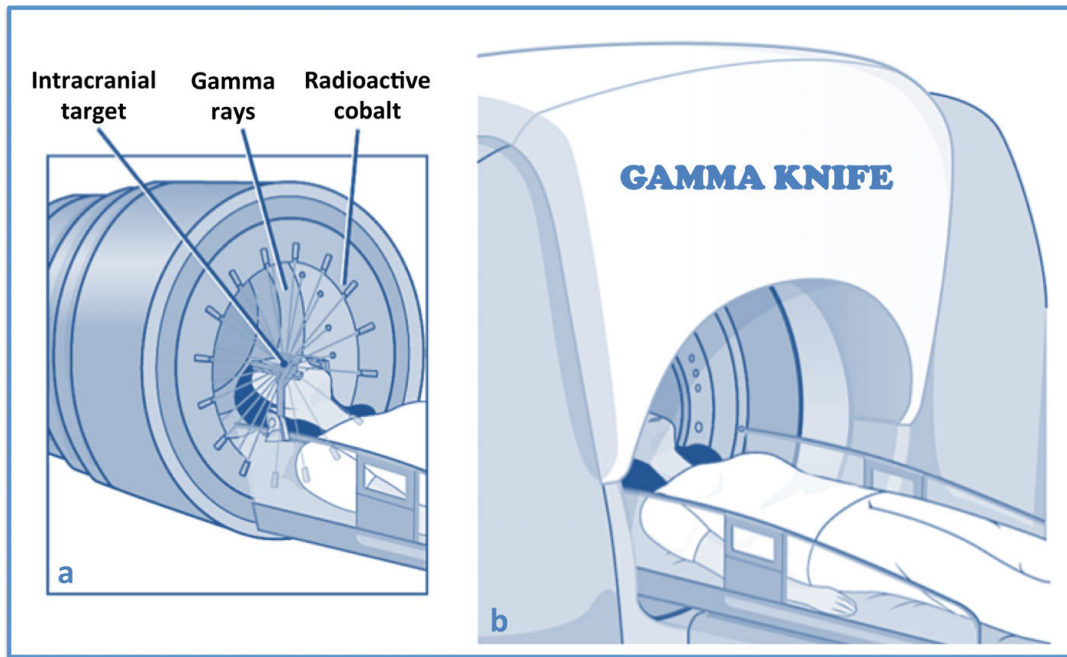


Figure 1: artistic representation of:
a- how the gantry of the Cobalt-60 machine is focusing Gamma radiation on the targeted region, while minimizing the amount of radiation that passes through the nearby regions; in the illustrated case, the patient has attached to the head a stereotactic frame; **b-** Gamma Knife machine (adapted with permission from <http://philschatz.com/chemistry-book/contents/m51203.html>)

1.1.2. The ventro-intermediate nucleus, as part of the thalamic nuclei

The thalamus is a paired diencephalic structure, centrally located between the cerebral hemispheres and the midbrain. Although occupying only 1% of total human body volume (approximately 15 cm³), it wires a broad array of functions, via densely interdependent connections between various cortical structures with basal ganglia, brainstem, spinal cord and cerebellum²². Furthermore, it controls information passing to and from the cerebral cortex, while conveying primary sensory inputs, integrating information across different networks, gating descending cortical outputs and modulating cortical laminar synaptic activity via reciprocal cortico-thalamo-cortico connections²³. Massive cortical projections bring each thalamic subpart (called nuclei), under the influence of motor, sensory and association areas of the cortical mantle.

The thalamus is considered a place of convergence of different major sensory and motor systems, in a very specific manner, at the level of each different nuclei. It integrates all these rather complex structures and distributes projections to specific areas of the cerebral cortex²⁴⁻²⁶. In this sense, it acts like a hub, relaying information between different subcortical areas and the cerebral cortex. The thalamus is playing also a role in the regulation of sleep, awareness and consciousness.

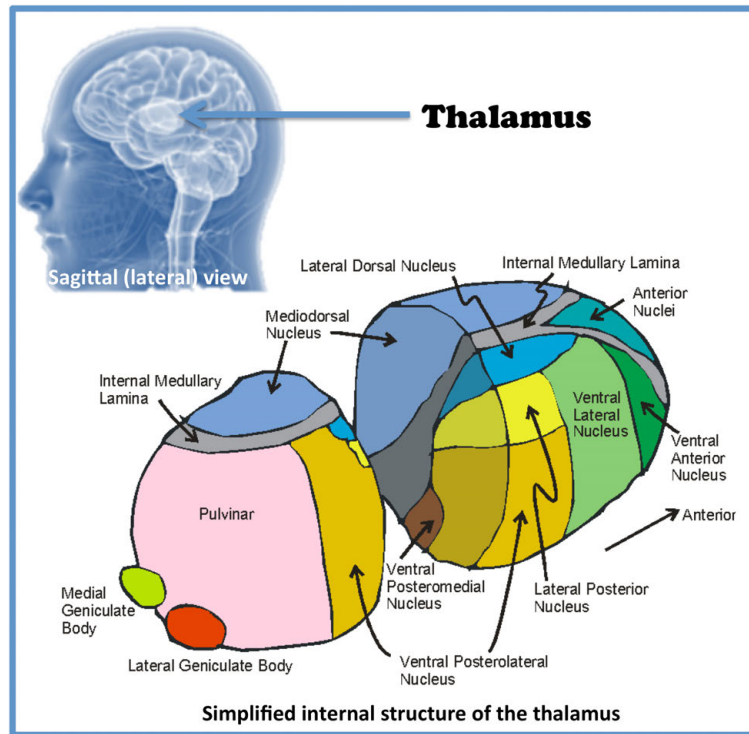


Figure 2: Overall vision of the anatomical location of the thalamus in humans, on sagittal (lateral, upper part) view; simplified view of the internal structure (lower part), as adapted, with permission from Doctor Jerry L- Prince, from “A novel contrast for DTI visualization for thalamus delineation”, Fan et al.²⁷, Fan X., Thompson M., Bogovic A., Bazin P.-L., Prince J., DOI: 10.117/12.844473, SPIE Medical Imaging 2010, San Diego, California, United States, Proc SPIE 762533

The current view on the thalamus considers this structure as separated into distinct clusters of neurons, grouped as more than 50 nuclei²⁸. These nuclei receive a particular, individual input and, moreover, send a particular afferent signal to one or several specific cortical regions, via the thalamo-cortical white-matter pathways^{25, 28}. In terms of nature of the incoming fibers, two groups of thalamic nuclei are classically considered and described by most of the authors, named the first and second order relays. The first order relay contains nuclei, which receive afferents from the ascending pathways, before they go to the cortex as output of sensory information, basal ganglia and cerebellum's. They principally transmit to primary cortical regions. The second order relay contains nuclei, which receive afferents mainly from the cerebral cortex and further transmits this information to another cortical area. They convey primarily to associative cortical regions. However, there is not an absolute barrier between them²⁹.

The nomenclature, as well as the number of thalamic nuclei, has been varying greatly depending on the reports. They have been previously delineated on an *ex vivo* basis, exploiting the differing chemoarchitectural and cytoarchitectural properties of the various cellular populations to identify unique, functionally specialized territories^{30, 31}. Whilst several parcellation schemes exist, Morel's atlas (based upon calcium-binding proteins for subdivision) is one widely accepted and divides the thalamus into five broad groups: anterior,

posterior, medial, lateral and reticular³⁰. Other parcellation methods have been proposed, including those based on structural Diffusion Tensor Imaging (DTI) (Wiegell et al.³², Najdenovska et al.³³) or functional MRI (Fan et al.²⁴). No matter the technique, or the computational approach, each type of nuclei is supposed to have its proper, well-defined, structure, function and connections, while using this approach. However, despite numerous advances, many aspects with regard to previously described nuclei separation techniques remain largely undiscovered²⁸.

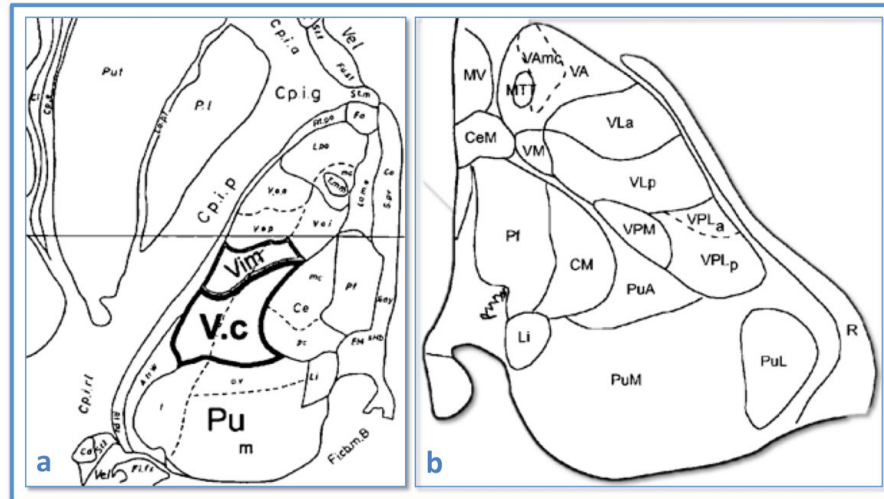


Figure 3: Illustration of parcellation of the thalamus, in axial plane, as depicted in: **a-** the Schaltenbrand's³¹ or **b-** Morel's atlas³⁰; while both are based on histological delineation, different subdivision patterns can be seen

The same limitations apply to the cytoarchitectonic definition of thalamic nuclei, including the Vim, at the level of the motor thalamus. One option, which might be considered, is a definition of the nuclei based on their subcortical afferents. There is no overlap between the cerebellar and pallidal and nigral afferent territories, although there are significant interdigitations. There is an anterior to posterior topographic organization of the thalamic ventral-lateral nuclei with the nigral and pallidal afferent receiving nuclei positioned anteriorly, followed by the cerebellar afferent receiving nucleus and then the sensory afferent territory in the most posterior position. However, there is a need for a better definition in human.

The ventro-intermediate nucleus (Vim, figure 3, a, adapted from Abosch et al.³⁴) is part of the ventral, motor group of thalamic nuclei. Among with the antero-lateral subdivisions, the former acts as a relay between the basal ganglia (e.g. ipsilateral globus pallidus), the contralateral cerebellum and the ipsilateral premotor and motor cortex³⁵. The interconnections with the basal ganglia and substantia nigra, but also with the red nucleus, make this structure important in movement control and motor coordination at large³⁶. The Vim was initially defined by Guiot and Albe-Fessard from electrophysiological recordings³⁷. It is organized in a somatotopic manner, with the leg-area lying laterally and the face-area

medially, measuring 2-4 mm in antero-posterior, 7-10 mm dorso-ventral and 4-6 mm medio-lateral³⁸.

1.1.3. Essential tremor

Human beings have left written archives about their tremors for thousands of years, with references in ancient Egypt, India, Israel, and Greece³⁹. Essential tremor (ET) is considered the most common movement disorders in adults⁴⁰. The hallmark manifestation is tremor, occurring during voluntary movements (i.e. kinetic tremor), at the opposite to the one appearing at rest³⁹. In the 19th century, the term «essential» was employed for a number of medical entities, which seems to have no evident medical cause. Charles Dana, a neurologist in New York, has coined the term ET in 1887, while documenting the presence of tremor in several large families⁴¹. The common use of the term «essential tremor» started by the mid of the 20th century and is referring to kinetic tremor, which is commonly familial, and for which no cause is known³⁹. The prevalence ranges between 0.4 and 3.9%³⁹.

The predominant clinical finding is the kinetic tremor of the arms. The frequency ranges between 4-12 Hz, and is usually inversely correlated with age⁴². Voluntary tremor occurs during writing, eating, dressing and other daily activities, impairing the patient's quality of life. Usually, there is a progressive worsening of this symptom, creating a progressive functional disability in multiple daily activities (Figure 4)⁴⁰. Head tremor is assumed to follow hand tremor, while considering a somatotopic spread of the involved parts of the body⁴³. It is related to several already supported features: older patient's age, older age of ET's onset, female sex and associated voice tremor⁴⁴. As directionality, three types are usually described: “yes-yes”, “no-no” and “round and round”⁴⁵. It is worth noting that aside motor manifestations, non-motor symptoms can be also present, including changes in visual reaction time⁴⁶, hearing impairment⁴⁷, cognitive deficits⁴⁸ or depressive symptoms⁴⁹.

The traditional view on ET, as a simple monosynaptic disease is currently being replaced by a broader definition, considering ET as a family of diseases, with a more complex set of clinical characteristics, which develop in a prescribed manner over time^{39, 41, 50}. Patients with ET who are sampled at different time points during their disease are also likely to have different clinical characteristics⁵⁰.

The diagnosis of ET is based on the medical history and physical examination performed by a health care professional. There is no single test to confirm the diagnosis. The anamnesis should include age of onset, family history, temporal evolution, exposure to eventual tremor-inducing drugs (e.g. Valproate, Lithium etc) or toxins (e.g. Mercury, Manganese etc). Neurological examination should assess distribution of tremor and

conditions of activation, include a visual estimation of the tremor's frequency range (low <4 Hz, medium 4-8 Hz, high >12 Hz).

Core diagnostic criteria are: bilateral action tremor of the hands and forearms (but not tremor at rest), absence of other neurological signs with the exception of cogwheel phenomenon and eventual isolated head tremor with no signs of dystonia. Secondary criteria are: long duration (more than 3 years), positive familial history and beneficial response to alcohol.

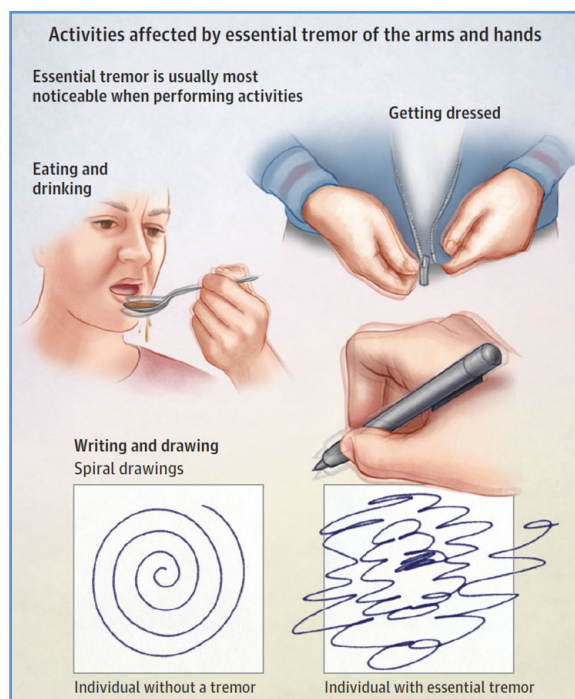


Figure 4: activities of daily living impaired by tremor: eating and drinking, dressing, writing (with permission from *Jama Neurology*, Muth *et al.*⁵¹, American Medical Association, DOI: 10.1001/jama.2016.16376)

Tremor severity can be assessed using standard questionnaire designed by Bain *et al.*⁵² (e.g. activities of daily living (ADL))⁵², tremor score on right treated hand (TSTH, e.g., right), from Fahn-Tolosa-Marin tremor rating scale⁵³ or the head tremor score using Tremor Research Group Essential Tremor Rating Assessment (TETRAS, range 0 to 3)

Although several hypotheses exist, ET underlying pathophysiology remains unknown (Figure 5 presents a broad view of what is considered tremor's circuitry, reproduced with permission from NEJM⁵⁴).

A first hypothesis commonly presumes **tremor as generated by abnormal oscillations within the motor cortex, the corresponding ipsilateral motor thalamic area (e.g. Vim) and the contralateral cerebellum (e.g. dentate nucleus)**, as parts of what is named the "tremor network"⁵⁵⁻⁵⁷. The "tremor network" hypothesis has been supported both by human electrophysiology⁵⁸ and neuroimaging studies^{55, 56}. Data from normal non-human primates have also shown Vim connections with the premotor and motor cortex and the cerebellum⁵⁹. Recent FC studies have previously shown, using resting-state fMRI (rs-fMRI), a prominent role of the Vim in the cerebello-thalamo-cortical pathway^{55, 56}. Furthermore, it is known that targeting of the Vim by standard surgical procedures generates good

therapeutic responses, with regards to tremor alleviation^{60, 61}. Hence, from this point of view, the cerebellum is considered to play a central role in the pathophysiology of ET⁶².

A second hypothesis is that **the inferior olivary nucleus (ION), induces a rhythmic oscillatory activity**, supposedly by reticulo-spinal and vestibule-spinal pathways, which has been reported by several animal experiments^{63, 64}. Moreover, in humans, Louis *et al.*⁶⁵ have done a systematic post-mortem study of microscopic changes in ION and did not detect any structural differences between ET cases and healthy matched controls. The same applied for functional neuroimaging positron emission tomography (PET) studies, which failed to identify any abnormal metabolic activity at this level⁶⁶. Both have pointed out towards the conclusion that if ION is involved in ET, there is no structural or metabolic modification⁶⁵. However, an isolated fMRI case-report, after opened surgical radiofrequency thalamotomy (RT), revealed significant activation within ION after the intervention⁶⁷.

A third hypothesis considers **ET as a progressive cell loss in the setting of a neurodegenerative disorder or a localized GABAergic dysfunction**^{68, 69}.

A fourth hypothesis links tremor with the visual system. This has not been specifically explored in modern studies until 2012⁷⁰ and further by the candidate using rs-fMRI in 2016, in the frame of the present thesis^{71, 72} or, more recently, by task-based fMRI⁷³. It has been previously demonstrated that in primates visuomotor arm tracking is followed by changes in the Purkinje cells in the cerebellum, which play a role in modulation of arm direction and speed⁷⁴. In humans, studies as early as the beginning of the 1960s^{75, 76} advocated for a decrease in physiological tremor while closing the eyes and further decrease in visual feedback.

1.1.4. The eye-hand coordination, a link with the visual system

The connection between visual areas, with part of the structures involved in tremor generation and specific circuitry, was subject of several studies, both in physiological and pathological tremor. It has been previously stated that vision is critical for performing basic motor tasks, particularly those requiring a degree of fine motor control and dexterity⁷⁷. Furthermore, reports of the tremor-vision association have provided subjects with an amplified view of their tremor⁷⁸. The hypothesis was that, in neurologically intact subjects, a potential tremor presence at the level of the distal segment is so small, that subtle changes in tremor amplitude cannot be detected by the visual system⁷⁹. One might think that by amplifying the tremor image (but not tremor itself), the visual system might be better capable to perceive the small amplitude tremor inherent to each limb segment. Furthermore, this type of reaction could potentially allow for greater control of the limb segment in question. This has not been conclusively demonstrated, as in a clear sense that augmented visual feedback would minimize finger tremor⁷⁸. However, this amplification approach is broadly adopted in microsurgery, so as to maximize the accuracy and precision⁸⁰. Most probably, while visual

feedback plays a role, other factors might be involved in tremor influence, such as the goal of the task, the number of the involved segments, the dexterity etc.

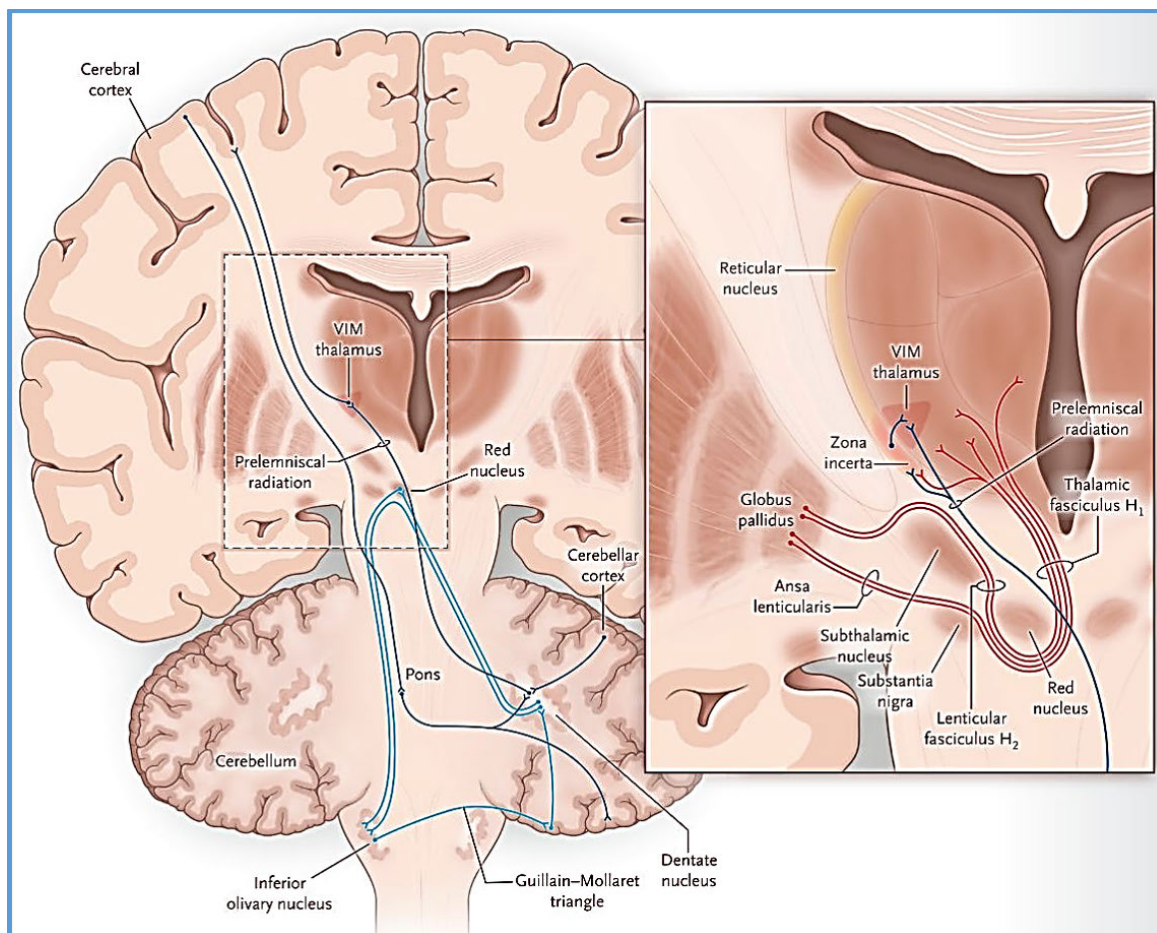


Figure 5: reproduced with permission from Haubenberger and Hallett⁵⁴ (*New England Journal of Medicine*, Copyright Massachusetts Medical Society): artistic representation of presumed pathways involved in the pathophysiology of ET: the cortico-ponto-cerebello-thalamo-cortical loop and the dentate nucleus-red nucleus-inferior olivary nucleus-dentate nucleus; are illustrated also the Vim, the zona incerta and the prelemniscal radiation, as areas successfully targeted in drug-resistant tremor

With regard to physiological tremor, Keogh et al.⁸¹ have investigated this feature, present in the upper limb of 8 adults, during performance of unilateral pointing task under conditions where the visual feedback, limb used and target size were altered. Postural tremor from the segments of the upper limb, forearm muscle electromyography (EMG) activity, and target accuracy measures were recorded and analyzed in the time and frequency domains. The authors concluded that physiological tremor output, observed in neurologically intact subjects, is not simply the product of intrinsic oscillations, but is task dependent and can be influenced by changes in the information provided to the subject. Changing the nature of the visual feedback resulted in increased tremor amplitude at the index finger. Furthermore, altering the nature of the visual feedback influenced tremor⁸¹.

With regard to tremor related to multiple sclerosis (MS) or cerebellar disorders, other studies suggested also that amplitude of postural tremor was influenced by changes in visual attention^{82, 83}. Moreover, in ET, Gironell et al.⁷⁰ analyzed 19 patients, while recording

neurophysiologic tremor with a tri-axial accelerometer transducer, attached to the dorsal surface of the index finger of the most affected hand. The authors concluded that tremor significantly improved in the absence of a visual feedback, in accordance with previous studies on MS⁸³. Possible hypotheses remained a visual component of tremor, but also that visual feedback might increase patient anxiety, expanding also in turn muscle activity and therefore tremor⁷⁰.

Interestingly, there is also prior evidence suggesting that the zona incerta (ZI, Figure 5), one of the proposed surgical targets for ET (for details on surgical targets see section 1.1.5.), could act like a link between the visual cortical sensory and brainstem motor system⁸⁴. This might be also related to the fact that structurally, ZI is known to receive a contingent of fibers from the occipital cortex. Furthermore, the authors suggested that the occipito-incertal pathway is selectively involved in visually guided behavior⁸⁴. More recently, the evidence of a visual subsector within the ZI has been added by Power et al.⁸⁵. This particular report has studied rats and suggested that ZI may be in position to integrate visual information together with the other somatosensory, motor and visceral information that it receives.

1.1.5. Surgical targets for drug-resistant essential tremor: brief overview

Primary treatment of ET is pharmacological [e.g., beta-blockers (mainly Propranolol), or Primidone, level A, established as effective⁸⁶], but its efficacy remains rather inadequate for some of the patients⁸⁷. In fact, 30% to 50% of them will not respond to either Primidone or Propranolol⁸⁸. Drug-resistant ET can benefit from standard open functional neurosurgery procedures, including deep-brain stimulation (DBS)⁶⁰ or radiofrequency thalamotomy (RF-T)⁶¹, which are further detailed in section 1.6. When the former are contraindicated, or due to reluctance to have foreign material inside the brain, patients can benefit from minimally invasive procedures, such as RS¹⁵ or, more recently, high-focused ultrasound (HIFU, producing a controlled thermocoagulation)⁸⁹, considered alternatives to RF-T.

The first surgical treatments for movement disorders were performed at the beginning of the 20th century, with a large variety of surgical targets. In 1932, Bucy was claiming decrease of tremor after interrupting the pyramidal system, with important postoperative deficits⁹⁰. In 1933, Putnam performed a posterolateral chordotomy and interrupted the proprioceptive input, in an attempt to decrease complications and relief tremor⁹¹. During the next decades, the methods used for interrupting basal ganglia's circuitry continued to be lesional (e.g. mesencephalic tractotomy⁹², stereotactic mesencephalotomy⁹³, anterior capsulotomy⁹⁴, coagulation of the basal ganglia nuclei, including pallidotomies and thalamotomies). In 1947, Spiegel and Wycs introduced the human stereotaxy, providing a reproducible method of navigating to an intended surgical target⁹⁵⁻⁹⁷. In 1952, Irving

Cooper⁹⁸, accidentally ligated the anterior choroidal artery, and the patient experienced tremor suppression, without motor loss during elective movement disorders surgery (e.g. mesencephalic pedunculotomy). In 1954, Hassler described lesioning of the ventral intermediate nucleus of the thalamus for parkinsonian tremor using stereotaxy⁹⁹. In 1962, Guiot, who was working with Albe-Fessard, defined the Vim as an electrophysiological concept and further surgical target for intractable tremor³⁷. However, the electrophysiological defined Vim is not identical with the entire Vim. The effects of surgery of the electrophysiological defined Vim are not necessarily totally restricted to the Vim itself, as defined cytoarchitectonically by Hassler, but could as well impinge on other subparts, such as the ventral oral posterior thalamic nucleus (Vop) or the subthalamic area. A very small RT lesion in this area, as small as 40 mm³, can alleviate tremor. In 1977, Velasco et al. proposed the posterior subthalamic area (PSA) as a surgical target for tremor¹⁰⁰. In the early 1980s, Ohye pioneered the selective Vim thalamotomy^{101, 102}. In 1987, Benabid et al. published the first results on DBS, which created a paradigm shift in the field of movement disorders¹⁰³. More recently, the zona incerta (ZI, figure 5) and its neighboring anatomic structure, the prelemniscal radiation, both part of the PSA, have been suggested as more effective targets for DBS in ET^{104, 105}. The proposed pathophysiological theories of these former targets are supposed to be related to direct modulation of the dentatorubrothalamic tract.

1.1.6. Surgical therapeutic approaches for drug-resistant essential tremor

Radiofrequency thalamotomy has been historically used since the early 1950s and is a stereotactic surgical procedure in which a small hole is made in the skull and then a lesion (destruction of cells) performed in the Vim¹⁰⁶. The former immediately arrests tremor on the opposite side of the body. Because the surgeon requires the assistance and cooperation of the patient during the surgery, the patient is awake throughout the procedure. This treatment is not reversible. Main contraindications are dysarthria and severe balance disturbance. It has an efficacy ranging between 73%-93%, but also potential complications, particularly dysarthria and impaired balance, especially when the procedure was performed bilaterally. Recently, a randomized trial between thalamotomy and thalamic DBS for various tremors showed in both short- and long-term follow-up that both procedures were effective for tremor control, but thalamotomy had more side effects and resulted in less improvement in quality of life than DBS¹⁰⁷. Among RF-T's advantages are lower costs as compared to DBS, no hardware remains, long-term efficacy^{61, 108}. However, persistent morbidity associated with thalamotomy, which occurs in fewer than 10% of patients, includes dysarthria, disequilibrium, weakness, and cognitive deterioration^{61, 108}. Bilateral thalamotomy is

associated with a high risk of dysarthria, occurring in as many as 29% of patients, and a risk of cerebral hemorrhage, and is usually avoided^{61, 108}.

Currently, continuous DBS is considered the reference technique and is an invasive treatment, involving the implantation of a medical device (e.g. brain pacemaker), which sends electrical impulses to specific parts of the brain (e.g. Vim for tremor, the subthalamic nucleus-for Parkinson’s disease). Despite the long history of DBS¹⁰⁹, its underlying principles and mechanisms are still unclear¹¹⁰. It is currently considered that electrical stimulation disrupts tremorogenic oscillations in the previously described pathophysiological loops (e.g. “tremor network”). However, it is also acknowledged that excitatory reciprocal thalamocortical loop is possibly capable of amplifying oscillations of any origin¹¹¹. Deep-brain stimulation directly changes brain activity in a controlled manner. Its effects are reversible (unlike those of lesioning techniques) and are one of only a few neurosurgical methods that allow blinded studies. Recently¹¹², it has been shown in thalamic slices from mice, that DBS causes nearby astrocytes to release adenosine triphosphate (ATP), a precursor to adenosine (through catabolic process); in turn, adenosine 1 receptor activation depresses excitatory transmission in the thalamus, thus causing an inhibitory effect that mimics ablation or lesioning. Deep-brain stimulation presents the risks of open surgical procedures (table 1), with major complications including hemorrhage and infections^{60, 107, 113-118}. Neuropsychiatric side-effects are also described, such as apathy, hallucinations, compulsive gambling, hypersexuality, cognitive dysfunctions and depression, that are potentially reversible¹¹⁹. These are treated with clinical and neuroradiological surveillance, corticoids or even surgery in accessible and life-endangering hematomas.

Intervention	Efficacy	Complications
1. Vim RF-T	73- 93% 30-80% (MS)	9-23% (PD) 16-41% (MS) up to 4% intracerebral hemorrhage
2. Vim DBS	71-94% (PD) 68-89% (ET)	up to: - 36% paresthesias - 18% dysarthria - 9% dystonia - 8% balance disturbance and limb weakness - 6% ataxia - 4% intracerebral hemorrhage
3. Vim GKR	73-93%	0-8.4%

Table 1 (*PD= Parkinson disease, ET= Essential tremor, MS= Multiple sclerosis): brief summary of the published data: as shown here, the rates of efficacy between Vim DBS and Vim GKR are quite similar, with lower complication rates and less invasiveness for the former; nevertheless, results are reported using heterogeneous methods and the targeting procedure-a crucial step- is operator-dependent

As an alternative to Vim DBS, Vim GKR is primarily indicated for drug-resistant ET and Parkinsonian tremor, but also for other types of tremors, as secondary indications

(multiple sclerosis, post-infarction, post-encephalitis)¹²⁰⁻¹²³. Because of the fact that the clinical response of Vim GKR is delayed in time and appears gradually¹²⁴, clinical and neuroradiological assessment is usually made at baseline, pretherapeutically, and is repeated at fixed intervals after (e.g. 3, 6, 9, 12, 18, 24 months and on yearly basis after^{122, 124, 125}). The immediate clinical evaluation after the procedure shows no visible changes in symptoms¹²⁴. The delay of improvement is usually around four months, ranging between three weeks and twelve months¹²⁵. The success rate varies between 73 and 93%, with a low complication rate ranging between 0 to 8.4%, for authors using the same range of prescription dose (e.g. 130-140 Gy)^{15, 126, 127}. Radiosurgery of the Vim has provided level IV evidence¹²⁶, including in the frame of prospective, single blind studies¹⁵. Favorable outcome has been documented on long-term basis, over 19 years: 93.2% improved in tremor, 60.3% tremor arrest or barely perceptible tremor¹²⁷. At last follow-up (median 54 months), tremor improvement was sustained in 96% of patients with initial tremor relief¹²⁷. Complications primarily include limited contralateral sensory loss or motor impairments, speech difficulties, hemorrhage and edema¹²²⁻¹²⁵. As an alternative to Vim DBS and more recently, Vim HIFU, which produces a controlled thermocoagulation, has emerged as a minimally invasive alternative^{15, 128}. High-focused ultrasound uses 1000 ultrasound rays for generating a focal lesion, which size and location are controlled via MR thermography, measuring in real time the temperature of the targeted area⁸⁹. A recent meta-analysis of the surgical treatments for tremor considered that the mean effect on tremor reduction was similar between Vim RF-T, Vim GKR and Vim HIFU, for a follow-up period, which did not have a significant influence on treatment effect size slope¹²⁹. The same applied for the analysis of complications.

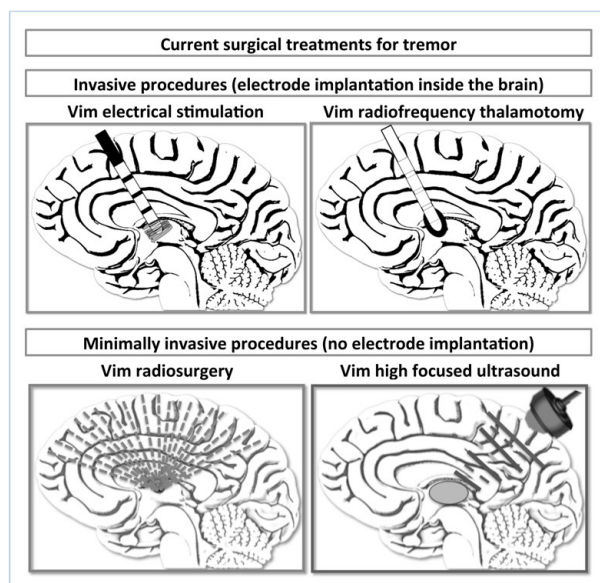


Figure 6: Surgical interventions for drug-resistant essential tremor: upper part, invasive procedures, with electrode implantation inside the brain: electrical stimulation (left), radiofrequency thalamotomy (right); lower part, minimally invasive procedures: radiosurgery (left), high-focused ultrasound (right), adapted from doi.org/10.1093/brain/awy096

1.1.7. Limitations of Vim radiosurgery for tremor

The thalamus was one of the first functional GKR targets, initially used by Leksell for the treatment of intractable pain of visceral origin, at the level of the dorso-medial nuclei group². Nowadays, GK thalamotomy (also named Vim RS or Vim GKR or even stereotactic radiosurgical thalamotomy) refers to targeting of the Vim nucleus for drug-resistant tremor. Vento-intermediate nucleus radiosurgery was pioneered in Sweden by Leksell's colleagues^{130, 131}, as well as in the United States¹³², in Japan¹²⁴, and in Europe (Marseille, France)¹⁵, as an alternative to stereotactic RT or DBS.

In ET, GKR has five main limitations: (1) indirect targeting, with (2) no intraoperative confirmation of the target, (3) delayed clinical effect, (4) inability to predict the radiological response (which is considered to be related, in most cases, with the clinical one)¹³³ and a (5) lack of understanding of its radiobiological effect.

(1) Indirect targeting:

Current MR imaging techniques, both at 1.5 and 3 Tesla (T), do not allow Vim's direct visualization (Figure 7). In this respect, the targeting is performed in indirect manner. For this former purpose, atlases can be used³¹, but also stereotactic coordinates, with respect to anterior and posterior commissure (AC-PC), as well as Guiot's diagram¹³⁴. However, none of the former account for inter-individual variability in target's location¹³⁵. Moreover, there is a lack of uniformity in the medical community.

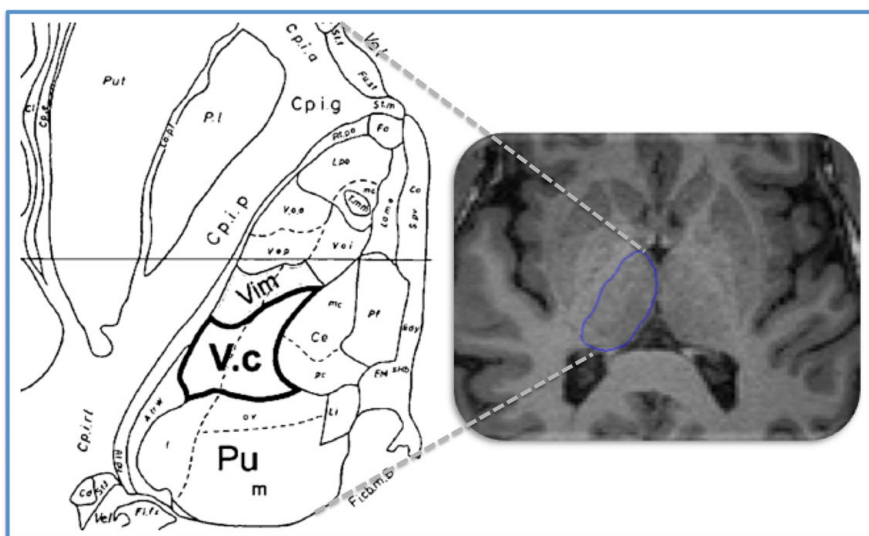


Figure 7: The thalamus appearance on T1 weighted imaging (right panel), with corresponding axial slice from the Schaltenbrand's atlas (left)³¹, modified and adapted from Abosch et al.³⁴; one can see the absence of intrinsic contrast for distinguishing different thalamic subparts, as the former appear like an homogenous region

The atlases show several subgroups of thalamic nuclei, divided based upon histological appearance on post mortem specimens³¹, but also by using electrophysiology¹³⁴ or *in vivo* anatomical studies²⁵. The main limitation of this parcellation comes from the reduced number of subjects and/or post-mortem specimens. Additionally, the same applies to how we can best normalize atlas-derived coordinates to a specific patient's brain. The

stereotactic coordinates, as well as the Guiot, are defined based upon anatomical landmarks, including the anterior and posterior commissure (AC and PC). Moreover, there is a variability in the location of thalamic nuclei in humans¹³⁶. Also, the dimensions of structures, such as the Vim, are very small, measuring, in its case, 2-4 mm (antero-posterior), 7-10 mm (dorso-ventral) and 4-6 mm (medio-lateral). No consensus exists regarding a “gold standard” targeting method, which accounts for an important variability. In this regard, there is a need of improving the targeting.

With these limitations, Vim GKR procedures (Figure 8) are performed in stereotactic conditions. After application of Leksell® coordinate G Frame (Elekta AB, Stockholm, Sweden), all patients undergo stereotactic MR imaging. Indirect targeting is performed using standard methodology by Guiot’s diagram, placed 2.5 mm above the AC-PC line and 11 mm lateral to the wall of third ventricle. A single 4-mm isocenter was used and a maximal prescription dose of 130 Gray (Gy) at the 100% isodose line.

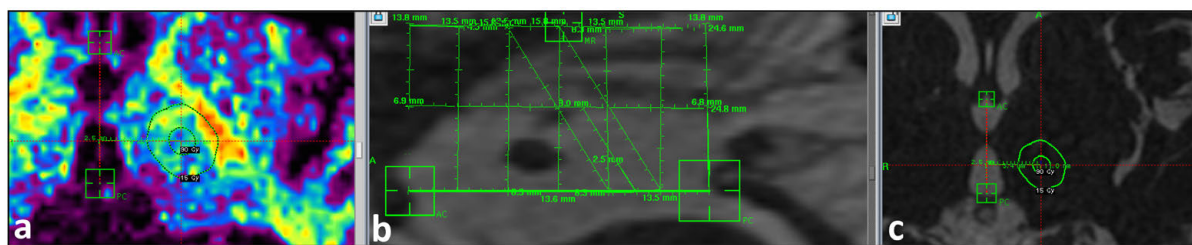


Figure 8: targeting of the ventro-intermediate nucleus of the thalamus by radiosurgery: **a**, use of non-stereotactic DTI, to visualize the internal capsule and limit the irradiation doses towards this structure; **b**, the quadrilatre of Guiot; **c**, the placement of a unique 4-mm shot, with the isodoses of 90 and 15 Gy colored in green

(2) Absence of the intraoperative confirmation of the target:

In the standard surgical procedures, such as Vim RT or DBS, there is the possibility of the intraoperative confirmation of the target, by the means of electrophysiology. As shown by previous studies, there is a difference between the “radiological” obtained Vim and the “electrophysiological” confirmed one, as high as 2 mm in approximately 35% and 1 mm, respectively, in 65% of the cases¹³⁷, which can account for different clinical results. This becomes particularly crucial in non-invasive techniques, such as Vim GKR. With regard to Vim GKR, there is no real intraoperative confirmation of the target.

(3) Delayed clinical effect:

The mean latency period till tremor alleviation after Vim GKR can be as high as 4 months (range 3 weeks, 12 months)¹⁵. Contrariwise, after DBS, tremor arrest is immediate.

(4) The inability to predict the MR signature at one year after Vim GKR (Figure 9):

This last aspect might have clinical implications with regard to tremor arrest. Unpublished data from the Marseille group¹³³ advocated for a correlation between the 1-year MR signature volume and the clinical outcome at one-year follow-up. Mainly, patients who fail to

improve after Vim GKR would display a significantly smaller, thalamic, 1-year MR signature volume, although undergoing a standard procedure. However, this fact should be cautiously interpreted, as other, much complex factors, might be involved. The shape of the lesion is described as typical (a spherical, high signal zone, with a blurred boundary and a central low-signal zone; approximately 5 mm diameter) or atypical (the central, low-signal zone is small and surrounded by a doughnut-shaped high-signal zone; approximately 10 mm diameter). Ohye et al.¹³⁸ suggested that atypical lesions could be associated with patient's age, cortical atrophy or symptom type (tremor, rigidity or dystonia) and hypothesized that increased radiation dose rate of Cobalt-60 sources may be responsible for this phenomena. Most of the patients will have a small reproducible lesion, some patients will show minimal changes on follow-up MR, while others might present string-like reactions along the border of the thalamus and along the internal segment of the globus pallidus. The former have larger MR signatures, which usually extend to the internal capsule or medial thalamic region, often involving streaking along the thalamo-capsular border. This might correspond to a population of “hyper-responders”. Ohye et al. suggested that 2% of the population might be hypersensitive to irradiation, although no predictive or risk factor has been identified. Thus, large individual variations were observed in response to Vim GKR^{123, 124, 139}. The same author¹⁴⁰ reported no correlation between these tissue reactions and tremor outcome. Kondziolka et al. studied the possible modulation of the response to GK using aminosteroid U-74389G, and showed that it reduces cytokine expression, normally seen after radiation injury¹⁴¹.



Figure 9: *a*, minimal MR signature; *b*, the classical “cocade” aspect; *c*, larger MR signature

(5) Lack of understanding of the radiobiological effect:

In fact, Vim GKR has no access to tissue for histological analysis, and follow-up is done on imaging only, which limits the knowledge of its biological therapeutic effect. Past histological evidence has been mainly limited to very few reports (Figure 10), of whom one is the historical series of GK thalamotomy performed by Leksell for intractable pain and further reported by Steiner et al.¹³¹. The radiation doses used were much higher, as compared to what we currently prescribe (e.g. 130 Gy), while the reported error of the target placement, as matched to the final result was as low as 1 mm. Furthermore, Leksell's view of the GK was clearly initially intended to mimic the lesional effects of a surgeon's knife, hence the name

given to the radiosurgery device. The second histological study by Kondziolka et al.¹⁴² evaluated the effect of a 100 Gy irradiation dose in the baboon. The authors concluded that radiosurgery at this dose (e.g. lower than in current clinical practice in Vim GKR), generates focal necrosis and axonal degeneration of the thalamus, 6 months after the procedure. More recently, the “cocade theory”²¹ advocated for a neuromodulatory effect of Vim GKR, while considering four different zone in and around the target: necrotic, subnecrotic, neuromodulation and no effect. In the same sense, Ohye¹⁴⁰ was the first to suggest in early 2000 that only the necrotic lesion itself was not enough to impact on tremor alleviation. In addition, he sustained the idea that the MR signature’s size, clearly visible one year after Vim GKR and induced by the former, was too small to account for the benefic clinical effect.

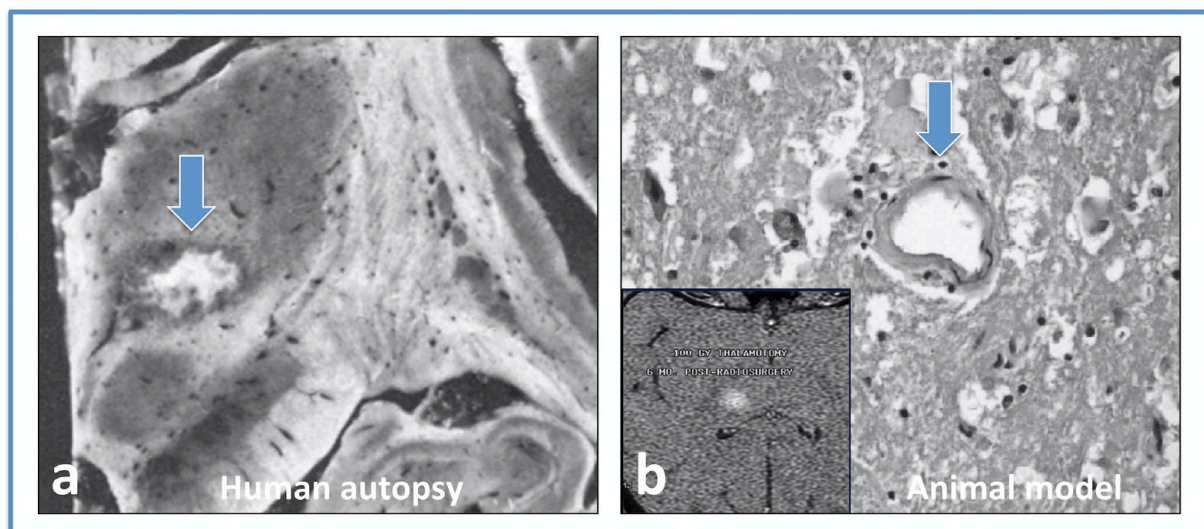


Figure 10: **a**, adapted from Steiner et al.¹³¹, first human autopsies after thalamotomy for pain; reproduced with permission from Springer Nature **b**, adapted from Kondziolka et al.¹⁴², 6 months after baboon irradiation, with 100 Gy, ventral thalamus (**main image**: hematoxylin and eosin stain, showing thalamic tissue within the radiosurgical target, with vascular hyalinization and wall thickening typical of radiation vasculopathy being prominent; **secondary image**, MRI of the irradiated zone); reproduced with permission from Karger Publishers

1.1.8. Addressing Vim’s GKR limitations using magnetic resonance imaging

In this thesis, we will explore several MRI modalities to answer the above-described limitations. The limitation related to the indirect targeting will be addressed using ultra high field MRI (7 T). The core of the present thesis, which is the understanding of the radiobiological effect of Vim GKR, will use structural (T1 weighted, T1w) and functional MR imaging. The state-of-art related to MR imaging in ET and methods used to analyze them are briefly described here after.

1.2. Neuroimaging context

1.2.1. Ultra high field 7 T MRI for thalamic nuclei visualization

During the past decade, a new usefulness of 7 Tesla images in functional stereotactic neurosurgical procedures (e.g. DBS) emerged, as advocated in several previous studies^{34, 143}.

In particular, Susceptibility Weighted Imaging (SWI) is an MR technique, which generates a unique image contrast, based on tissue sensitivity to magnetic susceptibility effects^{144, 145}. The term magnetic susceptibility, in a broader sense, is used to describe the degree of magnetization in an object resulting from an external field¹⁴⁶. Recent studies suggest that anatomical deep gray matter structures are better visible on 7 T MRI sequences, especially on susceptibility weighted imaging (SWI), but not only, as compared with the currently used 3 T in clinical practice^{34, 143, 147, 148}. This could be of particular benefit, especially for minimally invasive techniques, such as GKR, due to the indirect targeting manner, with no intraoperative confirmation of the target by electrophysiology (e.g. for Vim GKR). Moreover, GKR uses a multimodal imaging approach, based upon, if possible, a direct visualization of brain structures and the targeting, with the one exception of Vim GKR.

The advantages of using MR images acquired at 7 T (with higher magnetic strength 7 T) is not only the improvement of resolution and the SNR, but also the gain of a superior sensitivity to contrast of magnetic susceptibility origin, that allows a better identification of various structures in the mid brain's area, not distinguished at 1.5 Tesla or 3 T. Susceptibility related contrast can be explored either via SWI¹⁴⁹ or by quantitative susceptibility mapping (QSM)¹⁵⁰.

In fact, SWI at 7 T allows the direct visualization of the main thalamic regions and the distinction from their surroundings. In the framework of a standard gradient echo imaging, SWI is built as a combination of MRI's signal's magnitude and phase, both strongly affected by the magnetic susceptibility and the tissue geometry. Several tissues, including de-oxygenated blood vessels, axonal lesions, air/tissue interface, as well as the calcium and iron-laden tissue, manifest unique magnetic susceptibility differences with respect to its surroundings¹⁴⁶. Consequently, for these tissues, SWI provides a more enhanced contrast than the standard T1, T2 or T2*-weighted imaging. Furthermore, it also provides a better visualization of deep brain structures, as previously stated. Another potential benefit of the 7 T SWI scanning is the high isotropic resolution (0.67 x 0.67 x 0.67 mm³), which would help provide more accurate segmentation and, as consequence, a differentiation of smaller details, as compared to the ones detected in the diffusion MR data.

Current indications include brain tumors, multiple sclerosis, cerebrovascular disease, epilepsy and aging related changes¹⁵¹⁻¹⁵⁵. A recent emergent field is represented by

neurodegenerative disorders^{156, 157}. The main limitations remain the inhomogeneous field, cost, limited availability and extensive contraindication for scanning¹⁵⁴.

In the field of functional neurosurgery, Abosch et al.³⁴ (Figure 11) were the first to explore the usefulness of the SWI, acquired at 7 T, *in vivo*, mainly as related to different basal ganglia subparts and with special interest for the subthalamic nucleus (STN). In fact, SWI clearly allowed the separation of globus pallidus intern from the globus pallidus extern and showed a boundary between the STN, the substantia nigra and the red nucleus. At the level of the AC-PC plane, a comparison with histological landmarks, such as those from the Schaltenbrand and Wahren's atlas¹⁵⁸ and a contrast modulation within the thalamus was considered to be able to directly determine the shape and the location of the pulvinar (Pu), the ventral caudalis (Vc), and seemed also of real value for Vim's visualization. The former appeared as a well-distinguishable structure, hyperintense, surrounded by darker regions.

The underlined observations have a qualitative character and were made based on data from a single subject. However, this work was a pioneering one, with respect to a direct discrimination of subparts of the complex thalamic architecture.

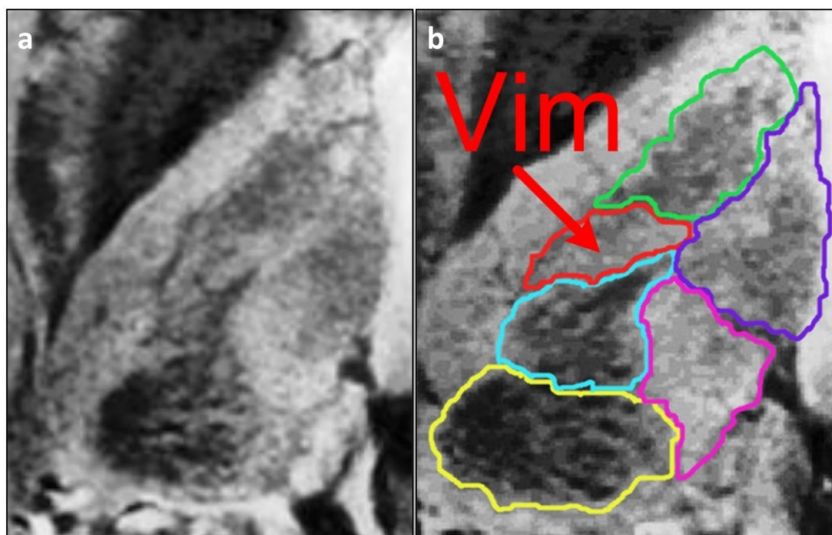


Figure 11: *a*, image extracted from Abosch et al.³⁴, showing SWI acquisition thalamic level (axial slice, right side); *b*, image acquired on a healthy subject at Center of Biomedical Imaging (CIBM), Lausanne, Switzerland, showing different thalamic subparts, including the Vim (courtesy and draw by E. Najdenovska)

1.2.2. 3 T MRI for exploring the radiobiology of radiosurgery

Structural neuroimaging approaches using conventional (1.5 and 3 T) MRI have provided new understanding with regards to tremor's pathophysiology in general, as well as to ET in particular⁶⁹. Computational approaches for analyzing high-resolution structural MRI (e.g. T1 weighted) can provide a powerful and non-invasive tool for characterizing individual and/or group differences in brain anatomy¹⁵⁹.

1.2.2.1. Voxel-based morphometry

1.2.2.1.1. General aspects

Voxel-based morphometry (VBM) is a neuroimaging analysis technique, which allows investigating focal differences between groups of subjects in white or gray matter (GM), by a well-established and robust methodology¹⁵⁹. In this thesis, Statistical Parametric Mapping is performed using MATLAB 2014a, 2014 (MathWorks, Boston, MA, USA) was employed for processing and analyzing the T1w MRI data.

In a nutshell, the anatomical MR images were normalized to the Montreal Neurological Institute (MNI) atlas, with voxel-size of $2 \times 2 \times 2$ mm. The normalization procedure allows the warped images to fit into a standard template brain. Furthermore, this establishes a voxel-to-voxel correspondence, between brains of different individuals and different shapes. It will enable to drive group statistics and to report the results in a standard coordinate system (e.g. MNI, which is based upon data from many individuals and is fully 3D, with data at every voxel; Figure 12).

They were further segmented in GM, white matter and cerebro-spinal fluid. Furthermore, they were spatially smoothed using a 8-mm full-width-at-half-maximum (FWHM) Gaussian Kernel in SPM12, to blur individual variations in gyral anatomy and to increase the signal-to-noise ratio. The smoothing procedure enables the subsequent voxel-by-voxel analysis, comparable to a region of interest approach, as the voxel will contain the average concentration of gray matter from around the voxel (where the voxel is characterized by the form of the smoothing kernel). The former is often referred as to GMD. In a structural MRI of the brain, the intensity of each volumetric pixel, or voxel, relates to the density of the gray matter in that region. The VBM technique is, in this sense, comparing brain structure on a voxel-by-voxel basis. After the classical preprocessing steps, the intensity values of the voxels are compared, to identify localized differences in GMD¹⁵⁹. A statistical model, adapted to the research question, can be used and further applied to the neuroimaging data.

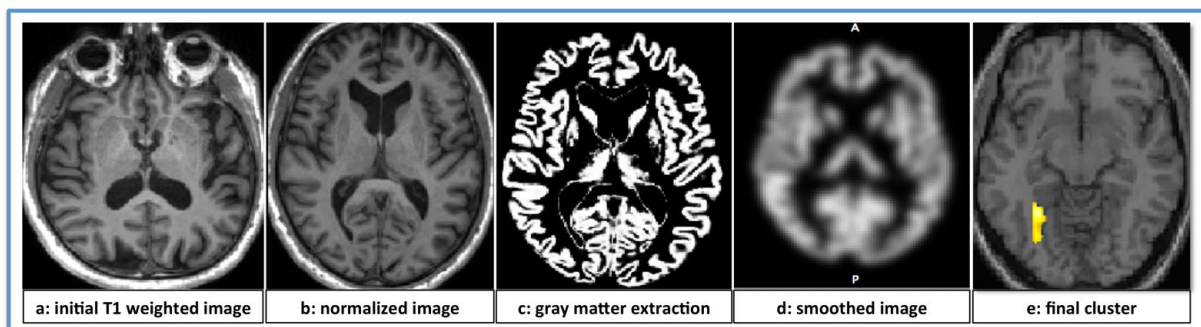


Figure 12: Preprocessing steps for VBM analysis: **a**, initial T1 weighted image; **b**, normalized images; **c**, gray matter extraction; **d**, smoothed image; **e**, final cluster (data from patients treated in CHU Timone, Marseille)

1.2.2.1.2. VBM in essential tremor

With regards to ET, VBM has been used for analyzing T1w imaging acquired at both 1.5 and 3 T MRI, with large spectrum of controversial findings¹⁶⁰⁻¹⁶⁸. However, all these studies have compared ET cases versus a group of healthy controls (HC). Daniels et al.¹⁶⁴ suggested that patients with predominant intention tremor show a relative expansion of GM areas involved in high order visuo-spatial processing (superior temporal, hippocampus, supramarginal gyrus, middle occipital); the authors hypothesized the existence of an adaptive mechanism, compensating the high demands of the visuo-spatial control of skilled movements in case of tremor. Quattrone et al.¹⁶⁸ advocated that patients with head tremor presented marked atrophy of the cerebellar vermis. Cerasa et al.¹⁶³ reported a reduction of the cerebellar volume in ET patients with and head tremor. Benito-Léon et al.¹⁶¹ have suggested multiple GM changes, at 3 T, in the bilateral cerebellum, bilateral parietal lobes, right frontal lobe and right insula. Bagepally et al.¹⁶⁰ advocated for widespread areas of GM atrophy in ET, including bilateral cerebellum and vermis, bilateral frontal, right superior parietal, middle temporal and occipital. Lin et al.¹⁶⁶ have found atrophy in ET within the caudate body, the middle temporal pole, precuneus or the superior temporal gyrus. Buijink et al.¹⁶² demonstrated a volume increase in cortical sensorimotor regions (bilateral precentral and postcentral) in ET patients with head tremor. Nicoletti et al.¹⁶⁷ found no white or gray matter atrophy in ET.

1.2.2.2. Resting-state functional MRI

1.2.2.2.1. General aspects

Functional MRI (fMRI) offers the possibility to safely and noninvasively image brain activity, with low spatial resolution and relatively good temporal resolution, as compared to other previous functional neuroimaging methods, such as positron emission tomography (PET). It is also evident during rest, despite the absence of a task-related cerebral activation, enabling the extraction of brain intrinsic connectivity networks¹⁶⁹. Resting-state functional magnetic resonance imaging (rs-fMRI) is a non-invasive technique that analyses spontaneous fluctuations of the blood-oxygen-level-dependent (BOLD) signal¹⁶⁹, corresponding to spatially segregated functional networks. Thus, it observes functional changes in the brain without requirement of a specific task, precluding the inadequacies of the task-designed fMRI. The intrinsic functional brain signals can be obtained with minimal patient compliance, which opens new avenues for the application of fMRI in the clinical realm¹⁷⁰. The main condition of resting-state is related to conscious and unconscious brain activity, which happens without premeditation or external stimulus. This is having as premise the fact that

brain is active even in the absence of a task, primarily driven by internal dynamics, with external events modulating, rather than determine, the activity of the system¹⁷¹.

There are two important aspects about the hemodynamic response that underlie basic qualities of BOLD fMRI (Figure 13) and further determine how the data should be analyzed. The first one is that the response is slow: although neuronal activity may last only milliseconds, the increase in blood flow that follows this activity takes about 5 seconds to reach his maximum; this peak is followed by a long undershot that does not return to baseline for at least the next 15-20 seconds. The second one is that the hemodynamic response can be, to a first approximation, be treated as a *linear time-invariant system*¹⁷². Mainly, a long train of neuronal activity can be determined by adding together shifted versions of the response to a shorter train of activity; the latest makes possible the creation of an upfront statistical model, describing the time course of hemodynamic signals that would be expected given some particular time course of neuronal activity, using *convolution*. Functional connectivity (FC; or interconnectivity (IC), if measured within the same network), as measured by correlations between time courses of the fMRI signals between segregated brain regions, has previously revealed neurological networks, including the motor one, such as in the seminal study of Biswal et al.¹⁶⁹. Evaluation of such connectivity offers an alternating approach for studying intrinsic networks interactions of the human brain. This approach has led to important new insights in many diseases, including in ET^{55, 56, 173, 174}, due to minimal patient cooperation and the possibility to obtain rich information, in a non-invasive manner¹⁷⁵. Numerous methods to extract functional connectivity or inter-connectivity (IC)—if within a functional network—have been suggested to measure temporal dependencies of neuronal activation between anatomically separated brain regions. Recent work in systems neuroscience has characterized several major brain networks that are identifiable in resting brain state¹⁷⁶. The general clinical applications drive from obtaining diagnostic biomarkers of a disease, identifying group differences of the former, or the effect of a punctual treatment in

longitudinal analysis etc¹⁷⁰.

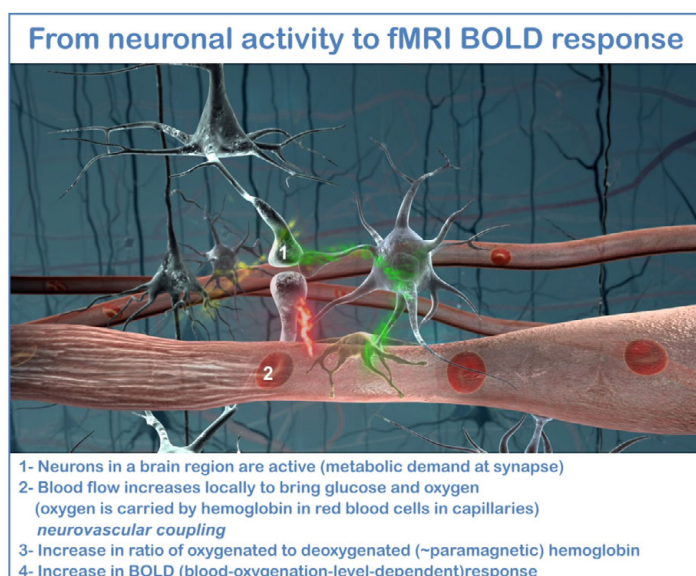


Figure 13: Artistic illustration of how we can pass from the neuronal activity to fMRI BOLD response (Courtesy of the USC Laboratory of Neuroimaging and Athinoula A. Martinos Center for Biomedical Imaging, Consortium of the Human Connectome Project-www.humanconnectomeproject.org)

1.2.2.2.2. Resting-state fMRI studies in ET

There are only a few observational rs-fMRI studies in ET^{56, 174, 175, 177, 178}. They are summarized in table 2. Benito-Léon et al.¹⁷⁵ used an independent component analysis (ICA, further detailed below) based approach to study resting-state networks, while the other reports use other methodologies, mainly to specifically probe the cerebello-thalamo-cortical network¹⁷⁹. Benito-Léon et al.¹⁷⁵ suggested that compared to HC, ET patients displayed increased FC in the sensorimotor and salience networks, and decreased FC in the cerebellum network; additionally, increased FC was observed between anterior and posterior default mode networks (DMN). Fang et al.⁵⁶ used a seed based approach and advocated that ET and HC cases share a similar Vim network, with changes in ET involving primarily the motor cortex (increase in FC)-cerebellum circuit. The same author used a different approach (e.g. regional homogeneity, ReHo)¹⁷⁷ and observed abnormal ReHo value of ET patients in the bilateral anterior cerebellar lobes and the right posterior cerebellar lobe were negatively correlated with the tremor severity score, while positively correlated with that in the left primary motor cortex. Using a seed-to-voxel connectivity analysis, Lenka et al.¹⁷⁴ showed decreased connectivity main of primary motor cortex with several cerebellum lobules, while compared to HC; furthermore, the thalamus on both hemispheres had increased connectivity with multiple posterior cerebellar lobules and vermis. Yin et al.¹⁷⁸ used amplitudes of low frequency fluctuation (ALFF) and demonstrated that patients showed significantly enhanced ALFF in the bilateral cerebral cortex, which is related to motor function, including the pre- and post-central gyrus, supplementary motor area and paracentral lobule; the larger ALFF value in the right precentral gyrus is related to a longer duration of tremor.

Study (year)	Methodology	Findings
Fang W et al. (2013) ¹⁷⁷	Regional homogeneity	abnormal ReHo values in: -bilateral anterior cerebellar lobes -right posterior cerebellar lobe *negatively correlated with the tremor severity score *positively correlated with that in left primary motor cortex
Gallea et al. (2015) ¹⁷³	Combined DTI, VBM, fMRI	Changes in supplementary motor area (ALFF)
Fang W et al. (2016) ⁵⁶	Seed (region-of-interest) based approach	ET and HC cases share a similar Vim network, with changes in ET involving primarily the motor cortex (increase in FC) -cerebellum circuit

Benito-Leon J et al. (2016) ¹⁷⁵	Independent component analysis (ICA)	- compared to healthy control, ET patients displayed increased FC in the sensorimotor and salience networks, and decreased FC in the cerebellum network; - additionally, increased FC was observed between anterior and posterior default mode networks
Yin W et al. (2016) ¹⁷⁸	Amplitudes of low frequency fluctuation (ALFF)	- ET patients showed significantly enhanced ALFF in bilateral cerebral cortex, which is related to motor function, including the pre- and post-central gyrus, supplementary motor area and paracentral lobule - the larger ALFF value in the right precentral gyrus is related to a longer duration of tremor
Lenka et al. (2017) ¹⁷⁴	Seed-to-voxel	- decreased connectivity main of primary motor cortex with several cerebellum lobules, while compared to HC ; - the thalamus on both hemispheres had increased connectivity with multiple posterior cerebellar lobules and vermis

Table 2: main findings from previous rs-fMRI studies in ET

1.2.2.2.3. Resting-state fMRI processing (pipeline)

The analysis of fMRI data is not straightforward. This is made complex by a certain number of factors, including: (1) data is subject to artifacts (caused by head movement); (2) there is variability in the data, which includes both between individuals and across time within individuals; (3) the dimensionality is very large, fact that implies a number of challenges, compared to small datasets with whom many scientists are familiar to work with. No matter the clinical context, but especially in patients with movement disorders, which was the case of those examined by the candidate in the frame of the present thesis, a quality control to ensure that artifacts do not corrupt data remains mandatory.

An overview of the general linear model is further detailed. The rs-fMRI preprocessing pipelines (including scrubbing) developed by the candidate in the frame of the present thesis (LTS-5, EPFL/Miplab, Campus Biotech) are further detailed in what follows.

1.2.2.2.4. The general linear model

The goal of an fMRI analysis is to analyze each voxel's time series, so as to see whether the BOLD signal changes or not during time. The tool, which is used to fit and detect this variation, is the general linear model (GLM), where the BOLD time series plays the role of a dependent variable, and the independent ones in the model reflect the expected BOLD stimulus time courses. Two aspects are important: one is to create GLM predictors that will model the BOLD signal as accurately as possible and the second is to model and to account BOLD noise and other sources of variation in the fMRI time series. The GLM is named "general", as it can be used for correlations, one-sample t-test, two-sample t-tests, analysis

of variance (ANOVA), or analysis of covariance (ANCOVA). We briefly present the GLM and its related aspects, such as parameters estimations, hypothesis testing and model setup for these various types of analyses.

The GLM methodology to fMRI data is primarily based on the premise that the hemodynamic response is a linear transformation of the underlying neuronal signal. The simplest model is a simple regression, containing a single independent variable: $Y = \beta_0 + \beta_1 X_1$. Linear regression models the linear relationship between a single dependent variable, Y , and a single independent variable, X , using the equation:

$$Y = \beta X + c + \varepsilon$$

The regression coefficient, β , reflects how much of an effect X has on Y ; ε is the error term and is assumed to be independently, identically, and normally distributed (mean 0 and variance σ^2). Multiple regression is used to determine the effect of a number of independent variables, X_1, X_2, X_3 etc, on a single dependent variable, Y . The different X variables are combined in a linear way and each has its own regression coefficient:

$$Y = \beta_1 X_1 + \beta_2 X_2 + \dots + \beta_L X_L + \varepsilon$$

The β parameters reflect the independent contribution of each independent variable, X , to the value of the dependent variable, Y (i.e. the amount of variance in Y that is accounted for by each X variable after all the other X variables have been accounted for).

This is simply an extension of multiple regression or alternatively multiple regression is just a simple form of the GLM. Multiple regression only looks at one dependent (Y) variable, whereas GLM allows us to analyse several dependent Y variables in a linear combination (i.e. multiple regression is a GLM with only one Y variable). In the GLM the vector Y , of J observations of a single Y variable, becomes a matrix, of J observations of N different Y variables. An fMRI experiment could be modeled with matrix Y of the BOLD signal at N voxels for J scans. However SPM takes a univariate approach, i.e. each voxel is represented by a column vector of J fMRI signal measurements, and it processed through a GLM separately (this is why we then need to correct for multiple comparisons).

The use of the GLM in different methodologies is presented below, with regards to each research project developed in Miplab (Campus Biotech).

Thesis objectives

The main objectives of the present thesis are:

In this thesis, we will explore two major limitations related to the targeting and the understanding of the radiobiology of radiosurgery for tremor. We first explore direct visualization of the Vim based on ultra high field 7 T MRI. The central core of the thesis is related to a better understanding of the radiobiology, using VBM and rs-fMRI analysis.

2.1. To address the limitation of indirect targeting (with E. Najdenovska, PhD)

2.1.1. *indirect landmarks of Vim localization (radiatio prelemniscalis, RAPRL)*

This was initially evaluated on a cohort of 32 patients, treated with left unilateral Vim RS. An extension of this cohort included 200 cases, for which the coordinates of the targeted Vim, as well as those of the RAPRL, have been extracted by the candidate. This former part is a work in progress.

2.1.2. Direct targeting at 7 Tesla. We have explored direct Vim's manual delineation on susceptibility weighted images (SWI); correlation with the quadrilatere of Guiot and other multimodal Vim segmentation methods

A comparison between 4 methods of Vim's definition has been performed: manual delineation on 7T SWI, targeting using the quadrilatere of Guiot (the candidate), 3T diffusion-based segmentation methods of motor nuclei and multi-atlas delineation employing the SWI features (E. Najdenovska).

2.2. Understanding the radiobiology of Vim radiosurgery

2.2.1. Voxel-based morphometry, for whom the statistical approach and respective results are further detailed below in chapter 3.

Two types of methodology have been employed: one was exclusively based on pretherapeutic GMD, attempting to predict the 1-year clinical response; the other considered longitudinal changes in GMD 1 year after Vim RS, as well as their interaction with clinical effect.

2.2.2. Resting-state functional MRI, for whom the statistical approach and respective results are further detailed below in chapter 3.

Three methodological types have been employed: (1) only using pretherapeutic data, attempting to predict the 1-year clinical response (using ICA and seed-to-voxel, further detailed below); (2) using changes in FC and IC between pretherapeutic and 1 year after Vim RS, in interaction with clinical effect (using ICA and seed-to-voxel); (3) discussing dynamic FC, using connectivity activation patterns (CAP).

Addressing the limitations of targeting

Publications related to this particular chapter:

a- Peer-review papers:

a.1. “Imaging of the Ventral Intermediate Thalamic Nucleus at 7T”

(Journal of Scientific Reports, Nature, under review)

E. Najdenovska, C. Tuleasca (equally contributor as first author), J. Jorge, P. Maeder, J. P. Marques, T. Roine, D. Gallichan, J.-Ph. Thiran, M. Levivier and M. Bach Cuadra

a.2. “Towards an automated segmentation of the ventro-intermediate thalamic nucleus”

Proceedings, CLIP workshop on the 20th International Conference on Medical Image Computing and Computer Assesed Intervention (MICCAI), in September 2017;

E. Najdenovska, C. Tuleasca, J. Jorge, P. Maeder, J.-Ph. Thiran, M. Levivier and M. Bach Cuadra; CLIP workshop on the 20th International Conference on Medical Image Computing and Computer Assesed Intervention (MICCAI), in September 2017;

b- Abstracts presented in oral or poster form, as preliminary reports:

b.1. “Gamma Knife radiosurgery of the Vim: segmentation of the thalamus, pilot study with simulation of targetting on 7 Tesla images and preliminary results in 3 consecutive cases” (poster presentation)

C. Tuleasca, E. Najdenovska, J. R. Marques, L. Xin, F. Vingerhoets, J.-Ph. Thiran, M. Bach-Cuadra and M. Levivier; Local MD-PHD retreat, 2013, Ecole Polytechnique Fédérale de Lausanne, Switzerland

b.2. „Ultra-high field (7 Tesla) MRI for Gamma Knife surgery targeting of the ventro-intermediate nucleus: a pilot *in vivo* study” (poster presentation)

C. Tuleasca, E. Najdenovska, L. Xin, J. R. Ferreira Marques, F. Vingerhoets, J.-Ph. Thiran, M. Bach Cuadra and M. Levivier; Joint Annual Meeting of the Swiss Society of Neurosurgery, Neurology and Neuropsychology, juin 2014, Zurich, Suisse;

b.3. “Vim’s anatomical landmarks: indirect targeting versus direct visualization“ (oral presentation)

E. Najdenovska, C. Tuleasca, J. R. Marques, J. Jorge, D. Gallichan, P. Maeder, J.-Ph. Thiran, M. Levivier, M. Bach Cuadra; «13th International Stereotactic Radiosurgery Society Congress», June 2017, Montreux, Switzerland

b.4. „Ultra-high field (7 Tesla) MRI for Gamma Knife surgery targeting of the ventro-intermediate nucleus: a pilot *in vivo* study” (poster presentation)

C. Tuleasca, Elena Najdenovska, Linjing Xin, José Rebelo Ferreira Marques, Francois Vingerhoets, Jean-Philippe Thiran, Meritxell Bach Cuadra and Marc Levivier; Annual meeting of the French Speaking Neurosurgical Society (SNCLF), December 2014, Paris, France

b.5. „Ultra-high field (7 Tesla) MRI for Gamma Knife surgery targeting of the ventro-intermediate nucleus: a pilot *in vivo* study on 5 healthy subjects and 2 patients” (oral presentation)

C. Tuleasca, E. Najdenovska, L. Xin, J. R. Ferreira Marques, F. Vingerhoets, J.-Ph. Thiran, M. Bach Cuadra and M. Levivier; 12-th International Stereotactic Radiosurgery Society Congress (ISRS), June 2015, Yokohama, Japan; Journal of Radiosurgery and SBRT, Volume 3, Supplement 1, page 149

3.1. Indirect landmarks: prelemniscal radiation (unpublished data)

New imaging modalities, such as diffusion tensor imaging (DTI) and colored fractional anisotropy (FA) mapping, enable visualization of the fiber tracts surrounding deep brain structures (e.g. basal ganglia). Thus, they can potentially be used to improve our abilities to accurately locate deep brain targets, including the antero-lateral thalamus, and further its subparts, such as the Vim¹⁸⁰. During the past two decades, new approaches have been developed, to automatically segment thalamic nuclei, based upon DTI¹⁸¹⁻¹⁸³. Magnetic resonance diffusion tractography (also called probabilistic tractography) and colored FA maps can be used to visualize white matter fibers *in vivo* and have many applications in neurosurgery³². Water diffusion within white matter is directionally dependent, which allows the generation of FA anisotropic maps and evaluation of associated movement vectors³². Indeed, FA maps can clearly identify major white matter bundles that are not otherwise readily discernable on the classical T1- and T2- weighted images^{32, 33}. Probabilistic tractography can be used to establish the structural connectivity profile of major thalamic target nuclei (and particularly the motor group, which includes the Vim) prior to functional neurosurgery^{181, 182}. Although some authors claim that the Vim nucleus can be identified with this technique, as part of the dento-rubro-thalamic tract¹⁸⁴, the extensive post-acquisition data processing is not currently compatible with routine Vim RS planning software and these techniques have yet to be validated in the clinic realm, on much larger cohort of patients.

We analyzed the possibility to use the stereotactic position of the radiation prelemniscalis (prelemniscal radiation, RAPRL, Figure 4, Figure 14) on colored FA mapping, and to correlate this position, as distance to the Vim, with safety and efficacy of the procedure. Our purpose was to investigate if these FA mapping can help to locate the Vim nucleus by identifying its borders, particularly the RAPRL, which lies below and behind the nucleus. This research has been based on the preliminary work from the Marseille's group, by Lefranc et al.¹⁸⁰. The main purpose was to find an indirect anatomical landmark, for Vim localization, which can be easily visualized. The RAPRL are located within the widest tract in this region. All the fibers run obliquely in a postero-inferior to antero-superior direction and thus form a funnel. These fibers arise in the mesencephalic reticular nuclei, pass through the substantia nigra to the thalamus (the Vim and ventral oralis anterior and posterior - Voa/Vop nuclei), ascend between the red nucleus, the subthalamic nucleus and the ZI and terminate within the Vop and Vim thalamic nuclei¹⁸⁵.

In an initial cohort of 32 patients, we have extracted the stereotactic coordinates for the RAPRL and the Vim RS isocenter. Posttherapeutic clinical data, including the tremor score on the treated hand, as well as the radiological data (type of response as from the Marseille's

impossible to use a stereotactic frame with this sequence. Thirdly, and as a consequence to the previous point, it is mandatory for us to co-register the FA mapping dataset with a stereotactic MRI dataset (e.g. the stereotactic reference) acquired on the day of Vim RS.

With the current state-of-art, the FA map can only provide additional information, if the quality of image co-registration process has been rigorously verified. Moreover, and as previously stated, it is well known that this type of registration process can reduce the accuracy of target identification. As it is difficult to quantify the extent of this former error, which may differ from one patient to another, the stereotactic localization of this landmark should be cautiously interpreted.

3.2. The Vim through multimodal imaging at 3 and 7 T

In this research project, we aimed at correlating four different modalities for defining the Vim (Figure 15):

- 1- targeting used in common clinical practice, by quadrilatere of Guiot (the candidate)
- 2- direct manual delineation on 7 Tesla susceptibility weighted imaging (the candidate)
- 3- automated diffusion MRI based thalamic subdivision (E.Najdenovska, PhD)
- 4- atlas-based Vim outline (E. Najdenovska, PhD)

The first method is defining the Vim based upon previous electrophysiological recordings¹³⁴, in functional neurosurgery, while the others three are directly using its anatomical structure. The second method is based only upon direct human-eye examination. The third approach is using local diffusion properties, as extracted from DWI. The fourth is based upon atlas-based segmentation tools, in an automated manner.

The primary aim was to be able to pass from indirect, to an direct Vim targeting. The secondary aim was to correlate, for the first time, different ways of defining this nucleus, of crucial importance in surgical targeting for drug-resistant tremor¹⁸⁷.

We further review the main methodological aspects, as well as their benefits and limitations, with the current state-of-art. We provide qualitative and quantitative details, to objectively analyze our results.

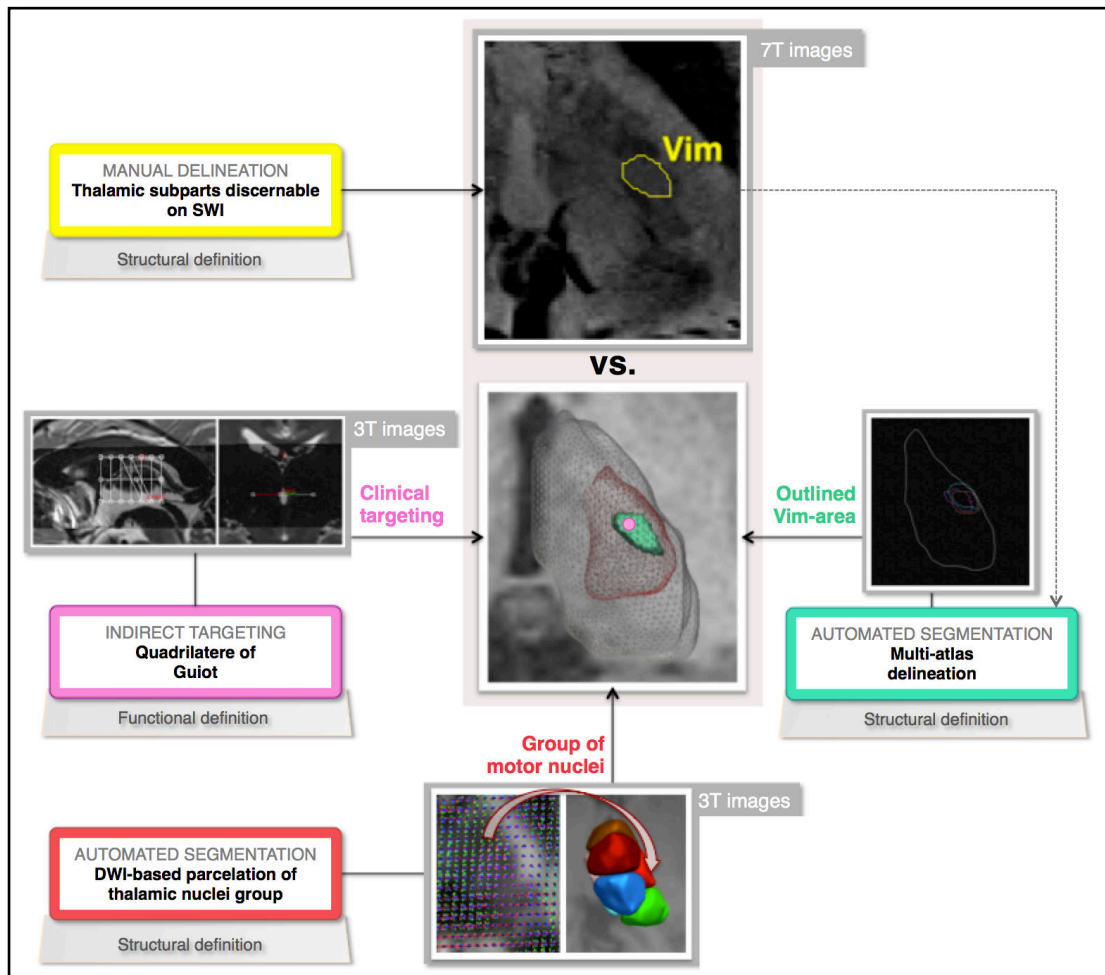


Figure 15: Schematic overview of the methods used to define the Vim in the present thesis¹⁸⁷ (*functional definition refers to its validation in functional neurosurgery)

3.2.1. Materials and methods

Participants

Nine healthy subjects were scanned at both 3 T and 7 T. Five of them were of relatively young age (mean age 25+/-2 years-old, male to female ratio 3:2, further referred as YS1-YS5, respectively). The remaining four were elderly subjects (mean age 67.2+/-9.5 years-old, male to female ratio 3:1, further referred further as ES1-ES4), with no particular brain disease and/or deformation caused by intracranial lesions.

MR imaging

The acquisitions at 3 T (TIM-Trio Siemens scanner, 32-channel head coil) included the standard clinical Vim RS protocol, as we would have done it in a real clinical realm: coronal T2-weighted, T2-weighted Constructive Interference Steady State (CISS)/Fiesta, T1-weighted (T1w, MPRAGE) and diffusion weighted images (DWI), acquired with 72 gradient directions and $b=1000 \text{ s/mm}^2$. At 7 T (68 cm-wide bore MRI system (Siemens Medical

solutions), 32-channel head coil (Nova Medical)) we acquired T1w MP2RAGE¹⁸⁸. For further details please refer to supplementary material.

Common image space

The analyses were acquired in the individual image space (for each subject), using as landmarks the anterior - posterior commissure (AC-PC) plane. For the young subjects, we first transformed the T2w into the AC-PC space, by employing 3D Slicer¹⁸⁹ and manually choosing 30 brain mid-plane points (done by the candidate). The resulting image was then used as a reference for the AC-PC alignment of the remaining sequences. More precisely, for each 3T contrast, with the exception of the DWI, we performed a rigid-body transformation (six degrees of freedom, DOF).

To correct the DWI Echo Planar Imaging (EPI) distortion, we registered the fractional anisotropy map (FA) to the MPRAGE with a non-linear transform using FSL FNIRT^{190, 191} (Analysis Group, FMRIB, Oxford, UK; performed by Elena Najdenovska). Moreover, the observed distortions in the frontal and the parietal cortex of the 7T data, were compensated with a 12-DOF linear transform between both skull-stripped 7T MP2RAGE and 3T MPRAGE. This transform was applied to the SWI rigidly (6-DOF) aligned beforehand to the corresponding MP2RAGE (done by Elena Najdenovska). All registrations¹⁹² were performed with 100000 voxel samples and Mattes Mutual Information as cost function. The outcome quality was assessed by visual inspection of the matching between the ventricles. After being transformed to the AC-PC space, all images were resampled to the T2 CISS spatial resolution (0.4x0.4x0.4 mm³) using linear interpolation.

Since the 3T images of the elderly cases were acquired directly in AC-PC space, the AC-PC transformation was not required in these cases. However, correspondence between the respective images was accordingly to the previously described flowchart for young cohort. After being transformed, all the images were interpolated to the voxel size of 0.5x0.5x0.5, defined by the T1 template in Montreal Neurological Institute (MNI) space¹⁹³. Figure 16 summarizes the registration process.

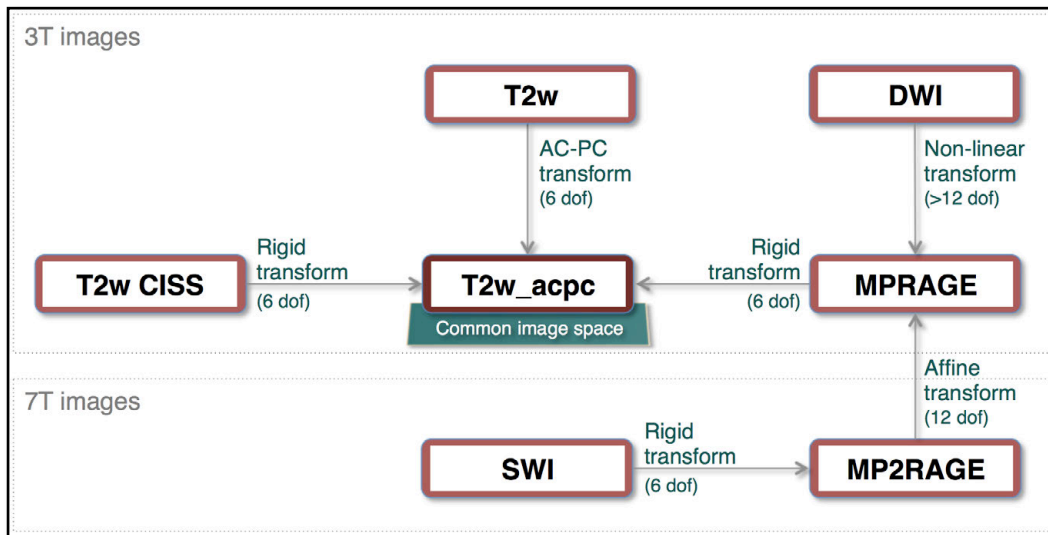


Figure 16: Schematic overview of the registrations applied for transforming into the common image space¹⁸⁷

3.2.2. Methods of Vim identification

3.2.2.1. The quadrilatere of Guiot

The quadrilatere of Guiot^{37, 194} is defined upon anatomical landmarks, including the standard AC-PC line, the height of the thalamus and the third ventricle's lateral wall, all easily recognizable on T2 CISS/Fiesta images and T2 coronal. The final position is at 11 mm from the third ventricle lateral border. The candidate performed this targeting in MITK 3M3 (German Cancer Research Center, Heilderberg, Germany).

As the targeting procedure was done outside of regular treatment-planning GKR software (which is the Leksell Gamma Plan, Elekta Instruments, AB, Sweden), the quadrilatere of Guiot was built independently six times for each subject, bilaterally and blindly, with an aim of assessing the reproducibility.

A sphere with 2 mm radius was drawn around each Guiot point, to simulate the 90 Gy isodose line, which virtually corresponds, if these cases were treated in a real clinical realm by Vim GKR, to the 1-year MR signature after the procedure²¹.

3.2.2.2. Manual Vim delineation on 7T SWI

The manual delineation of the Vim on 7T SWI was primarily based upon the previous observations of Abosch et al.³⁴ and the Schaltenbrand and Wahren atlas¹⁹⁵ also used as reference in the mentioned study.

The thalamic lateral border and the internal capsule are well distinguishable on the 7T SWI. Having as reference the Shaltenbrand's atlas, the Pulvinar as well is directly and easily recognizable in the axial SWI plan (in green, Figure 17, A). Superior to it, in axial plan, is the ventro-caudalis nucleus (Vc) appearing as a dark region (Figure 17 A, bright-violet) and

immediately posterior to a narrower zone, with brighter image intensity, that is considered the Vim (Figure 14 A, yellow). Above it, ventro-oralis (Vo) appears (Figure 17 A, bright-blue) as another dark area, defining the superior border of the Vim. Additionally, the visualization of the medio-dorsal group allows the identification of the mesial Vim border.

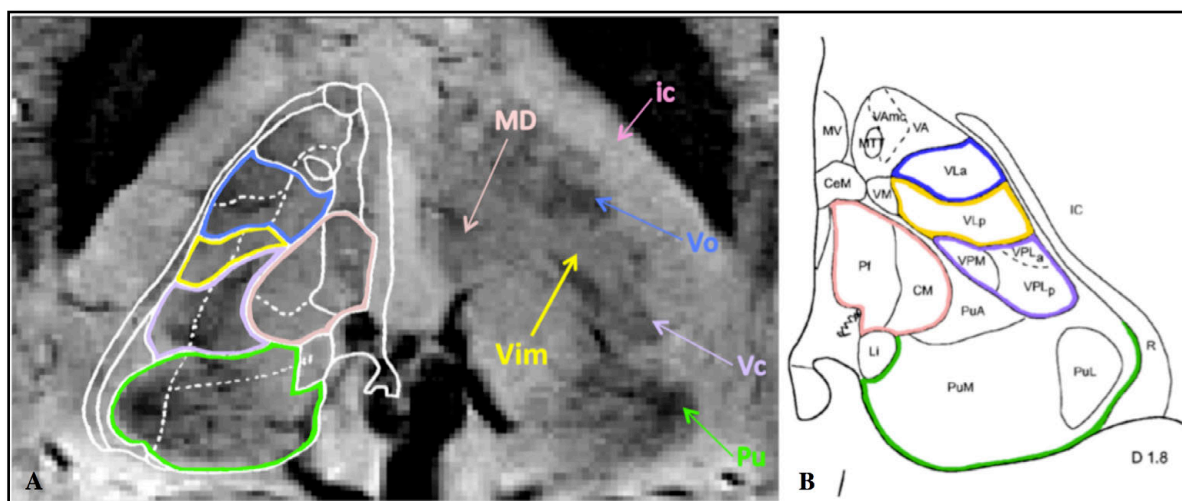


Figure 17: Illustration of the visible structures corresponding to the thalamic area in axial view on the SWI acquired at 7T, based upon the illustration from the pioneering work of Abosch et al.³⁴. In panel A the SWI features are compared with the Schalterbrand atlas (plate 53 Hd +3.5) superimposed on the right thalamus. The arrows and the respective color contours indicate the nuclei: Vim, Pulvinar (Pu), ventro-caudalis (Vc), ventro-oralis (Vo), the medio-dorsal group (MD) and the internal capsule (ic). The shown SWI image is part of the dataset used in this study. Panel B gives a corresponding axial plate of the Morel's atlas where the (same) color (shade) matches appropriate regions of the Shalterbrand's atlas, while keeping the same nomenclature used in each one of them. In fact, considering the Morel's atlas³⁰ nomenclature, Vim is part of the Ventro-Lateral-posterior nuclei, which furthermore, together with ventro-lateral anterior and ventro-posterior nuclei form the VLV cluster¹⁸⁷

3.2.2.3. The automated 3T dMRI-based segmentation

Doctor Elena Najdenovska performed this segmentation, based upon a methodology she developed and which has been already published in 2017³³. Mainly, this approach was to segment the thalamus in 7 thalamic subparts, including the ventro-lateral ventral cluster (VLV; nomenclature from Morel et al.³⁰), which is considered to include the Vim. Additionally, Dr Najdenovska was able to subdivide the VLV in three different subparts, using particular diffusion features.

3.2.2.4. Multi-atlas segmentation

Dr Najdenovska performed this part of the project. Having the manual delineation of the Vim for all the subjects, we used the multiatlas technique for automated segmentation of individual Vim in leave-one-scenario.

3.2.3. Quantitative analysis

The intra-subject reproducibility of the Guiot targeting was estimated by the Euclidian distance between the target points for each individual hemisphere, by taking as reference the

first targeted point.

The volumes of the manual Vim and automated VLV delineation were evaluated using the Dice Coefficient¹⁹⁶, measuring their overlap. An overlap greater than 70% was considered a good match.

3.2.4. Qualitative analysis

The four investigated approaches provide outcomes, which have different sizes. In fact, they range from a simple single point to a group/volume of nuclei.

To better assess their spatial distribution, the VLV, as well as the manually delineated Vim's area, were further subdivided in eight geometrical subregions. More specifically, for each region of interest (e.g. VLV from DWI) or the manually delineated Vim, we calculated the smallest rectangular cuboid containing all non-zero voxels, whose mid-plane isolated the superior from the inferior part, the posterior and the ventral part (Figure 18).

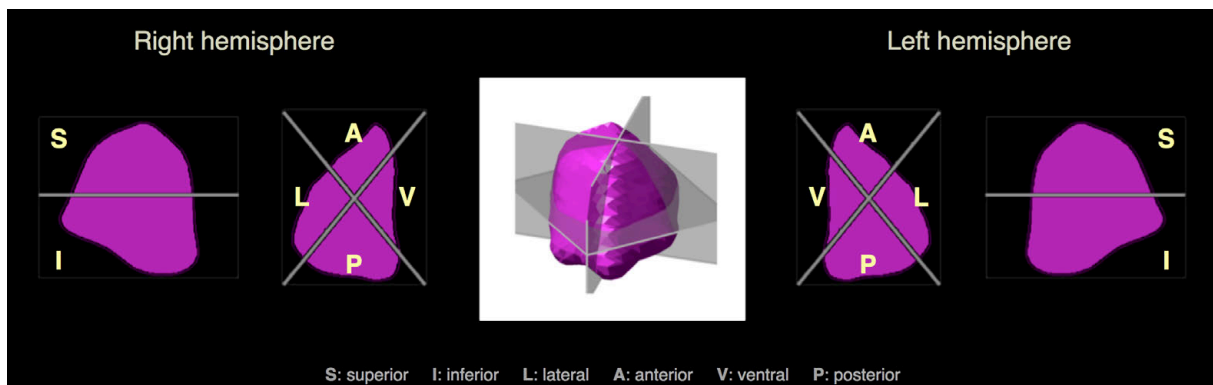


Figure 18: Schematic representation of the ROIs separation in 8 regions, in 2D and 3D view (middle). The labeling of the subparts is done according to the hemispheres to which the ROI belongs¹⁸⁷.

3.2.5. Results

3.2.5.1. The points from the quadrilateres of Guiot

The obtained points from the individual targeting (6 times per side and per subject, as previously stated) using the quadrilateres of Guiot were either overlapping or differing by one voxel, for all nine subjects involved in this study. The maximum intra-subject difference was less than 1.3 mm, confirming the accuracy and reproducibility of the former (see the boxplots for the YS1 to YS5 in Figure 19).

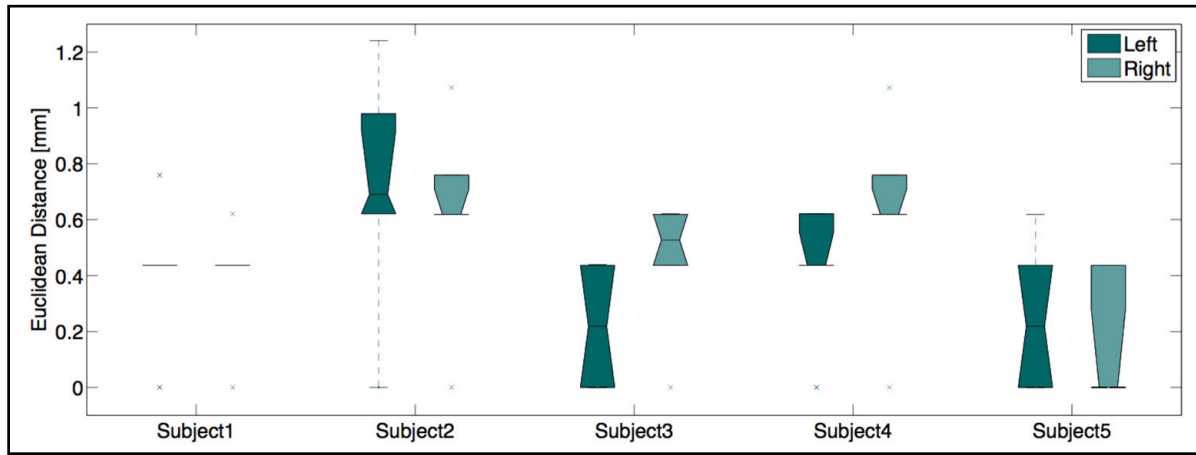


Figure 19: Boxplot showing the difference between the six targeting points obtained by the quadrilatere of Guiot for each subject respectively (in the healthy subjects, YS1 to YS5)¹⁸⁷

3.2.5.2. Manual Vim delineation on 7 T SWI

The Vim was identified and manually delineated in both hemispheres for eight out of nine subjects. In the ninth case, which was a younger subject, only the right Vim area was distinguishable. On the left side, a blood vessel made difficult to discriminate any contrast difference, which could have corresponded to the Vim (Figure 20). Hence, in total, the candidate was able to manually delineate 17 Vim (8 subjects x 2 sides, plus only 1 side for the ninth subject).

The manual delineation was nonetheless challenging and time-consuming. The borders of the Vim were not unquestionably discernable, due either to the lack of image intensity contrast, or the presence of small blood vessels, that sometimes could have been confounded with the surrounding nuclei. Moreover, the image intensity and its contrast variations differed between subjects and different age ranges.

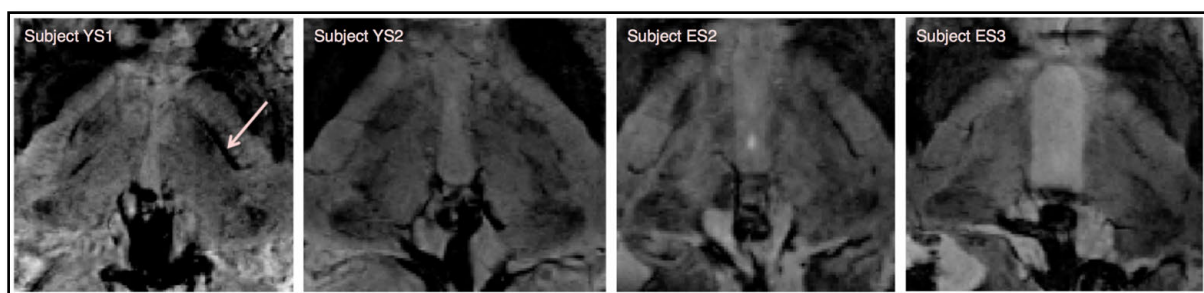


Figure 20: Illustration of the difficulties encountered for the manual delineation of the Vim regarding the image contrast on SWI acquired at 7T and the presence of blood vessels in the targeted area. We can observe that the contrast varies between subjects, but also between the two groups, young (here YS1 and YS2) versus the elderly (ES2 and ES3). The arrow for Subject YS1, illustrates the relatively big blood vessel passing through the left targeted thalamic region that prevented manual discrimination of the Vim. The presence of small vessels surrounding the Vim can be observed in each panel¹⁸⁷

The manually delineated volumes were in the range of 35.5 to 94.5 mm³ and occupying 0.4-1.5% of the total thalamic volume (Table 3).

V o l u m e	Vim								VLV			
	Manual delineation				Multi-atlas segmentation				Diffusion-based outline			
	Left		Right		Left		Right		Left		Right	
	mm ³	normalized	mm ³	normalized	mm ³	normalized	mm ³	normalized	cm ³	normalized	cm ³	normalized
YS1	/ [*]	/ [*]	77.6	1%	/ ^{**}	/ ^{**}	/ ^{**}	/ ^{**}	1.1	15%	1	14%
YS2	76.3	1%	82	1.1%	66.9	0.9%	71.6	1%	1.3	17%	1.3	18%
YS3	83.3	1.5%	82.9	1.2%	28.5	0.5%	44.4	0.6%	1.1	18%	1.1	16%
YS4	82.8	1.1%	73	1.1%	42.4	0.6%	42.4	0.6%	1	14%	0.9	15%
YS5	67.2	1%	78.7	1%	43	0.6%	41.5	0.5%	1.2	19%	1	15%
ES1	93	1.2%	94.5	1.3%	42.7	0.6%	23.7	0.3%	0.9	13%	0.8	13%
ES2	58	0.5%	56.5	0.5%	19.4	0.2%	44.9	0.4%	1.4	14%	1.4	15%
ES3	81.5	0.9%	65.5	0.8%	32.4	0.4%	9.7	0.1%	1.2	15%	1	14%
ES4	71.4	1.1%	69.1	1%	20.2	0.3%	6.1	0.1%	0.7	13%	0.8	13%

Table 3: The calculated volumes of the manually delineated Vim (7 T SWI) and the VLV cluster (DWI). The presence of a blood vessel made impossible the manual delineation of the Subject YS1's right Vim (^{*}) and therefore this subject was not considered in the analysis of multi-atlas segmentation (^{**}).

3.2.5.3. Correlation between the manual delineation and the Guiot's points

The Guiot's points were always inside, or on the border of the manual delineation. Considering the geometrical subdivision, in seven out of nine cases, Guiot's points were in the ventral part of the manual delineation.

3.2.5.4. Comparison with the automated methods

3.2.5.4.1. Automated 3T dMRI-based segmentation

For all nine subjects, the thalamic parcellation showed similar segmentation patterns, as previously reported for a larger cohort of 35 healthy subjects¹⁹⁷. The segmented ventro-lateral ventral (VLV) cluster, which is the outline of interest since it encloses the motor-

related nuclei, with Vim as integrated part¹⁹⁷, represented the expected spatial extent. Its volume ranged between 740 and 1400 mm^3 or 13-19% of the corresponding thalamic volume.

The VLV cluster constantly included the manually delineated Vim outline. In average, the size of the diffusion based segmented VLV was 15 times bigger than the manual one. With respect the spatial localization assessed via the geometrical subdivision (Figure 18), for 16 out of 17 cases the manual Vim outline was found in the inferior VLV, in the last case being around the mid-plane. Furthermore, the manual outline was always next to the lateral VLV border and for 15 cases lied in this cluster anterior/anterior-lateral part. For the remaining two cases, the Vim outline was around the respective in-plane diagonal.

3.2.5.4.2. Multi-atlas segmentation

To ensure an equal contribution from both hemispheres, the subject with no manual outline of the Vim (YS1) was not considered for building the multi-atlas framework. The remaining eight subjects were analyzed. Hence, by applying the leave-one-out (LOO) scenario, seven atlases were used per hemisphere.

The multi-atlas segmentation outlines were fairly comparable to the manual delineation (Figure 21), with the exception of one subject (ES3). For the former, within the right hemisphere, this methodology failed to provide an outline overlapping with the manual delineation. The calculated Dice overlap was 45.1+/-12.9% for the left and 45+/-26.37% for the right hemisphere. The individual Dice coefficients are given in Figure 22 together with the visual representation of the outcome.

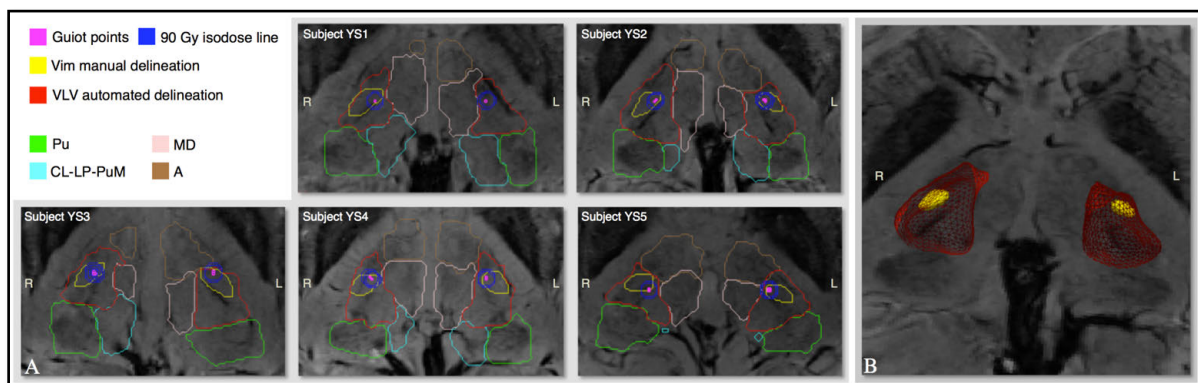


Figure 21: Visual representation of the comparison between the methods. Panel A give the results in axial view of each young subject respectively (YS1-YS5), while panel B shows a 3D view of the Subject YS2's outlined Vim, as well as its localization inside the VLV cluster and within the thalamus. Among the shown findings, the Guiot points are given in magenta, the manual Vim delineation in yellow and the automatically segmented VLV cluster in red. The remaining automatically delineated clusters shown in panel A are: Pulvinar (Pu), medio-dorsal (MD) and the anterior (A) group of nuclei as well as the cluster enclosing the centro-lateral and the lateral posterior nuclei along with the medial part of the Pulvinar (CL-LP-PuM). It can be seen that for all the subjects the Guiot points are always inside and/or on the border of the manual delineation, which furthermore is observed in the anterior-lateral part of the VLV cluster close to its lateral bord¹⁸⁷.

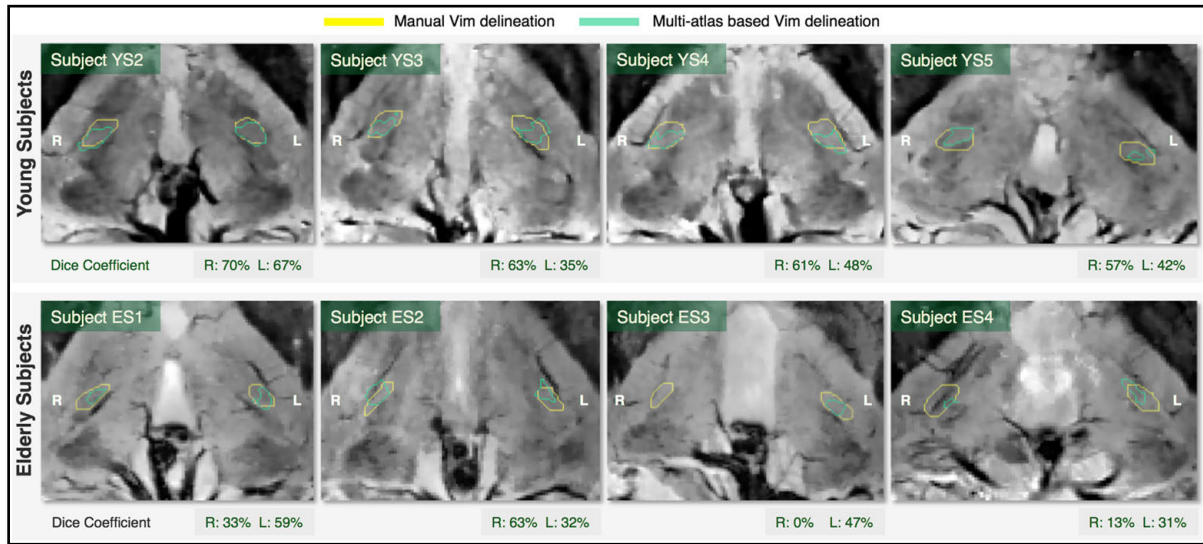


Figure 22: Visual comparison between the manual delineation and the multi-atlas outline of the Vim. The Dice coefficient estimates the overlap between the two outlines.

3.2.6. Discussion

This part of the thesis aimed at improving the targeting. The primary aim was to replace the current indirect methods with direct ones, and to aim for reproducibility and standardization. We compared four different strategies for defining the Vim, a common target in functional neurosurgery for drug-resistant tremor and particularly ET. The neuroimaging protocol analyzed here included only healthy volunteers. Furthermore, we combined two different expertises (medical doctor and engineer), in a multimodal-imaging framework, including both 3 and 7 T images.

We observed that the clinical targeting points, defined by the commonly used in quadrilatere of Guiot in clinical practice are, for 77.8% of the cases, in the ventral part of the Vim's manual delineation 7T SWI. In fact, by representing the aimed region in a functional neurosurgical manner, the Guiot targeting allocates only a point and, in consequence, is limited in providing a full structural discrimination of the Vim. In this context, our findings indicate a confined localization of the clinically aimed points inside a structural outline that should be further investigated in terms of structural and functional connectivity for potentially obtaining advanced target-related insights. Moreover, an extension of this study on larger dataset could possibly lead to a robust prediction of the neurosurgical target inside the Vim borders.

The qualitative inspection also suggested that Vim's manual delineation, 15 times smaller than the size of the VLV, is mainly enclosed, in 88.2% of the studied cases, in the inferior anterior-lateral division of that cluster. Such findings reveal a constrained area, which would most likely correspond to the Vim within a region automatically delineated by computer-assisted image-analysis techniques, which has not been demonstrated previously.

Moreover, it could be further explored in other studies by an automated segmentation of the Vim, based exclusively on individual subject-related data.

The proposed multi-atlas segmentation framework shows promising potential of delineating the Vim area in automated manner. The outcome tends to slightly underestimate what is considered to be the corresponding Vim volume, but considering the size of the investigated structure we could argue that the obtained outline, with the exception of 2 cases (ES3 and ES4 right Vims), is rather acceptable. In terms of overlap, the Dice Coefficient greater than 70% is considered as good match. However, this measure is more sensitive to elongate structures, such as the Vim, rather than the rounded ones and, therefore, it could bias the estimation of the overlap¹⁹⁸.

We assume that the quality of the outcome from the proposed multi-atlas segmentation is closely related to the use of SWI-intensity instead of T1w or T2w lacking in intrathalamic contrast variation. Consequently, when the 7T SWI is available, it could be used as an alternative or as an initialization of a subject-related Vim segmentation, either manual or automated. Nevertheless, we expect an improvement of the presented findings with an extension/ adaptation of the number of employed atlases to its optimum¹⁹⁹. Moreover, all these findings apply, for the moment, only to healthy volunteers, and not to ET patients.

Although our main focus was the Vim, this study also provides validation of the automated dMRI-based clustering as complementary to the directly visualized SWI thalamic nuclei. For example, in SWI, the Pulvinar appears as the most-posterior distinguishable thalamic feature, very dark laterally and brighter next to the ventricles. In agreement with previously reported findings¹⁹⁷, we see that the green Pu-cluster contour delineates mainly the darker nuclei part and, a portion of medial Pulvinar (the brighter part), is enclosed in the CL-LP-PuM cluster. Furthermore, the spatial extent of the MD cluster generally coincides to the equivalent group of nuclei. All these findings support, above all, the spatial distribution of the VLV and thereupon, our outcomes related to this cluster.

Our study has several potential limitations. The first is related to the fact that the protocol was acquired only in healthy volunteers. The measure in which the same findings would be applicable in ET patients remains to be further elucidated by other studies. Moreover, the manual delineation on the 7T SWI data is, however, a time-consuming task, as the Vim borders are not always obvious, mainly because of the presence of blood vessels, a low local image contrasts or contrast variability across subjects, inside the thalamic area. Moreover, there was inconsistency in terms of the contrast variation between the cohorts representing different age scale. Namely, the elderly subjects presented poorer contrast that brought more difficulty in direct visualization of the Vim in those cases. In consequence, we assume having contour erring towards underestimation of the Vim extent. This could also

be deduced from the calculated volumes (Table 3), which are near the lower limits of what is considered the correct range³⁸. Additionally, in the scope of the mentioned contrast-related drawbacks, even the multi-atlas segmentation could be potentially troubled.

Additional SWI analysis indicated that the image intensity contrast could also depend on the head orientation inside the scanner. This could be caused by anisotropic contributions to the local tissue susceptibility. For instance, white matter fibers have significant anisotropic susceptibility²⁰⁰. Depending on the head orientation relative to the static MR field, the local susceptibility-based perturbations of the field may differ, and the resulting effects may thus show significant changes in contrast. Anisotropic voxels may also add different partial volume effects depending on the head orientation. Further improvements regarding these limitations, such as vessel removal or contrast standardization²⁰¹, should be addressed, in order to make the 7T SWI even more powerful and robust tool for Vim discrimination.

Nevertheless, the present study suggests a superiority of the SWI, acquired at 7 T, over the existing MR sequences acquired at 3 T, in terms of more precise characterization of the Vim as an individual structure. Moreover, we propose two new approaches for an automated Vim localization. If 7 T SWI data is available, the multi-atlas segmentation could be employed. However, considering the fact that the number of 7T scanners is limited worldwide, the automated detection of the Vim area inside the 3 T dMRI-based VLV cluster could also be used as an alternative.

Further studies on a larger dataset are needed to confirm the reported findings. Improvements could also enclose multi-atlas segmentation based on 7T SWI only. Additionally, given the potential of the automated dMRI-based segmentation, we assume that combining it with the 7 T SWI information appears as complementary, but both of them based on the individual anatomy, would further lead to an accurate Vim outline. Moreover, including data from ET patients and applying the same protocol will elucidate the concern of its applicability in patients. However, in our experience, problems related to movement make the SWI difficult to interpret. Other sequences, such as the T1 weighted, can be imported in the GammaPlan (Elekta Instruments, AB, Sweden) and might be of further help (Figure 23).

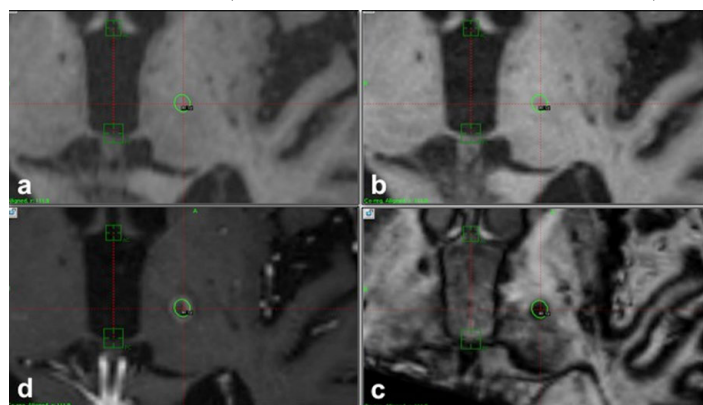


Figure 23: *Superimposed dosimetry with the 90 Gy isodose line (green) to the: (a) therapeutic images, 3T; (b) 3T 3 months follow-up MRI, with no visible change; (c) 7T 3 months follow-up MRI with visible structural changes and (d) 3T 6 months follow-up MRI; please note that 7T already shows a visible MR signature corresponding to the targeted area, while at 3T nothing was yet visible at 3 months*

Understanding the radiobiology of radiosurgery: structural changes

Publications related to this particular chapter:

Peer-review papers:

1. **"Assessing the clinical outcome of Vim radiosurgery with voxel-based morphometry: visual areas are linked with tremor arrest!"**, Acta Neurochirurgica
Constantin Tuleasca, Tatiana Witjas, Elena Najdenovska, Antoine Verger, Nadine Girard, Jerome Champoudry, Jean-Philippe Thiran, Dimitri van de Ville, Meritxell Bach Cuadra, Marc Levivier, Eric Guedj, Jean Régis (DOI 10.1007/s00701-017-3317)
2. **"Right Brodman area 18 predicts tremor arrest after Vim radiosurgery for tremor"**, Acta Neurochirurgica
Constantin Tuleasca, Tatiana Witjas, Dimitri van de Ville, Elena Najdenovska, Antoine Verger, Nadine Girard, Jerome Champoudry, Jean-Philippe Thiran, Meritxell Bach Cuadra, Marc Levivier, Eric Guedj, Jean Régis (DOI 10.1007/s00701-017-3391-x)

4.1. General aspects

We have previously underlined, in the state-of-art of the present thesis (see Chapter 1 of this thesis, *Introduction*) the fact that ET's pathophysiology remains largely undiscovered, despite several hypotheses. Moreover, the intimate mechanism by which tremor stops after Vim RS are also unknown. Additionally, RS is based only upon multimodal neuroimaging analysis for targeting and follow-up evaluation, with no access to anatomopathological analysis, with the sole exception of very few reports^{131, 142, 202}.

In the frame of the present thesis, the candidate employed advanced imaging techniques and complex computational approaches, to try to shed new light on tremor appearance in general and of its further arrest after Vim RS in particular. This included both structural (T1w) and functional (resting-state fMRI) analysis. While a part of the methodology is based on prior hypothesis (e.g. Vim as a core of the “tremor ax”), other aspects don't employ any prior hypothesis and could reveal new and unknown aspects. For uniformity reasons were analyzed only patients with right-dominant ET, while other types of tremor (Parkinsonian, multiple sclerosis etc) were excluded.

4.2. Main hypothesis

Gamma Knife radiosurgery for ET is classically performed with the aim of inducing a small area of necrosis after several months, clearly seen at 12-months follow-up MR²⁰³. In this respect, by the expected radiobiological effect, it mimics a histologically destructive one, compared to the one produced by a RT¹⁰⁷. However, Ohye¹⁴⁰ was the first to suggest that the necrotic lesion solely was not sufficient to produce tremor alleviation. Moreover, he advocated that the magnitude of the lesion induced by Vim GKR was too small to account for the benefic clinical effect. Similarly, the proposed «cocade theory», advocates for 4 distinct zones that might appear after Vim RS, including necrotic, subnecrotic, neuromodulatory and no effect²¹. Additional data from intraoperative electrophysiological studies in DBS after initially successful and further relapse ET have provided new insight. In fact, in a research work done by the candidate¹⁴ which confirmed findings from previously published reports^{140, 204} it is suggested a clear reorganization of the neuronal core inside (accounting for the initial effect) and at the periphery of the necrotic lesion (accounting for a latter effect).

In this respect, our main hypothesis was that structural changes after Vim GKR, in relation with clinical effect, might appear in parts of the previously described “tremor ax”. Our secondary hypothesis was that GMD alterations might be further present in other, remote areas, outside the previous, as part of distant structural and functional reorganization.

4.3. Voxel-based morphometry analysis

4.3.1. Relationship between clinical improvement and GMD changes between pretherapeutic and 1 year after Vim GKR state⁷²

4.3.1.1. Methodological aspects

Group separation

It has been previously advocated that medication diminishes TSTH by approximately 50%²⁰⁵ in around 50% of cases. In this sense, to consider Vim GKR at least as effective as medication, clinical responders (R) were considered those with at least 50% amelioration of TSTH 1 year after the procedure, to account for the delayed clinical effect¹⁵.

Patient population

Thirty-eight cases were analyzed. All benefitted from left unilateral Vim GKR for right dominant tremor.

Thirty-one (81.6%) patients were R (>50% 1-year TSTH improvement) and 7 (18.4%) NR (<=50% 1-year TSTH improvement).

Mean overall improvement in TSTH was 62.6% (standard deviation 32.3; range 0-100%) and in the R subgroup was 75.2%. No difference in clinical characteristics was found between R and NR (age, gender, tremor severity before Vim GKR; $p>0.05$). No side effect was found 1 year after Vim RS.

Statistical analysis

The between groups SPM (T) GMD maps were obtained using an analysis of variance (ANOVA) full factorial model, at a height threshold (voxel-level significance) of $p<0.05$, corrected for multiple comparisons for the cluster (FWE, family-wise error method). Secondly, if no change was initially found using FWE correction, with a less constraint voxel-threshold of $p<0.005$, only corrected for the cluster volume to avoid type II errors as recommended²⁰⁶. Age, gender and the type of tremor were used as nuisance variables. Was evaluated the interaction between clinical response and time, mainly between R versus non-responders (NR) patients, with the different time frame (baseline versus 1 year after Vim RS), so as to identify the eventual structural changes in GMD. The primary aim was to find differences between groups (R versus NR) in interaction with the time point (before and after Vim RS).

The SPM analysis was done by medical staff (the candidate, Eric Guedj-Nuclear Medicine from Marseille) that was not involved in the indication for treatment, the RS

procedure or follow-up evaluation. Gray matter density was further extracted from statistically significant regions. For correlation between GMD and TSTH improvement, STATA version 11 (STATA Corp LLC, College Stations, TX, USA) was used, and p values evaluated with Spearman correlation coefficient.

4.3.1.2. Results: changes in GMD between R and NR, during time

Changes in GMD between R and NR with time showed left temporal pole (Brodmann area, BA 38; cluster 1), and a larger cluster [kc= 135 (left occipital; cluster 2) > kc=124 (left temporal), indicating the number of voxels in each cluster; Figure 24] within the left occipital area ($p_{unc}=0.04$ for the first cluster, $p_{unc}=0.03$ for the second cluster). The former included, beside the left BA 19, the V4, V5, and parahippocampal place area (PPA)⁷².

Interestingly, GMD was lower at baseline in the NR group for both regions and at 1 year had a median value similar to the R groups (which presented a slight decrease in GMD)⁷².

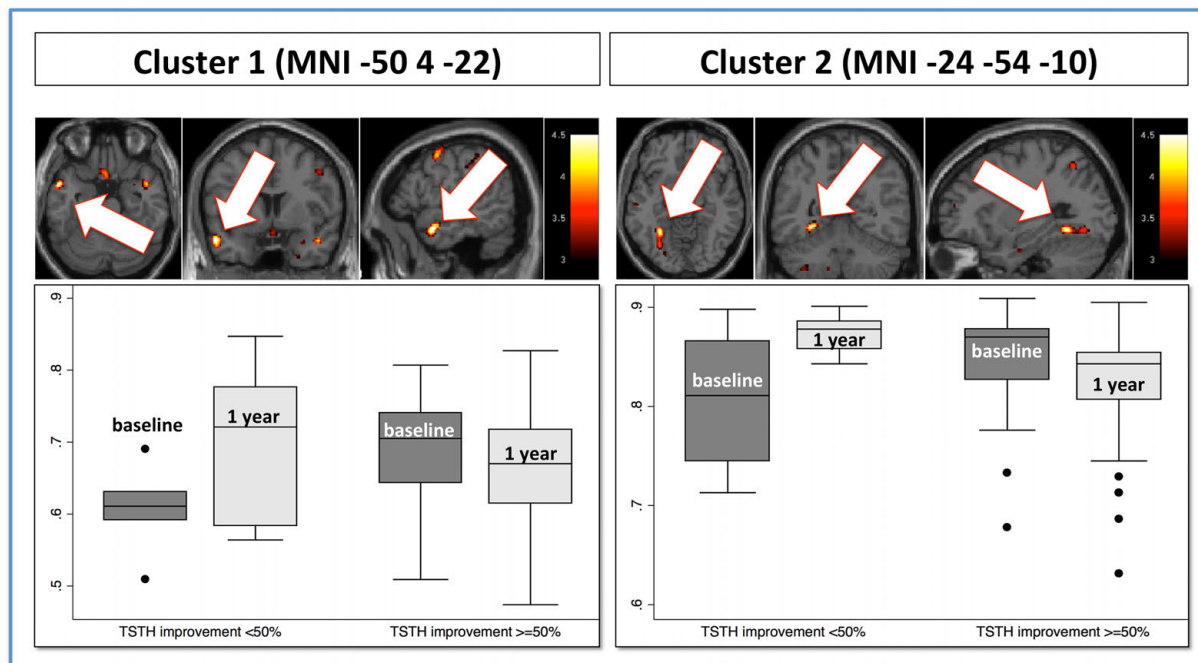


Figure 24: global overview of GMD at baseline and 1 year for left temporal pole and visual association area, depending on clinical response ($\leq 50\%$ TSTH improvement, versus $> 50\%$ TSTH improvement; it is of interest that for both clusters (temporal and occipital), for a TSTH improvement $\leq 50\%$, the baseline values are lower as compared with the ones for TSTH improvement $> 50\%$; at 1 year, the NR patients achieve a median value comparable to that of R at baseline, while the former remain stable;

Furthermore, higher GMD decrease between 1 year and baseline correlated with better TSTH improvement (Spearman $\rho = 0.01$; figure 25, left and right).

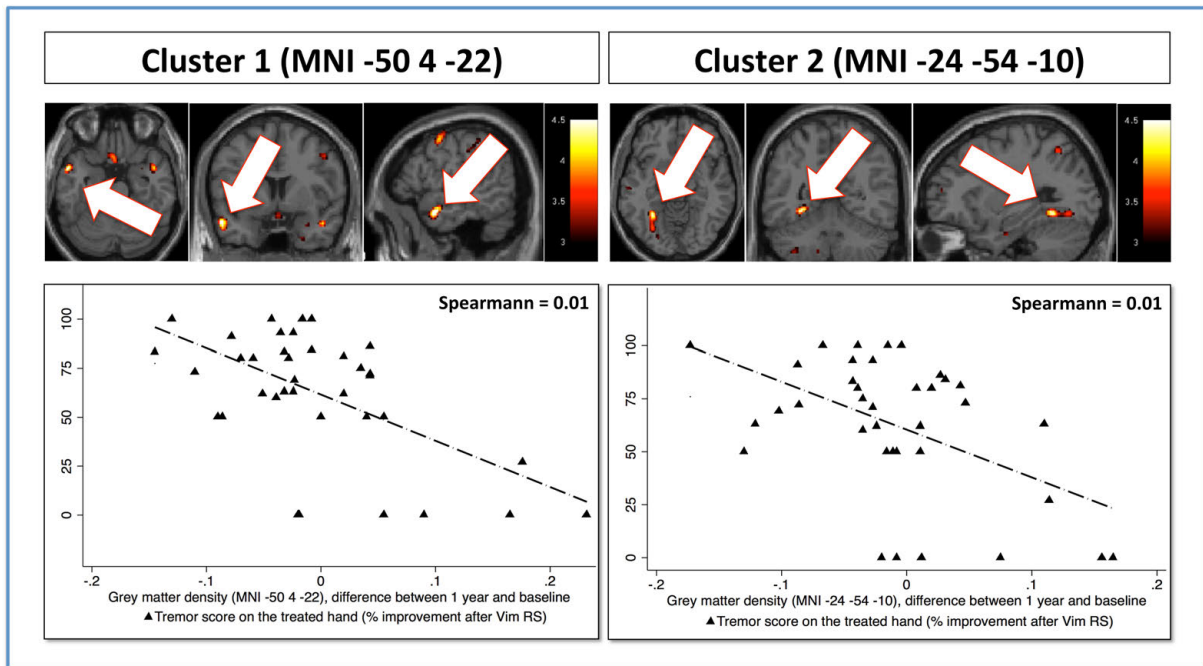


Figure 25: correlations between TSTH improvement and differences in GMD (Spearman= 0.01 for both clusters); left- temporal cluster, right-occipital cluster

For cluster 1 (left temporal pole), higher baseline GMD predicted better improvement (Spearman= 0.004; Figure 25, left). The GMD increase at 1 year after Vim GKR was fairly similar for both clusters in NR, while it tended to zero in R (figure 26, right).

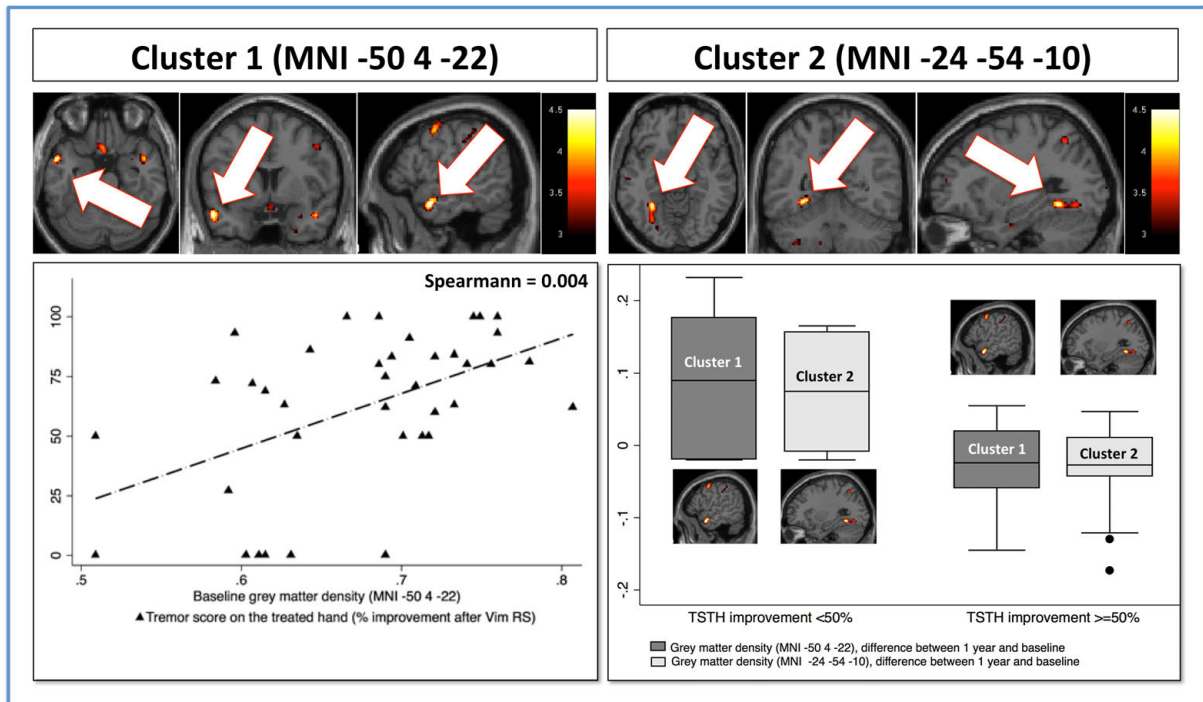


Figure 26: left, correlation between pretherapeutic GMD (left temporal cluster) and 1 year TSTH improvement (Spearman= 0.004); right, illustration of GMD increase (for the NR) and respectively no change (for R), as structural differences between R and NR during time, before and after Vim GKR, presented by clusters (1=left temporal and 2=left occipital, with a sagittal illustration for each one of them)

4.3.1.3. Summary of findings and anatomical relevance

In this first VBM research project, we investigated GMD changes one year after Vim GKR, in relationship with clinical effect. To the best of our knowledge, this was the first analysis of this type. We reported changes in GMD, correlated with clinical effect, between R and NR within left temporal pole (BA 38) and a larger cluster including left occipital lobe (BA 19, V4, V5, and parahippocampal place area), as statistically significant⁷².

The involvement of left temporal pole and occipital, BA 19 together with the PPA is a very interesting and novel finding, suggesting a distant effect of Vim RS. This distant effect was part of the study hypothesis and was confirmed by our result. Left temporal pole is mainly involved in visual (« what and where » visual pathways distinction) and emotional (visual processing of emotional images, emotional attachment) functions, processing phonological properties of written words, sign language or complex auditory processing²⁰⁷. The visual cluster actually extends beyond the BA 19, and includes parts of V4 and V5 and the PPA (posterior subdivision). Visual area V4 is part of extrastriate visual cortex²⁰⁸ and is considered involved in orientation, spatial frequency and color, but also long-term plasticity or stimulus salience. Interestingly, is gated by signals coming from the frontal-eye-fields (FEF)²⁰⁹. This brief overview of the anatomical relevance would be of special interest in patients with ET: in a crowded visual scene, all factors that could help distinguishing the target include color, shape and eye movements are of importance. Moreover, an important role of the PPA is the locomotor monitoring towards local and distant environment.

The role of visual association areas was described for the first time as statistically significant and thus relevant in tremor improvement after Vim RS. We postulated that how the “tremor network” (cerebello-thalamo-cortical pacemaker) modulates these structural changes in remote areas remains unknown. The anatomical connections between the primary motor cortex and visual areas might be of relevance, as previously advocated by other authors²¹⁰, for sensory guidance of movements (e.g. eye-hand coordination).

We advocated that our findings might prompt towards the necessity to recruit in the targeting specific visuomotor networks.

4.3.2. Correlation between pretherapeutic GMD and 1-year tremor improvement after Vim GKR²¹¹

4.3.2.1. Methodological aspects

Patient population

Were analyzed 52 patients (male to female ration: 30:22; mean age 71.6 years, range

49-82, standard deviation 6.9). All benefitted from left unilateral Vim GKR for right dominant tremor.

Statistical analysis

Statistical Parametric Mapping was employed to create a flexible Anova factorial model. Exclusively, pretherapeutic T1w imaging were used, and TSTH improvement was added as a covariate, using the corresponding continuous values, per subject, with the corresponding GMD maps, individually. The aim was to depict a pretherapeutic anatomical cluster, which correlates best with tremor arrest, 1 year after Vim GKR. The uncorrected p value at cluster level was set at ≤ 0.05 and for the peak level < 0.001 .

The SPM analysis was done by medical staff (the candidate, Dimitri Van de Ville-Miplab, Campus Biotech, Eric Guedj- Nuclear Medicine, Marseille) not involved in treatment indication, Vim GKR procedure or follow-up evaluation. Grey matter density was further extracted from statistically significant regions. For correlation between GMD and TSTH improvement, STATA version 11 (STATA Corp LLC, College Stations, TX, USA) was used, and p values evaluated with Spearman correlation coefficient.

4.3.2.2. Results: right visual association area (Brodmann area 18, V2)

Mean 1-year TSTH overall improvement was 67.8% (range 0-100%, standard deviation 32.9). No side effect was encountered. The vast majority of patients presented a left thalamic “cocade” MR signature on follow-up MRI, which is classically considered associated with the clinical response in Marseille’s experience^{14, 15}. Nevertheless, four patients, with severe pretherapeutic tremor, were considered clinical non-responders but had a visible thalamic lesion on follow-up MRI, while eight patients were considered clinical responders and had a smaller lesion on follow-up MRI.

The only statistically significant cluster was right BA 18 (visual association area V2; MNI 12, -74, -4; $p_{\text{uncor}}=0.05$, $K_c=71$; figure 27²¹¹). Higher pretherapeutic GMD correlated with better TSTH improvement (Spearman= 0.002; figure 27).

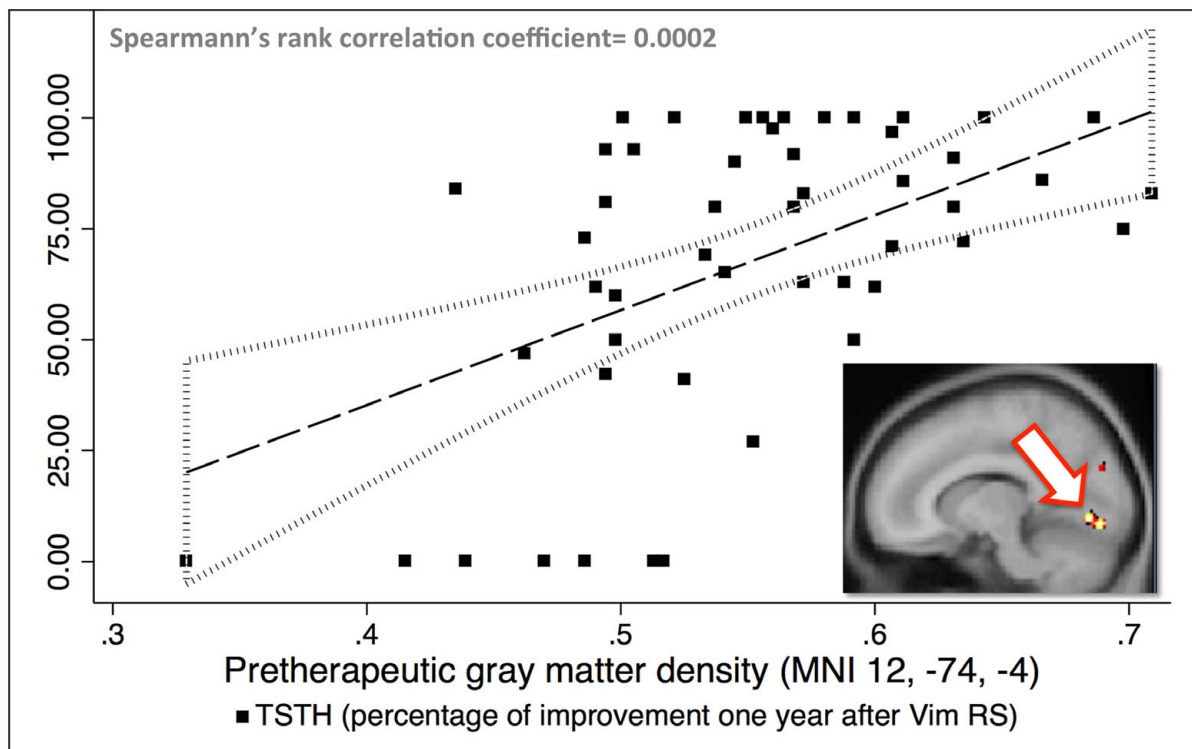


Figure 27: higher pretherapeutic GMD predicts better 1-year TSTH improvement

4.3.2.3. Summary of findings and anatomical relevance

We report higher pretherapeutic GMD within right Brodmann area 18 statistically correlated with better 1-year TSTH improvement after Vim GKR for ET.

Visual association area V2, part of the prestriate cortex, is the second major area of the visual cortex. Most of the neurons are regulated to simple visual features such as orientation, spatial frequency, size, color and shape. This region receives connections from the V1 and sends strong connections to the V3, V4 and V5 areas. It is mainly involved in visuo-spatial information processing²¹². Other roles include detection of light intensity, detection of patterns, discrimination of finger gestures or orientation-selective attention²¹³. In fact, according to some functional studies, it participates additionally in visual priming and visual attention²¹⁴.

4.3.3. Preliminary hypothesis with regard to the present VBM studies

It has been beforehand conjectured that visual areas must be linked to the motor ones, as a need for sensory guidance of movement of hand and fingers²¹⁰, and further in motor regulation. This aspect, of sensory guidance of movements, would be of crucial importance in the case of our patients. Several hypothesis would explain a connection between visual and motor areas: one would be a direct visual input to motor areas (by caudate nucleus and claustrum), a second a modulation by the corpus callosum (mediating tasks in which the

visual cortex on one part of the body is linked to the contralateral motor cortex), and a third that cerebellum might play the essential role of calibrating the relationship between visual and somatosensory/motor information²¹⁰.

In our opinion, these findings^{72, 211} should rather be seen as complementary, not exclusive. Both VBM research projects point out towards the involvement of the visual association areas in tremor arrest after Vim GKR. Furthermore and together, they show that lower baseline GMD in these visual areas (independently if right or left) and in the left temporal pole, was associated with lower 1-year TSTH improvement. Some other additional aspects should be taken into account, due to their relevance. Firstly, it is known that several visual functions (e.g. detection of light intensity, feature extraction or detection of patterns etc) simultaneously activate both BA 18 and 19, which are in close anatomical location, while being integrated part of a common brain network. Secondly, with regards to the visual perception, it is now well acknowledged that it is not carried out in a unique area, but involves many other different parts of the cerebral cortex^{215, 216}, receiving primary input from V1. Typically, the corresponding processing of different information streams continues beyond V1. Many outputs go to V2 (e.g. BA 18), relate to motion analysis and this information is further process in V3 (e.g. BA 19) and then V5, the medial temporal (MT) cortex (part of the PPE) and medial superior temporal (MST) cortex. Thirdly, with regard to functions related to visual association cortex, electrophysiology data suggest sensitivity to motion-delineated forms²¹⁷ and its role as a differentiation point between the '*what*' and '*where*' visual pathways. Additional involvement is in visuospatial information processing, horizontal saccadic eye movements, orientation-selective attention and tracking visual motion patterns²¹⁵. These functions involve both hemispheres and do not limit to a certain unilateral and individual area (no matter if V2 or V3, V4 etc). Fourthly, from methodological point of view, as previously detailed, the research questions were different. Lastly, the cerebellum might play the crucial role of adjusting the link between visual and somatosensory/motor information²¹⁰, as “calibrator”, which might be of special interest in ET.

4.3.4. Strengths of both VBM projects

Our research questions were not conducted to support any of the existing physiopathological theories. Thus, our findings might shed new light on tremor generation and further tremor arrest after Vim GKR. We could consider ET as a family of diseases, rather than a uniform entity⁵⁰. In this sense, we might find adaptive structural MR changes appear during disease course and, depending on these changes, the “reset” of the “tremor network” might be either easier or more difficult after Vim GKR. With regard to this, some of the patients, depending on their phenotype, might develop structural MRI changes making them more “sensitive” or “resistant” to Vim RS, as a trait of ET subclinical phenotype.

Other advantages of the VBM analysis are related to an unbiased and objective procedure, fully automated, not based on regions of interest and which is more exploratory. Furthermore, it depicts differences and/or changes at a global and local scale.

4.3.5. Limitations

The limitations of our study are mainly related to the absence of a blinded neurological examination and those of the VBM method (preprocessing steps, statistical challenges etc). With regard to the former, VBM can be very sensitive to various artifacts, including brain misalignment (with eventual spurious results), misclassification of tissue structures, differences in folding patterns and in cortical thickness¹⁵⁹. All these processing steps could confound the statistical analysis. Moreover, the interpretation of GMD changes could become challenging in small structures, such as components of the basal ganglia. Although our findings have anatomical significance, they would still ideally need to be validated by a neuropathological confirmation one day. Furthermore, VBM was not initially aimed for subcortical structures, and the complicated anatomy of some specific regions may obstruct the automatic processing of this method. With regard to the studied population, in the first project, only 7 (18.4%) of the patients were non-responders. This sample size is rather limited and also imbalanced as distribution between the R and NR. In this sense, our findings should be replicated in a separate and larger cohort, including one containing more NR. There was no randomization, which could allow the direct comparison with a control population of non-treated ET patients.

Understanding the radiobiology of radiosurgery: resting-state functional MRI changes

Publications related to this particular chapter:

a- Peer-review papers:

a.1. "Pretherapeutic functional neuroimaging predicts tremor arrest after thalamotomy", *Acta Neurologica Scandinavica*- one of our illustrations gave the cover page
Constantin Tuleasca, Elena Najdenovska, Jean Régis, Tatiana Witjas, Nadine Girard, Jerome Champoudry, Jean-Philippe Thiran, Meritxell Bach Cuadra, Marc Levivier, Dimitri van de Ville (DOI 10.1111/ane.12891)

a.2. "Clinical response to Vim's thalamic stereotactic radiosurgery for essential tremor is associated with distinctive functional connectivity patterns", *Acta Neurochirurgica*- one of our illustrations gave the cover page

Constantin Tuleasca, Elena Najdenovska, Jean Régis, Tatiana Witjas, Nadine Girard, Jerome Champoudry, Jean-Philippe Thiran, Meritxell Bach Cuadra, Marc Levivier, Dimitri van de Ville (DOI 10.1007/s00701-017-3456-x)

a.3. "Pretherapeutic functional imaging allows prediction of head tremor arrest after thalamotomy for essential tremor: the role of altered interconnectivity between thalamolimbic and supplementary motor circuits", *World Neurosurgery*

Constantin Tuleasca, Jean Régis, Elena Najdenovska, Tatiana Witjas, Nadine Girard, Jerome Champoudry, Jean-Philippe Thiran, Meritxell Bach Cuadra, Marc Levivier, Dimitri van de Ville (DOI 10.1016/j.wneu.2018.01.063)

a.4. "Ventral-lateral motor thalamus abnormal connectivity in essential tremor before and after thalamotomy", *World Neurosurgery*

Constantin Tuleasca, Elena Najdenovska, Jean Régis, Tatiana Witjas, Nadine Girard, Jerome Champoudry, Faouzi Mohamed, Jean-Philippe Thiran, Meritxell Bach Cuadra, Marc Levivier, Dimitri Van de Ville (DOI 10.1016/j.wneu.2018.02.055)

a.5. "Visually-sensitive networks in essential tremor: evidence from structural and functional imaging", *Brain*

Constantin Tuleasca, Jean Régis, Elena Najdenovska, Tatiana Witjas, Nadine Girard, Jean-Philippe Thiran, Meritxell Bach Cuadra, Marc Levivier, Dimitri van de Ville (DOI 10.1093/brain/awy094)

a.6. "Pretherapeutic motor thalamus resting-state functional connectivity with visual areas predicts tremor arrest after thalamotomy for essential tremor: tracing the cerebello-thalamo-visuo-motor network",

World Neurosurgery (accepted for publication, in press)

Constantin Tuleasca, Jean Régis, Elena Najdenovska, Tatiana Witjas, Nadine Girard, Jean-Philippe Thiran, Meritxell Bach Cuadra, Marc Levivier, Dimitri van de Ville

b- Abstracts presented in oral or poster form, as preliminary reports:

b.1. "Functional connectivity of the human thalamus in essential tremor before Gamma Knife thalamotomy: a seed-based resting-state fMRI study" (poster presentation)

Constantin Tuleasca and Elena Najdenovska, Nadine Girard, Alessandra Griffa, Jerome Champoudry, Antoine Dorenlot, Romain Carron, Tatiana Witjas, Jean-Philippe Thiran, Jean Régis, Meritxell Bach-Cuadra, Marc Levivier; MD-PHD local Retreat, Ecole Polytechnique Federale de Lausanne (EPFL); October 2015

b.2. "Resting-state fMRI reveals tremor network alterations in Parkinson's disease versus essential tremor"(poster presentation)

Constantin Tuleasca, Elena Najdenovska, Alessandra Griffa, Nadine Girard, Jerome Champoudry, Tatiana Witjas, Jean Régis, Jean-Philippe Thiran, Meritxell Bach Cuadra, Marc Levivier, Dimitri Van de Ville; Joint Annual Meeting, Swiss Society of Neurosurgery and Swiss Society of Neuroradiology, June 2017, Bern, Switzerland

b.3. “Visual association, motor and attention networks are involved in recovery of drug-naïve essential tremor patients after stereotactic radiosurgical thalamotomy: a resting-state fMRI study” (poster presentation)

Constantin Tuleasca, Elena Najdenovska, Jean Régis, Tatiana Witjas, Nadine Girard, Jérôme Champoudry, Mohamed Faouzi, Jean-Philippe Thiran, Meritxell Bach Cuadra, Marc Levivier and Dimitri Van De Ville ; Lausanne MD-PHD retreat, Lausanne, Switzerland, November 2017

b.4. “Visual association, motor and attention networks are involved in recovery of drug-naïve essential tremor patients after stereotactic radiosurgical thalamotomy: a resting-state fMRI study” (poster presentation)

Constantin Tuleasca, Elena Najdenovska, Jean Régis, Tatiana Witjas, Nadine Girard, Jérôme Champoudry, Mohamed Faouzi, Jean-Philippe Thiran, Meritxell Bach Cuadra, Marc Levivier and Dimitri Van De Ville ; Alpine Brain Meeting, Champéry, Switzerland

b.5. “Implication of visual, motor and salience networks from resting-state fMRI in recovery of drug-naïve essential tremor patients after stereotactic radiosurgical thalamotomy” (présentation orale)

Constantin Tuleasca, Elena Najdenovska, Jean Régis, Tatiana Witjas, Nadine Girard, Jérôme Champoudry, Mohamed Faouzi, Jean-Philippe Thiran, Meritxell Bach Cuadra, Marc Levivier, Dimitri Van de Ville; Leksell Gamma Knife Society Meeting, March 2018, Dubai, United Arab Emirates

b.6. “The role of 1-year MR signature after stereotactic radiosurgical thalamotomy for essential tremor: functional reorganization of dorsal attention and salience networks” (présentation orale)

Constantin Tuleasca, Elena Najdenovska, Jean Régis, Tatiana Witjas, Nadine Girard, Jérôme Champoudry, Mohamed Faouzi, Jean-Philippe Thiran, Meritxell Bach Cuadra, Marc Levivier, Dimitri Van de Ville; Leksell Gamma Knife Society Meeting, March 2018, Dubai, United Arab Emirates

b.7. “Pretherapeutic functional connectivity of ventro-lateral thalamus with visual networks predicts tremor arrest after stereotactic radiosurgical thalamotomy for essential tremor: a resting-state fMRI study” (présentation orale)

Constantin Tuleasca, Elena Najdenovska, Jean Régis, Tatiana Witjas, Nadine Girard, Jérôme Champoudry, Mohamed Faouzi, Jean-Philippe Thiran, Meritxell Bach Cuadra, Marc Levivier, Dimitri Van de Ville; Leksell Gamma Knife Society Meeting, March 2018, Dubai, United Arab Emirates

b.8. “Higher MR signature volumes 1 year after stereotactic radiosurgical thalamotomy are associated with a particular patient’s functional profile: a resting-state fMRI study” (oral presentation)

Constantin Tuleasca, Elena Najdenovska, Jean Régis, Tatiana Witjas, Nadine Girard, Jérôme Champoudry, Mohamed Faouzi, Jean-Philippe Thiran, Meritxell Bach Cuadra, Marc Levivier, Dimitri Van de Ville; Leksell Gamma Knife Society Meeting, March 2018, Dubai, United Arab Emirates

b.9. “Pretherapeutic functional neuroimaging predicts tremor arrest after thalamotomy for essential tremor” (oral presentation)

Constantin Tuleasca, Elena Najdenovska, Jean Régis, Tatiana Witjas, Nadine Girard, Jérôme Champoudry, Mohamed Faouzi, Jean-Philippe Thiran, Meritxell Bach Cuadra, Marc Levivier, Dimitri Van de Ville; Swiss Congress of Radiology, May 2018, Lausanne, Switzerland

5.1. Important methodological aspects: general preprocessing and scrubbing

The general principal of BOLD signal and rs-fMRI analysis, including the GLM, have been previously detailed in the introduction section. The preprocessing and statistical aspects, as well as the different research projects, are further described here.

With the state-of-art of the current literature, two common types of preprocessing pipelines may be used. We developed both of them in the EPFL-LTS 5 in the current project. They are tightly connected with the use of further particular software suites for fMRI statistical analysis. Since motion is an important potential confounding factor in these clinical populations, we first computed Power's framewise displacement index for each time point²¹⁸. When it exceeded 0.5mm, the corresponding frame was "scrubbed" along with one preceding and two following ones (for a total of 5 for one time-point exceeding the upper limit allowed). Only the remaining frames were further considered. One preprocessing pipeline mainly the FSL/AFNI® packages and further on the REST® software²¹⁹. It includes: (1) image reconstruction (IRM), (2) transformation of DICOM format to Nifti, (3) mcflirt function with selection of the middle fMRI image for further registration, (4) head motion correction, (5) signal stabilization, (6) registration of the T1 to fMRI, (7) spatial smoothing, (8) temporal band pass filtering and detrend, (9) extraction of the regressors (white matter and cerebro-spinal fluid), (10) the extraction of a brain mask in whom the connectivity analysis will be done, (11) statistical analysis (seed-based method) in REST®, (12) normalization. The second preprocessing pipeline has been implemented in SPM® and is further used for independent-component analysis, using GIFT®. It includes: (1) image registration (all fMRI to the first time point, 6 degrees of freedom), (2) image registration of fMRI to T1, (3) normalization i.e. registration: T1 to MNI (12 degrees of freedom), voxel size becomes 2 mm³ and (4) smoothing (FWHM= 6 mm). We propose a brief overview of the main preprocessing steps, in Figure 28.

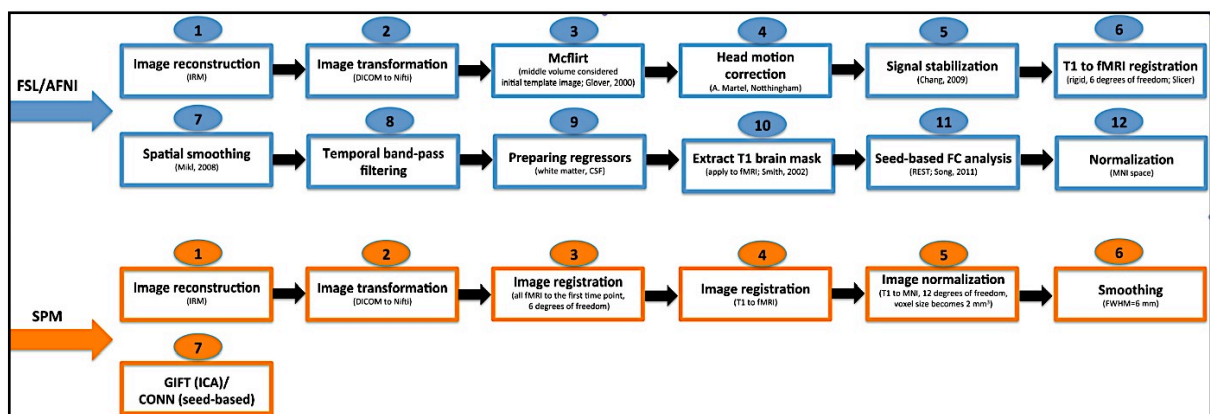


Figure 28: two pre-processing pipelines developed in LTS-5, Swiss Federal Institute of Technology

Variable	Mean	Standard deviation	Minimum	Maximum
Age (y)	70.1	9.8	49	82
Duration of symptoms (y)	38	19.5	6	70
ADL baseline	29.1	12	13	49
ADL (% improvement)	82.9	27.3	0	100
Right total tremor amplitude (TSTH)	18.6	5.5	8	30
TSTH* (% improvement)	67.3	28.2	13.3	100
Head tremor score baseline (normalized)	-0.3	0.8	-1.2	0.8
Head tremor score (% improvement, normalized)	1.3	0.04	1.2	1.4
Quest baseline	46	15.1	29	80
Quest (% improvement)	24	16.1	2	47
Time to improvement (months)	3.3	2.7	0.2	10

Table 4: Basic demographic data

5.2. Patient population

We prospectively included 17 consecutive patients (right-sided tremor, drug-resistant) treated only with left unilateral Vim GKR in Marseille, France, between September 2014 and August 2015^{71, 220-223}. This study received approval (CHU Timone, CPPRB1) from the Ethical Committee of the Marseille University Hospital. Written informed consent was obtained from all patients. All cases were referred by a movement disorders neurologist (TW).

Baseline tremor (by TW) and neuroimaging assessment (on a single 3 T MR machine, Siemens Skyra, Munich, Germany, T1 and rs-fMRI, n=17) was performed. The vast majority of patients didn't have medication anymore, usually for inefficacy reasons. However, the clinical evaluation was done under the pharmacological therapy (if one had such in a minority of situations), while the scanning in the drug-naïve state. Same protocol was repeated one year after Vim RS (n=17). The mean age was 70.1 years (range 49-82). The mean duration of symptoms was 38 years (range 6-70) (table 4). The mean time to tremor improvement in the present series was 3.32 months [standard deviation (std) 2.7, range 0.2-10].

5.3. Radiological answer: MR signature volume 1 year after Vim GKR

Mean MR signature volume 1 year after Vim GKR was 125 mm³ (standard deviation 162, 2-600 mm³). This volume was drawn individually on T1 Gadolinium-injected MR, 1 year after Vim GKR, considered definitive radiological answer in our experience²²⁴. To ensure volume calculation accuracy, each patient MR was imported in LGP. This was co-registered with therapeutic images. The 90 Gy isodose line, which corresponds to final MR-signature in our experience^{21, 224}, was projected to the 1-year result and matched perfectly the MR-signature. Manually, using LGP segmentation tools, volume was individually drawn and further automatically calculated by the software. There was no correlation between 1-year

MR signature volume and ADL drop ($p > 0.05$), but there was with TSTH drop ($p = 0.01$).

5.4. Motion scrubbing (see previous pre-processing steps)

At baseline, pretherapeutically, the mean number of frames taken out was 35 (median 15, range 0-135) and at 1 year was also 35 (median 15, range 0-150).

5.5. Statistical analysis

Three different fMRI computational approaches were used: (1) ICA, seed-based approach and dynamic connectivity with connectivity activation patterns (CAP). Resting-state data was analyzed in Lausanne, Switzerland, by two persons not involved in patient selection, radiosurgery procedure or follow-up course (the candidate, supervised by Professor Van de Ville, MIP::Lab, Campus Biotech, Geneva).

5.5.1. Independent component analysis

In signal processing, ICA is a computational method that allows separating a multivariate signal into additive subcomponents²²⁵. This is performed assuming that the subcomponents are non-Gaussian signals, and that they are considered statistically independent from each other. Independent component analysis is a special case of blind source separation. A simple application of the ICA was considered the “cocktail party problem”, where the underlying speech signals are separated from a sample data consisting of people talking simultaneously in a room. It has been used in a variety of situations, including neuronal spike sorting²²⁶ or removing artifacts, such as eye blinks, from EEG data²²⁷.

With regards to our patients, group-level independent component analysis (ICA) was applied to decompose rs-fMRI data into components of temporally coherent spontaneous activity using GIFT ICA Toolbox (USA, <http://icatb.sourceforge.net>)²²⁸. Two type of analysis were done.

5.5.1.1. Only using baseline, pretherapeutic data (n=17)

Methodological aspects²²⁰

The concat-ICA approach is data-driven and considers the concatenated data of 17 pretherapeutic scans²²⁹. The total number of independent components (ICs) was set to 20, which is common setting in literature to identify large-scale distributed networks (Figure 29).

Visual inspection of IC maps revealed neurological meaningful patterns; no components were excluded for further analysis.

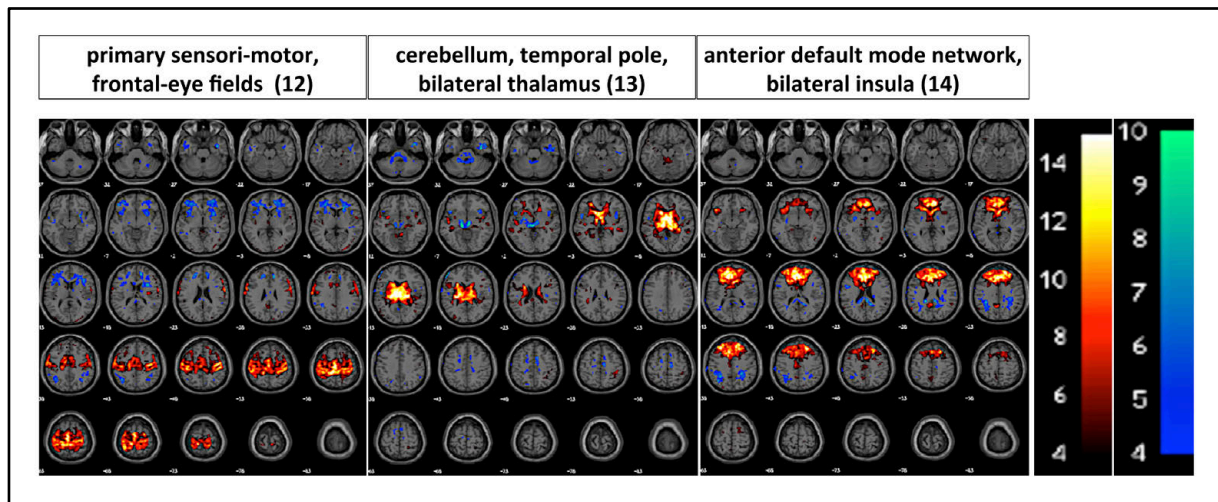


Figure 29: Illustrative example of 3 networks generated by the ICA approach²²⁰

For rs-fMRI data, Anova was implemented in SPM12 as a *flexible factorial model*. This analysis was made on each component, by using the subject-level maps. As we wanted to apply the model to each component, we used a Bonferroni correction to deal with number of models (20). For each component, subject-level spatial maps that represent strength of inter-connectivity in a large-scale network at baseline, were fed into general linear model that included the difference in points for ADL and TSTH between 1 year after Vim RS and baseline pretherapeutic values. This allowed assessing whether voxels correlated significantly with tremor improvement. Within each linear model, we use cluster-level Gaussian random field theory to correct for testing whole-brain voxels, but, since the linear model is applied to each component separately, we also additionally applied Bonferroni correction to deal with multiple comparisons (20) and report corrected p -values. In order to exclude possible confounders, using the same methodology, no statistically significant cluster was found while assessing correlations with the pretherapeutic tremor scores. This was of particular interest in order to exclude a relationship between baseline scores and their respective drop in points 1 year later, which could have been reflected in our results. Furthermore, age, disease duration, or time-to-response after Vim RS were not statistically correlated with baseline brain interconnectivity measures (Spearman's rank correlation coefficient >0.05 , using Stata version 11, Stata Corp LLC, College stations, TX, USA).

Results

We report three networks, which revealed statistical significant clusters. For ADL improvement, we found network 12 (composed by bilateral motor network, frontal eye-fields-FEF) and network 13 (composed by bilateral thalamus, cerebellum). For TSTH improvement, representative was network 14 (composed by bilateral insula, mesial prefrontal cortex).

For network 12 (Figure 30, table 5), we found a significant cluster within and adjacent to inferior olivary nucleus (ION). The more positive inter-connectivity at baseline between ION and network 12, the higher the drop in points on the 1-year ADL score. This result thus represents connectivity between bilateral motor cortex and FEF with the ION.

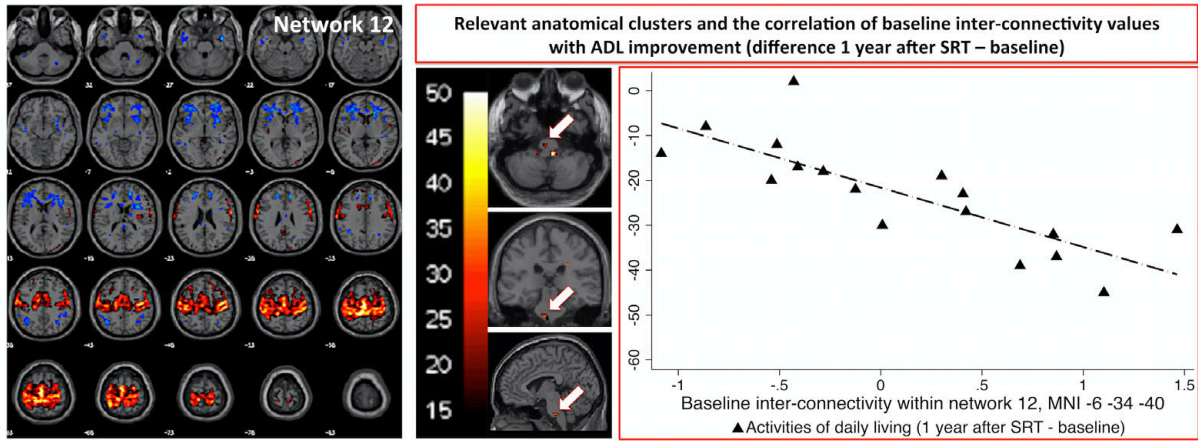


Figure 30: Interconnectivity within network 12, between bilateral motor cortex and FEF with ION, reproduced with permission from doi.org/10.1111/ane.12891

For network 13 (Figure 31, table 5), we found significant clusters within right (predominant) and left motor cerebellum lobule V. The more positive inter-connectivity at baseline between the former and network 13, the higher drop in points on the 1-year ADL score. This result thus represents connectivity between the bilateral thalamus and right motor cerebellum lobule V.

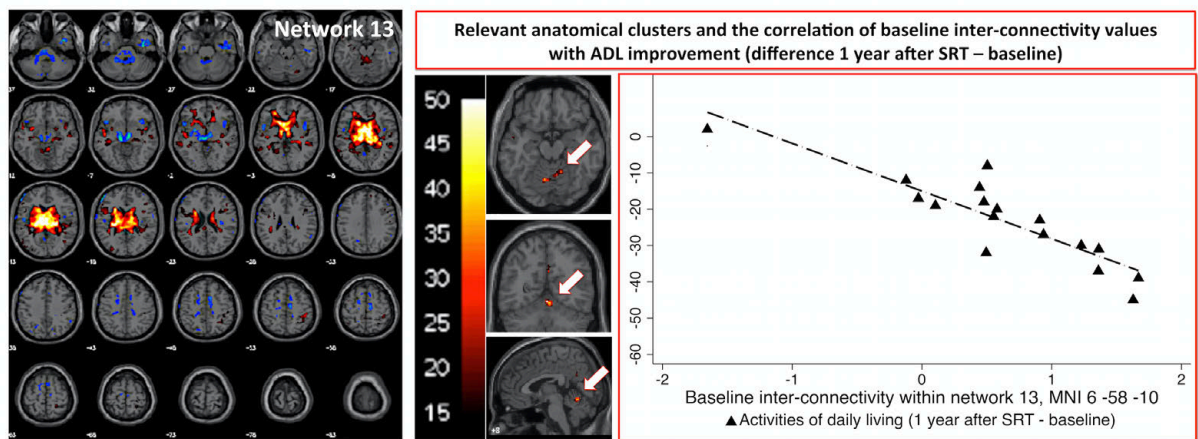


Figure 31: Interconnectivity within network 13, between bilateral thalamus with left cerebellar lobule V, reproduced with permission from doi.org/10.1111/ane.12891

For network 14 (figure 32, table 5), we found significant clusters within right medial rostral prefrontal cortex, known as right BA 10. The more positive inter-connectivity at baseline between the former and network 14, the higher drop in points on the 1-year TSTH score. This result thus represents connectivity between anterior default-mode network and bilateral insula with the right BA 10.

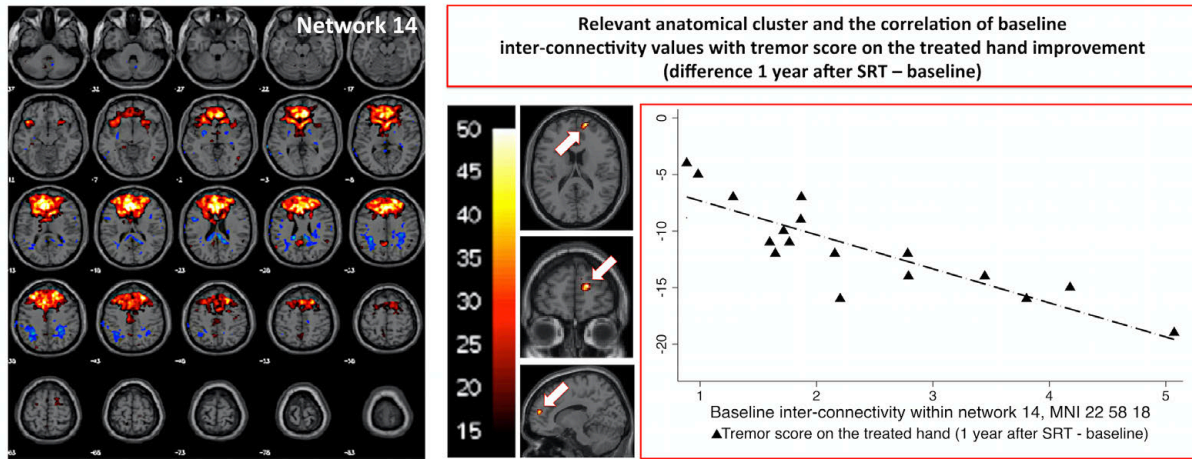


Figure 32: Interconnectivity within network 14, between DMN and salience with BA 10, reproduced with permission from doi.org/10.1111/ane.12891

Network	Inter-connectivity between the network and the relevant anatomical cluster	MNI	p FWE corrected	Kc (cluster size)
12	Inferior olivary nucleus (correlates with ADL improvement)	0 -26 -42 -6 -34 -40	0.015	62
13	Right and left motor cerebellum lobule V (correlates with ADL improvement)	6 -58 -10 -4 -62 -16	0.000	135
14	Right rostral prefrontal cortex (BA 10) (correlates with TSTH improvement)	22 58 18	0.005	79

Table 5: summary of main findings, reproduced with permission from doi.org/10.1111/ane.12891

Summary and anatomical relevance

Our findings reveal, for the first time, that functional network measures, extracted from pretherapeutic resting-state fMRI, correlate with a drop in standard tremor scores one year after Vim GKR, for both ADL and TSTH. For ADL improvement, the inferior olivary nucleus showed higher inter-connectivity with network including bilateral motor cortex and FEF, as well as motor cerebellum lobule V with the network constituted by bilateral thalamus. For TSTH improvement, right mesial aspect of BA 10 showed higher inter-connectivity with anterior default-mode network and bilateral insula. Of note, ADL is a global tremor score, involving many aspects, while TSTH is only related to a specific aspect (e.g. the hand). In this sense, neuroimaging distinction of two different clinical evaluations is not necessarily astonishing.

The first network (network 12 in our study) encompasses bilateral motor cortex and frontal eye-fields, interconnected with left inferior olivary nucleus. Historically, based upon oscillatory-pacemaking properties, inferior olivary nucleus has been proposed as primary driver of ET pathogenesis due to its implication in learning and timing of motor behavior²³⁰, meaning an involvement in control and coordination of movements, sensory processing and cognitive tasks. Two types of input are particularly of interest: one allowing for movement learning (actions), and other for posture and balance maintaining (maintenance reflexes)²³¹, which could be relevant in the context of ET patients. There are four major electrophysiological theories about the role of the inferior olivary nucleus: timing, learning, comparator and “network oscillations”. Timing theory (Welsh *et al.*²³²), suggests the

existence of an oscillatory clock, offering proper scheduling of command signals for appropriate motor domains; same was supported by Yarom and Cohen²³³, considering motor deficits or tremor appearance as a manifestation of a damaged timing mechanism. Consequently, ET would reflect maladjustment in timing of muscle activation. Learning theory states that climbing fibers to the inferior olive provide the cerebellar Purkinje cells with an error signal indicating an eventual scarce motor activity. Comparator theory postulates that climbing fibers of inferior olive provide cerebellar Purkinje cells with a signal error that indicates inadequate motor activity. “Network oscillations” theory, suggested by Yarom and Cohen²³³, states that each neuron by itself cannot exhibit oscillatory behavior, but only when a network of electronically coupled neurons is formed. The role of ION versus cerebellum has been debated for decades as being main actor in ET’s pathogenesis. Louis *et al.*⁶⁵ have done a systematic post-mortem study of microscopic changes in inferior olivary nucleus and did not detect any structural differences between ET cases and healthy matched controls. The same author has recently made an extensive review and considered we should put the model of the ION as tremor generator at rest²³⁴. The same applied for functional neuroimaging positron emission tomography studies, which failed to identify any metabolic activity at this level⁶⁵. Both have pointed out towards the conclusion that if inferior olivary nucleus is involved in ET, there is no structural or metabolic modification, which would be directly related to this disease⁶⁵. However, an isolated fMRI case-report, after opened surgical radiofrequency thalamotomy, revealed significant activation within inferior olivary nucleus after surgery⁶⁷.

The second network (network 13) encompasses bilateral thalamus and tremor drop relates to higher inter-connectivity with bilateral (right predominance) motor cerebellum lobule V. In humans, DBS⁶⁰ or RT⁶¹ of the cerebellar thalamic nucleus (i.e. Vim) induce tremor arrest²³⁵. Additional findings from rs-fMRI studies suggest that the cerebellar thalamus (e.g. Vim) and the cerebellum are involved in the mechanism of ET⁵⁶. Data from electrophysiology (Hua *et al.*), after single neurons awake mapping of the ventral thalamus in patients with ET prior to open radiofrequency thalamotomy, suggested that during tremor, Vim had a significantly higher proportion of “tremor neurons” compared to other thalamic areas⁵⁷. These findings were considered inconsistent with the olivo-cerebellar model previously described, which supposes motor cortex been driven through thalamic connections (which would be a combination of networks 12 and 13 in the present study). Schnitzer *et al.*²³⁶ used magnetoencephalography and revealed a motor network involving the contralateral primary motor cortex, premotor cortex, thalamus, brainstem and ipsilateral cerebellum. A meta-analysis of neuroimaging studies²³⁷ revealed that sensorimotor tasks activated the anterior lobule V (and adjacent lobule VI), with additional foci in lobule VIII. Lobule V is mainly associated with motor control. Furthermore, motor and somatosensory representations show largely overlapping activation patterns, with major cluster focused in lobule V²³⁷. The motor and somatosensory coordinates were right lateralized, in patients with right-handed tasks (as in the present study, right hand tremor and right lobule V activation), consistent with established ipsilateral cerebellar somatotopy and homunculi²³⁷.

The third network (network 14), rather astonishing at a first sight, includes anterior DMN and bilateral insula; inter-connectivity of right mesial aspect of Brodmann area 10 relates to 1-year drop in TSTH. Brodmann area 10 is considered as the only prefrontal area that has predominant interconnections with the supramodal cortex in prefrontal cortex (corresponding to network 14), anterior temporal or cingulate cortex. This area is relevant for cognitive tasks and by extension non-motor features in ET. Functionally, Semendeferi *et al.*²³⁸ advocated for a specific increase in connectivity, especially with other high-order association areas, underlying the role in initiative taking and the planning of future actions, trademarks of human behavior. Ramnani *et al.*²³⁹ stated that due to its particular connectivity patterns, would additionally play a crucial role in highest level of integration of multiple sensory modalities, coming from auditory, visual and somatic sensory systems, which would help to integrate outcomes from multiple cognitive operations. Gilbert *et al.*²⁴⁰ have designed a “conjunction-type” fMRI study using a series of tasks that measure the construct of interest. Brodmann area 10 was activated when people switched from either stimulus-oriented to stimulus-independent attending. The authors suggested that medial BA 10 (as in our findings) is involved in promoting attention towards the external environment, as, for example, in situations that require a particularly fast response to external stimuli.

With regard to the present findings, the real central node of ET remains to be established. Moreover, two alternative theories could be supported by our results. A pacemaker theory, with three possible anatomical locations: the left ION, the right cerebellar lobule V or the BA 10, as well as the components with whom they share interconnectivity, including the motor network, the thalamus, or the anterior node of the DMN and insula. Our findings don't answer the dilemma whether the cerebellum versus the ION would be the central core of the disease. A network theory would advocate for the presence of one versus multiple networks, of whom one coupling motor cortex with the ION, the second the thalamus with motor cerebellum, and a third between the anterior default-mode network and bilateral insula and the BA10. Whether the former act in synchrony or disassociated remains to establish by further studies.

In the light of what has been described above, one could suppose that the eventual oscillatory regulator in ET should have a resetting mechanism. It is most probably that by stimulation (such as Vim DBS) or ablative (such as Vim RT, Vim GKR or Vim HIFU) procedures, this regulator stops ticking at the appropriate time. Furthermore, it gives a new onset, occurrence and terminations within the system's oscillations, under a new neuronal control. Our method was not specifically designed to support existing physiopathological theories, and thus these findings shed new light on the implication of networks and their alterations on tremor generation.

5.5.1.2. Using both pre- and posttherapeutic data, as single patient group (n=17 subjects x 2 time-points, n=34)⁷¹

Methodology

Data-driven analytic approach we employed considered the concatenated data of the 34 scans (17 subjects X 2 time-points, pretherapeutic and 1 year after Vim GKR). Total number of components (c) was set to 20, which is a setting commonly used in literature for identifying large-scale distributed networks. After visual inspection of maps at group level, 2 (components 1 and 3) out of 20 components were excluded. The other 18 were kept for subsequent analysis, as they showed neurologically relevant spatial patterns type.

For rs-fMRI data, analysis of variance (ANOVA) was implemented in SPM12, as a *flexible factorial model*, on each component, by using individual subject-level maps, to take into account time point (pretherapeutic *versus* 1 year after Vim GKR), response (groups 1 and 2, further detailed below), and interactions between. Bonferoni correction was used to deal with number of models (20). We then report corrected *p*-values using conventional cluster-level family wise error (FWE) correction. For correlation between IC values and previously detailed tremor scores, STATA version 11 (STATA Corp LLC, College Stations, TX, USA) was used.

For relevant IC values, there was no influence of age ($p > 0.05$). The influence of disease duration was statistically significant only for c9 (see below). The 1-year MR-signature volume correlated only with IC strength between bilateral motor areas (c13, further detailed) with right visual association area (see below).

Results

Group definition for further statistical analysis

Currently available medications improve tremor in approximately 50% of patients and Propranolol, most commonly used, reduces tremor amplitude by approximately 50%²⁰⁵. To consider a therapeutical effect of Vim RS at least as effective as medication, we conventionally divided patients in two groups: 1, $\leq 50\%$ improvement in TSTH ($n=6$, 35.3%) and 2, $> 50\%$ improvement ($n=11$, 64.7%). There was no difference in age ($p=0.86$) or duration of symptoms ($p=0.41$) between groups. There was a tendency towards higher thalamotomy volumes in group 2 ($p=0.06$, mean in group 1= 0.044 ml (std 0.04, range 0.002-0.127 ml); mean in group 2= 0.17 ml (std 0.187, range 0.027 - 0.600 ml). This group separation is the same as the one proposed for the first VBM research project⁷², on a different population of patients.

Interaction between time-point and clinical response

We report statistically significant IC within 2 networks. The first is salience, involving bilateral superior frontal gyri and insular areas (c9) with left claustrum and putamen. The

second is bilateral motor network (c13), left cerebellum lobule VI and FEF with right visual association cortex, right BA 19.

For left claustrum and putamen, corresponding boxplots are shown in figure 32. At baseline, IC were positive in group 1 and remained further so, while being close to zero in group 2 (figure 32, corresponding boxplots on time effect depending on group). Functional connectivity differences (between 1 year and baseline) actually related to TSTH improvement, allowing a separation of group 1 from group 2 (main figure 33, right).

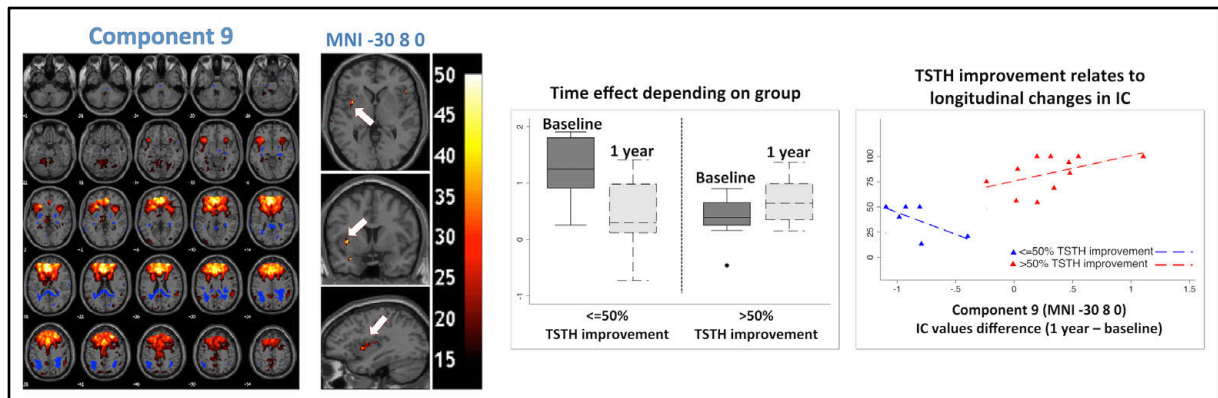


Figure 33: Main component 9 (IC with MNI -30 8 0), from left to right: anatomical images, boxplots and corresponding values by group, as well as difference in IC 1 year after Vim GKR, allowing a clear separation between groups, reproduced with permission from doi.org/10.1007/s00701-017-3456-x

For right visual association area, corresponding boxplots are shown in figure 34. At baseline, they were negative in group 1 and inversely positive at 1 year, while being close to zero in group 2 (figure 34, corresponding boxplots as time effect depending on group). Moreover, a decrease in IC at 1 year was related to TSTH improvement, allowing a separation of group 1 from group 2 (Figure 34, right). Spearman's rank correlation coefficient=0.01).

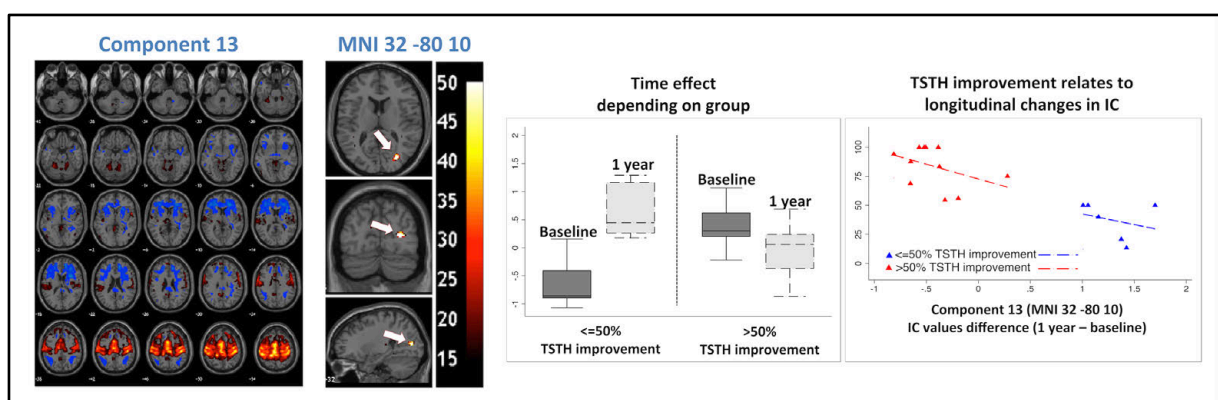


Figure 34: Main component 13 (IC with MNI 32 -80 10), from left to right: anatomical images, boxplots and corresponding values by group, as well as difference in IC 1 year after Vim GKR, allowing separation between groups, reproduced with permission from doi.org/10.1007/s00701-017-3456-x

Main effect of time point

We report statistically significant IC within two networks. The first is right dorsal attention network (c2) with the left anterior ventro-lateral prefrontal cortex (VLPFC). The second is salience network (c9) IC with fusiform gyrus, with a cluster including parts of right visual area V5, the former illustrated in Figure 34 (right side).

Figure 34 illustrates, on the right side, the reminiscent of the salience network, which showed altered interconnectivity with right fusiform gyrus and V5 (FWE= 0.000, right image, upper part). For this former network, opposite results are seen as compared with the one described in interaction between clinical effect and time, in network (c13), between bilateral motor cortex, FEF and left cerebellum lobule VI, with right visual association cortex, right BA 19 (as previously described). Overall interconnectivity values decreased from slightly positive to the opposite slightly negative values (Figure 34, left image, middle part). Furthermore, patients who alleviated less (group 1) presented slightly positive pretherapeutic interconnectivity (which decreased to median of slightly negative symmetric, close to zero, one year later), while those who alleviated more (group 2), had pretherapeutic negative median values (close to zero, which slightly increased to a median of zero one year later) (Figure 34, right image, lower part). The results are presented as compared with the one from the interaction between time (pre- and one year post-therapeutic, as previously described) with clinical effect, of which network interconnectivity strength between c13 with right visual BA 19 related to tremor arrest after Vim RS (FEW= 0.001, Figure 34, left, upper part²⁴¹). Both pretherapeutic interconnectivity (Figure 34, right, middle part), as well as difference between 1 year and baseline, related to TSTH improvement after Vim GKR. Furthermore, patients who alleviated less presented negative pretherapeutic interconnectivity (which increased to median positive values one year later), while those who alleviated more, had already positive pretherapeutic values (which decreased to a median of zero one year later) (Figure 35, right, lower part). We concluded, based upon the previous, that Vim GKR seems to bring interconnectivity in the visual areas back to normal for all patients, but the ones who had this region more functionally integrated pretherapeutically had much larger benefit.

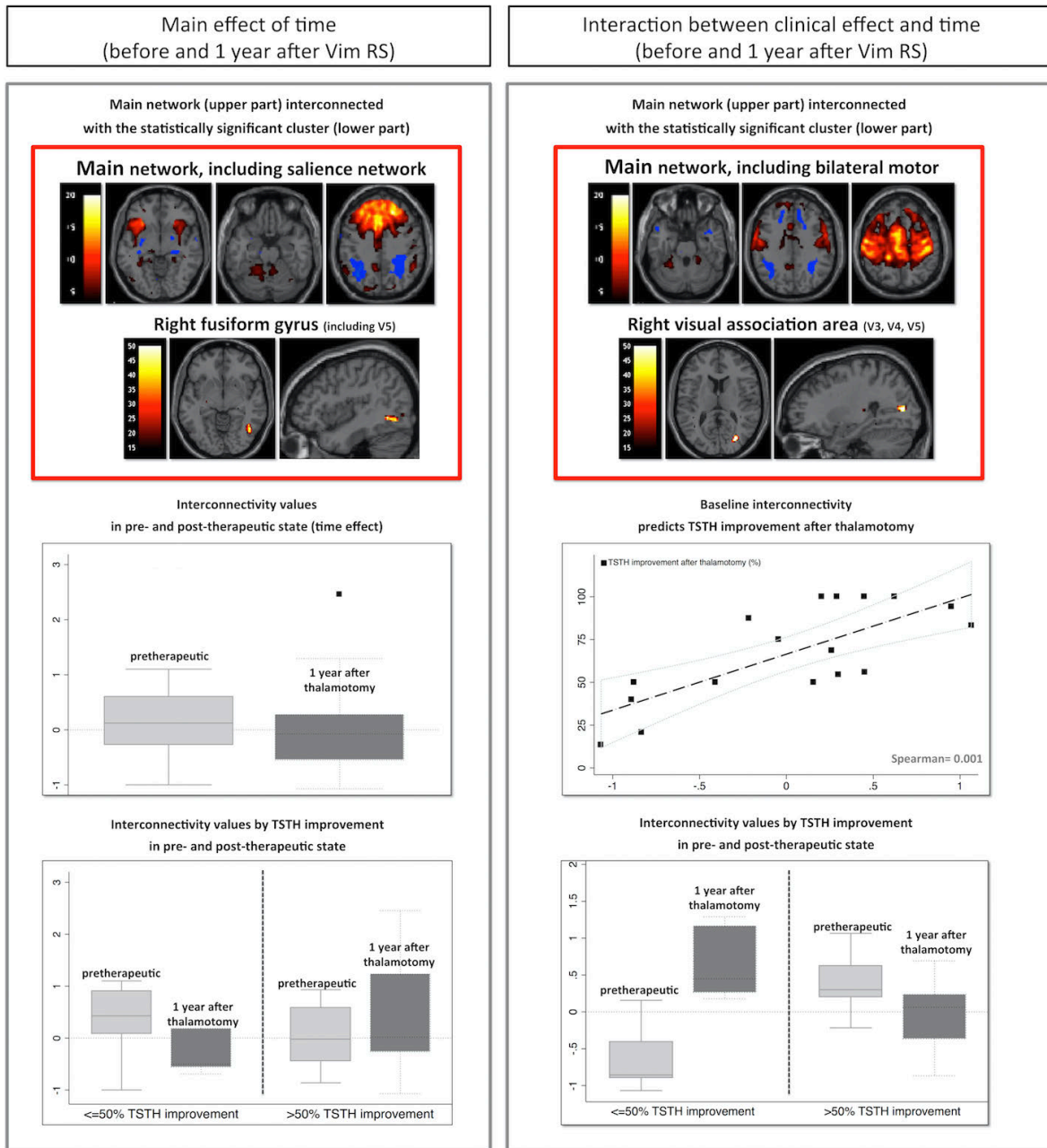


Figure 35: Adapted from *Brain*²²³, with permission: right, main effect of time: upper part, interconnectivity between the main network, including remnant salience network with right fusiform gyrus (including V5); middle part, boxplot illustration of overall interconnectivity values in pre- and posttherapeutic states; lower part, boxplot illustration with regard to the group clinical effect (with less or equal and more than 50% improvement); left, interaction between clinical effect and time: upper part, interconnectivity between the main network, including left cerebellum lobule VI, frontal eye fields and bilateral motor cortex with right visual association area (Brodmann area 19, including V3, V4 and V5); middle part, pretherapeutic interconnectivity predicts tremor score on the treated hand improvement 1 year after Vim RS (Spearman rank correlation coefficient 0.001); lower part, boxplot illustration with regard to the group clinical effect (with less or equal and more than 50% improvement).

Summary and findings and anatomical relevance

In this research project, we report TSTH improvement correlated with IC strength between salience network with left claustrum and putamen, as well as between bilateral motor cortex, FEF and left cerebellar lobule V with right visual association area. Longitudinal

changes showed additional associations in IC strength between salience network with fusiform gyrus.

To summarize, we show two different relevant circuitry with regards to our patients: one is related to a basal ganglia network, while the second to visual association areas, the former linked with M1.

The basal ganglia circuitry is briefly overviewed. The input and output of claustrum is related to almost all regions of cortex (including cingulate, visual areas in occipital lobe, entorhinal cortex, and temporal areas)²⁴². Furthermore, we identified that the anterior dorsal part, found here, connects with motor and somato-sensory cortex. Main functions include: cross-modal perception²⁴³, coordination of matching between visual and tactile modalities²⁴⁴, and has even been invoked as important to consciousness²⁴². The putamen, by its connections to substantia nigra and globus pallidus, plays a major role in movement regulation, motor learning, preparation, sequences, tasks and amplitude, limb movement control, and as part of motor system that is mobilized to take action, or influences various types of learning²⁴⁵.

With regards to the visual circuitry (e.g. visual association area), several hypotheses with regards to their relevance have been already discussed in each discussion section of the VBM projects. One appealing theory with regard to the present findings would be visual input to caudate nucleus and claustrum and further to M1²⁴⁶, explaining appearance of the former in another component from the same analysis. Another would give the cerebellum the role of a “calibrator”. Other functions of the visual association cortex are related to feature extraction, attentional and multimodal integrating functions. Furthermore, electrophysiology data suggest sensitivity to motion-delineated forms²¹⁷ and its role as a differentiation point between the ‘*what*’ and ‘*where*’ visual pathways. Additional involvement of the visual association cortex is in horizontal saccadic eye movements, visuospatial information processing, orientation-selective attention and tracking visual motion patterns²¹⁵.

The fusiform gyrus, interconnected here with salience network, is mainly involved in high-level vision as part of the ventral visual stream (“what” pathway) and various neural pathways related to recognition. It encompasses the middle temporal area (V5), and plays a major role in motion perception, integration of local motor signals into global percepts, and guidance of some eye movements. Major projections include eye movement-related areas (e.g. FEF). It is worth noting that both V5 and V6 have high myelin content, a characteristic that is usually present in brain structures involved in fast information transmission.

5.5.2. Seed based approaches^{221, 222}

5.5.2.1. General concept

In a seed based approach, we used rs-fMRI to characterize the antero-lateral, motor

thalamus, temporal correlations at whole brain level. This is based upon the prior hypothesis of the “tremor network” and its successful targeting in drug-resistant tremor (e.g. at the Vim level), in which a core role is played by the motor thalamus within this network. Seed-based FC was obtained as correlations between the VLV’s time courses and the one of every other voxel. One-year MR-signature volume was always located inside VLV and did not correlate with any reported seed-FC measures ($p>0.05$).

5.5.2.2. Main hypothesis

Our first hypothesis was that pretherapeutic FC is impaired within the previously described “tremor network” as compared with HC, based upon recent fMRI studies and existing physiopathological theories^{55, 56, 247}. However, beside the main Vim’s role in tremor propagation and its altered thalamo-cortical connectivity in ET⁵⁶, recent studies have specified an increased FC of sensory-motor and salience networks in ET as compared with HC²⁴⁸. Our second hypothesis was that Vim GKR would not only generate changes within the thalamo-cortical network, but also produce a functional reorganization of salience networks.

5.5.2.3. Methodological aspects and VLV extraction from diffusion MR data

More exactly, ventro-lateral ventral nucleus (VLV, nomenclature from Morel et al.³⁰) was used a region-of-interest (ROI), to encompass the lack of direct Vim’s visibility in current 3T MRI. Furthermore, it allowed a uniform segmentation procedure.

The VLV was obtained individually, by Dr Najdenovska, using an automated, robust and reproducible method for thalamus parceling, while exclusively exploring local thalamic diffusion properties across both healthy subjects and patients with ET (pretherapeutic data), and already published²⁴⁹. In fact, nomenclature for motor thalamus subdivisions has varied between authors and species. For consistency reasons, we will refer only to Vim and VLV in the present research part.

Left and right VLV, seed-to-voxel FC maps were generated individually using the REST package²¹⁹ (e.g. seed-to-voxel implementation), that computes FC of a ROI (e.g. left and right VLV) and any other voxel in the brain. Furthermore, they were normalized applying the Montreal Neurological Institute (MNI, Montreal, Canada) template, using SPM 12 (London, United Kingdom). The resulting connectivity maps were statistically analyzed at the group level with SPM 12, using a variety of different tests: 1- one-sample t-test for evaluating left and right pretherapeutic VLV seed-based FC; 2- a regression analysis (ANOVA flexible factorial), using a general linear model, for assessing pretherapeutic rs-fMRI FC, which would relate to 1-year ADL, TSTH and head tremor arrest; 3- a two-sample t-test, to asses

alterations in FC between the pretherapeutic state and the HC; 4- a paired t-test to assess changes in FC between pre- and post-therapeutic state. The ET population was described above. Ten healthy controls (HC) were enrolled (age and gender matched) with a mean age of 70.4 years (median 71; range 59-83 years; male to female ratio: 4:6).

We first applied an uncorrected height threshold of $p < .001$ followed by a $p < .05$ FWE- or FDR-corrected cluster-size threshold. All the presented scatter plots are statistically significant results and were made using Stata (version 11, Stata Corp LLC, College stations, TX, USA).

We assessed the potential confounders. The classical MR signature volume, visible 1 year after Vim RS, was always located inside left VLV cluster (as an example please see figure 36 for methodological aspects). Moreover, there was no statistically significant correlation between this volume and the FC values. Also, no difference was found between left and right FC ($p > 0.05$).

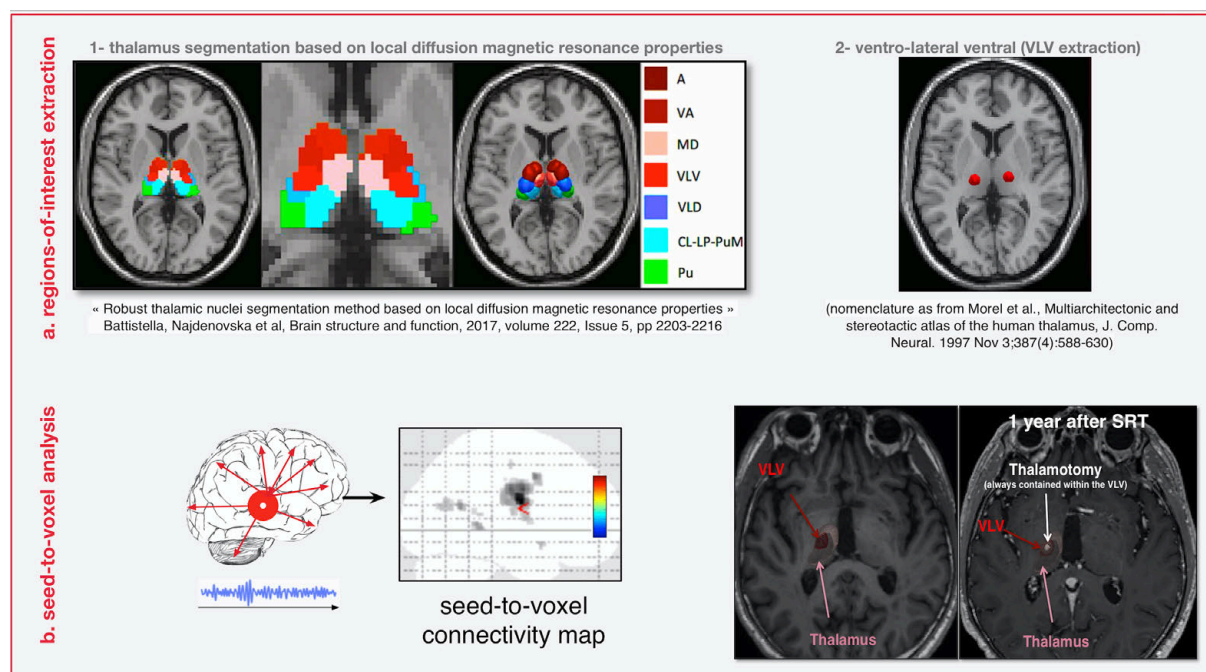


Figure 36: a- region-of-interest extraction by Dr Najdenovska, using a methodology, which has already been published; b- brief and artistic overview of the seed-to-voxel approach, with the 1-year MR signature volume always contained inside the VLV cluster (permission for reproducing this figure is not required, but the journal article need to be cited²²¹)

5.5.2.4. Results

Left and right VLV FC

There was no statistically significant difference between left and right FC ($p > 0.05$).

Pretherapeutic FC predicts 1-year tremor improvement

We report statistically significant correlations between pretherapeutic left VLV FC

with right visual association area (BA 19), which predicted 1 year ADL drop ($p_{unc}=0.02$ - SPM result, more positive FC associated with better improvement; figure 37, a)

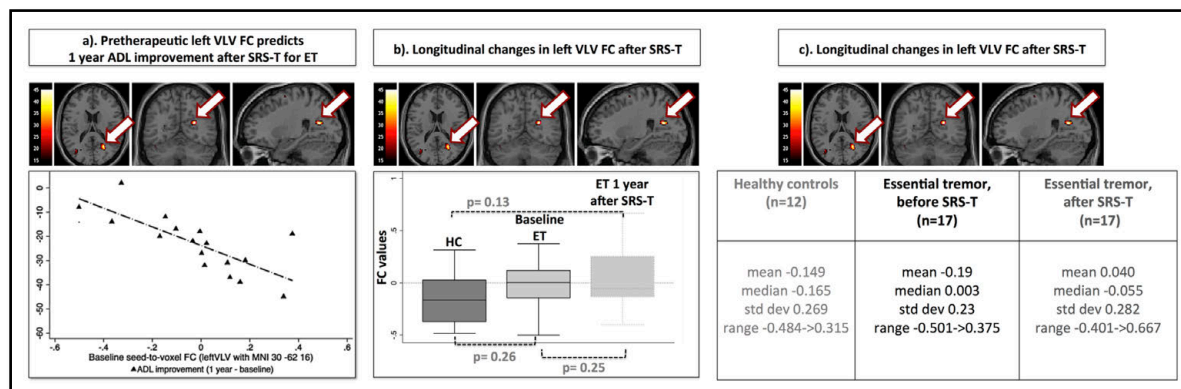


Figure 37: a- illustration of left VLV seed-to-voxel FC maps (with right visual association area), which predicts 1 year ADL's improvement; b- boxplots with the FC values for HC, baseline ET and ET 1 year after SRS-T; c- the illustration of mean, median, standard deviation and range for each of the groups (permission for reproducing this figure is not required, but the journal article need to be cited²⁵⁰)

While in HC the mean and median left VLV FC values were -0.149 and -0.165, in pretherapeutic state they were -0.19 and 0.003 and in post-therapeutic state 0.040 and -0.055, respectively. For details please see figure 3 (b and c, with the respective boxplots and mean, median, standard deviation and min and max values). However, there was no statistically significant difference between the FC values for HC and ET before SRS-T (two sample t-test, $p=0.26$), or between the former and 1 year after SRS-T (paired t-test, $p=0.25$).

The patients who alleviated more in terms of ADL drop were those with an increase in FC values 1 year after SRS-T, as compared to pretherapeutic state.

Furthermore, pretherapeutic left VLV FC with left fusiform gyrus (BA 37) predicted 1 year head tremor score improvement ($p_{unc}=0.04$ - SPM result, more negative FC associated with better improvement; figure 38, a). While in HC the mean and median leftVLV FC values were 0.053 and 0.044, in pretherapeutic state they were 0.272 and 0.215 and in post-therapeutic state 0.08 and 0.022, respectively. For details please see figure 38 (b and c, with the respective boxplots and mean, median, standard deviation and min and max values).

There was a statistically significant difference between the FC values for HC and ET before SRS-T (two sample t-test, $p=0.05$), or between the former and 1 year after Vim GKR (paired t-test, $p=0.5$). Moreover, there was no statistically significant difference between HC and 1 year after Vim GKR. The patients who alleviated more were those with a drop in FC values, getting back to similar values, as the ones of the HC.

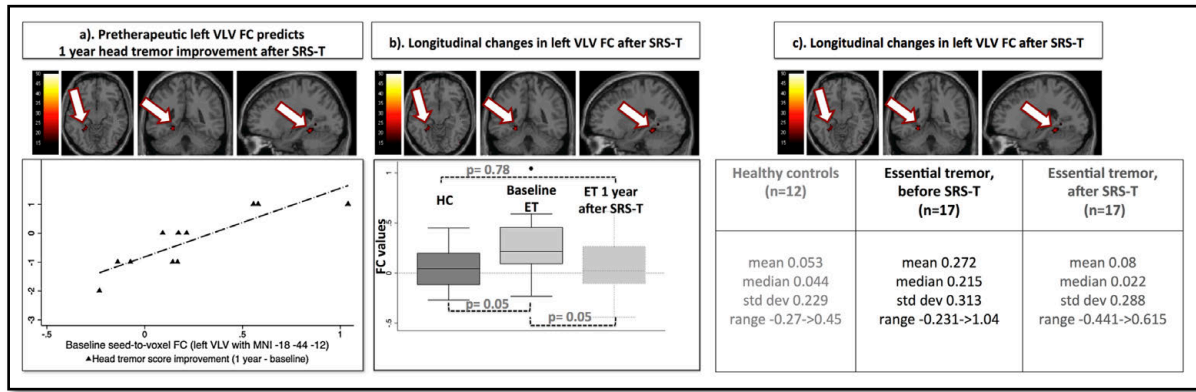


Figure 38: a- illustration of left VLV seed-to-voxel FC maps (with left fusiform gyrus), which predicts 1 year head tremor improvement ($n=11$, for pretherapeutic head tremor score ≥ 1); ; b- boxplots with the FC values for HC, baseline ET and ET 1 year after Vim GKR; c- the illustration of mean, median, standard deviation and range for each of the groups (permission for reproducing this figure is not required, but the journal article need to be cited²³⁰)

VLV altered FC in pretherapeutic drug-naïve ET as compared with HC

Drug-naïve ET, compared with HC, showed decreased (median negative value) FC between the left VLV and the following clusters: left primary somatosensory area (inferior part, $p_{FWE-corr}=0.035$), pedunculopontine nucleus ($p_{FWE-corr}=0.003$) and dorsal anterior cingulate cortex (BA 32, $p_{FWE-corr}<0.001$). Furthermore, a decreased pretherapeutic FC with the primary somatosensory cortex (Spearman=0.04) and pedunculopontine nucleus (PPN, Spearman= 0.01, Figures 39 and 40) correlated with baseline ADL. Drug-naïve ET, compared with HC, revealed increased left FC with left visual association cortex (BA19, $p_{FWE-corr}=0.005$, Figure 41) and left superior parietal regions (BA 7, $p_{FWE-corr}=0.014$).

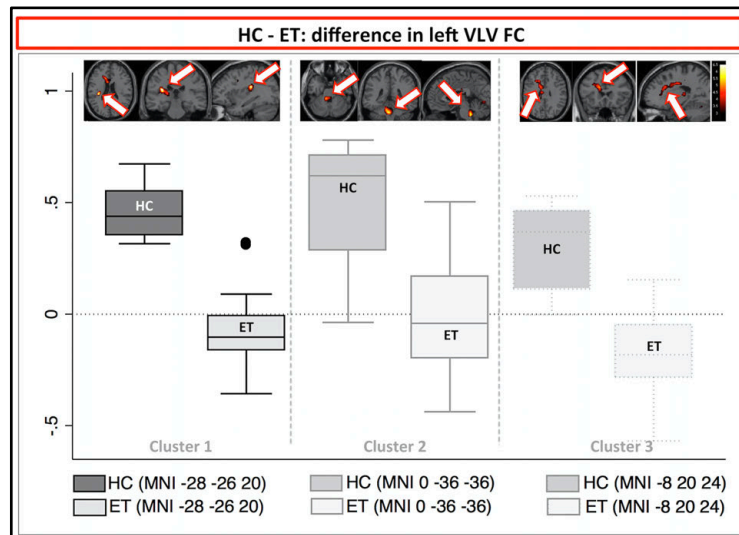


Figure 39: Difference in FC between HC and ET in (from left to right): left primary somatosensory area, pedunculopontine nucleus, and dorsal anterior cingulate (permission for reproducing this figure is not required, but the journal article need to be cited²²¹)

Pedunculo pontine nucleus FC with left VLV (correlation with baseline ADL)

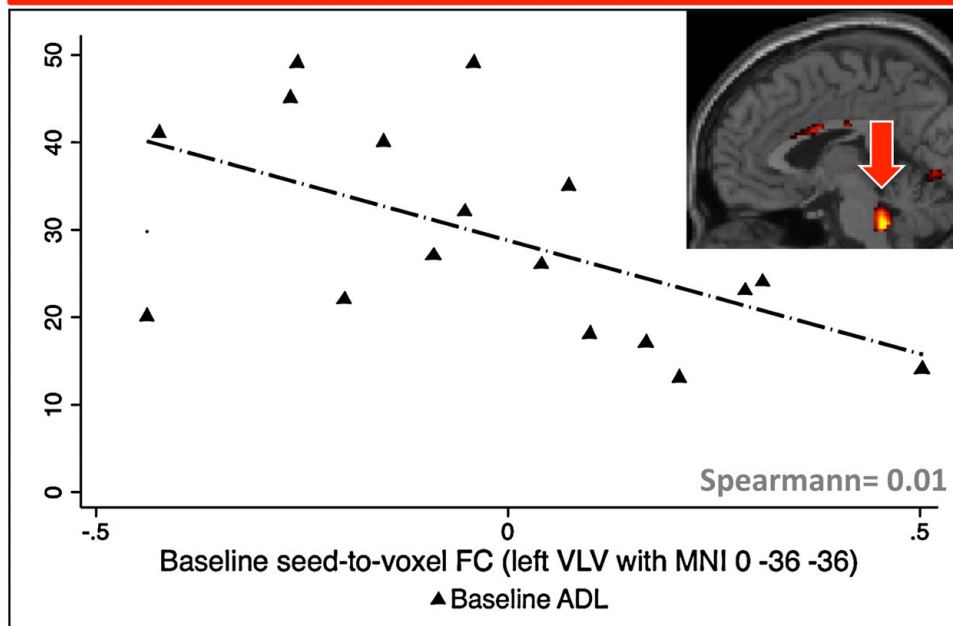


Figure 40: decreased pretherapeutic FC of left VLV with pedunculo pontine nucleus as compared with HC (Spearman= 0.01) correlates with baseline ADL (permission for reproducing this figure is not required, but the journal article need to be cited²²¹)

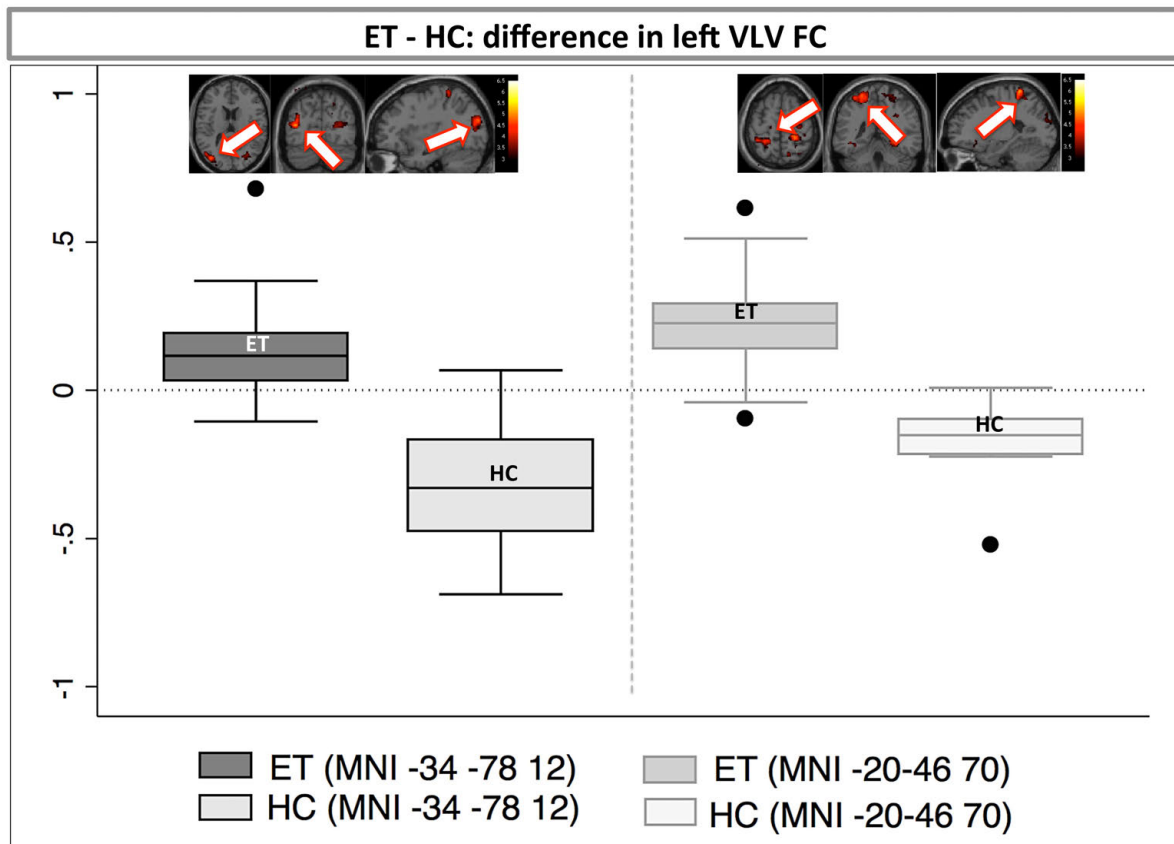


Figure 41: ET patients, as compared with HC, showed increased left FC with left visual association cortex (BA19, $p_{FWE-cor}=0.005$) and left superior parietal regions (BA 7, $p_{FWE-cor}=0.014$) (permission for reproducing this figure is not required, but the journal article need to be cited²²¹)

Changes in VLV FC between pre- and post-therapeutic state

We found a decrease from pretherapeutic positive FC to a median value close to zero 1 year after Vim GKR (Figure 42, from a to d) between left VLV with the following clusters: right insular and orbito-frontal cortex (BA 47, $p_{\text{FWE-cor}}=0.000$), right BA 40 (posterior parietal, supramarginal gyrus, $p_{\text{FWE-cor}}=0.002$), left BA 13 (anterior insula, $p_{\text{FWE-cor}}=0.000$) and right BA 44 and 8 (inferior frontal gyrus and FEF, $p_{\text{FWE-cor}}=0.002$).

On the other hand, an increase from pretherapeutic negative FC to a median close to zero 1 year after Vim GKR is reported for left VLV FC with right supplementary motor area (SMA, $p_{\text{uncor}}=0.015$).

The boxplots are illustrated in Figure 42, both for pre- and posttherapeutic state (1 year after Vim GKR).

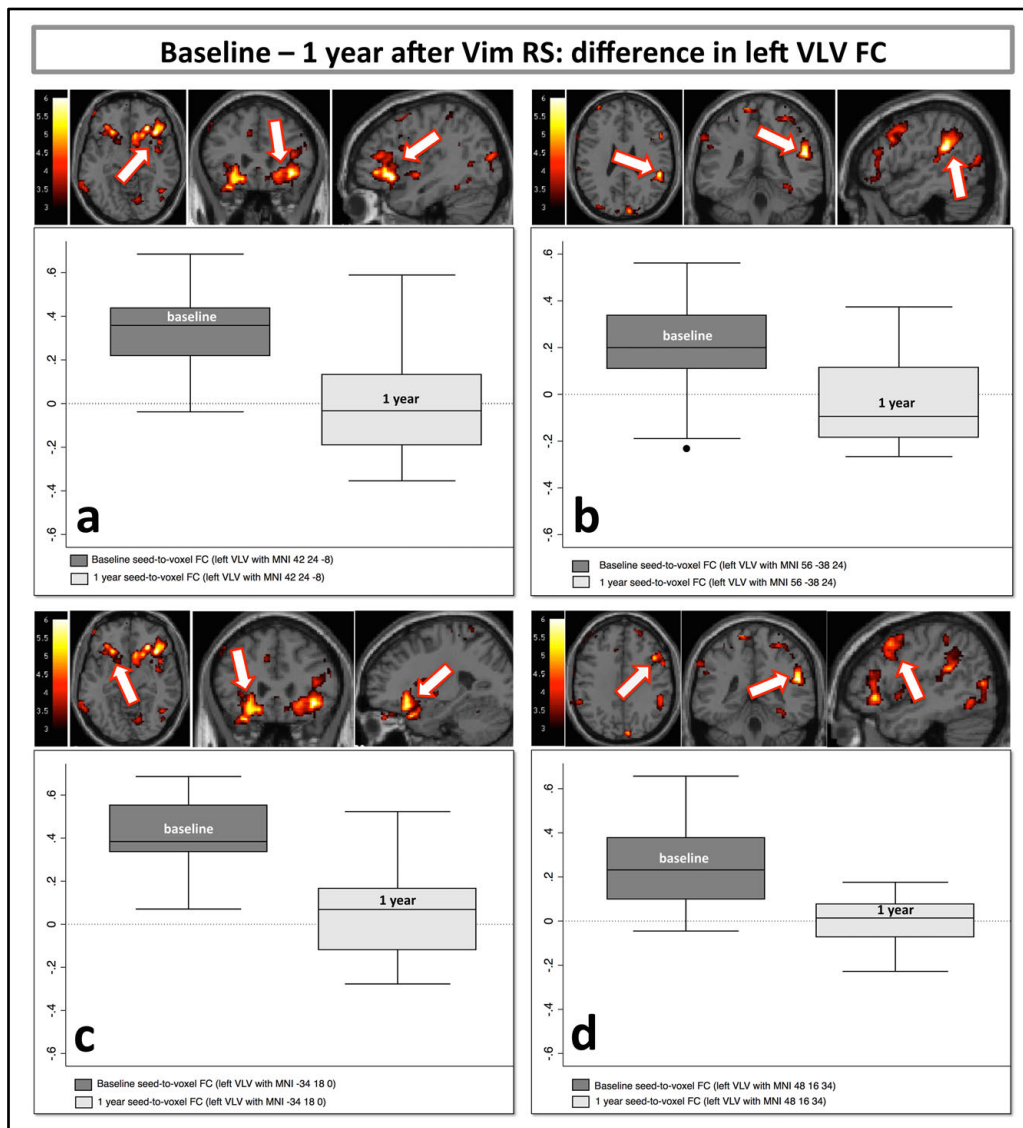


Figure 42: Illustration of differences of left VLV seed-to-voxel FC values for the statistically significant clusters in pretherapeutic – 1 year after Vim GKR: right insular and orbito-frontal (a), posterior parietal cortex (b), left anterior insular cortex (c), right inferior frontal gyrus and frontal-eye fields (d) (permission for reproducing this figure is not required, but the journal article need to be cited²²¹)

5.5.2.5. Summary and anatomical relevance

In this part of the thesis research project, we focused on FC of the ventro-lateral thalamus, the most commonly used surgical target (e.g. Vim) for tremor.

With regards only to baseline rs-fMRI data, we report that pretherapeutic left VLV seed-FC correlates both with 1-year tremor drop (ADL and head) after Vim GKR. Furthermore, pretherapeutic FC between left VLV and right visual association area relates to one-year drop in ADL after Vim GKR (more positive FC between left VLV and right visual areas associated with better improvement). In fact, patients with largest difference in left VLV FC with respect to pre- and posttherapeutic state did have the largest benefit in ADL improvement from the Vim GKR. Pretherapeutic FC with left fusiform gyrus correlates with 1-year head tremor drop in points (more negative FC associated with better improvement). Here, there was a statistically significant difference between HC and pretherapeutic state, as well as between the pre- and posttherapeutic state. In fact, altered FC of the left VLV in ET went back to values close to the ones in HC after SRS-T. Moreover, patients with a drop in FC did have the largest benefit with respect to head tremor improvement.

We hypothesized that altered FC between the ventro-lateral thalamus with parts of the so-called “cerebello-thalamo-cortical” loop would predict tremor and time to tremor arrest. In the light of the previous, we postulated that a cerebello-thalamo-visuo-motor network is involved in tremor generation and further arrest after Vim GKR.

The ventro-lateral thalamic connections have been previously described by numerous studies. Using structural neuroimaging (e.g. tractography), Hyam et al.²⁵¹ suggested that Vim’s connections are with ipsilateral M1 and contralateral cerebellum. In a recent structural (e.g. diffusion clustering of thalamic nuclei) study³³, it has been advocated a structural connectivity between VLV with contralateral cerebellar peduncle and ipsilateral M1 and red nucleus. More recently, a functional neuroimaging study (Fang et al.⁵⁶) used also ROI approach and evaluated time-courses of Vim in ET as compared with healthy controls. The authors reported FC increase between Vim and M1 area in ET, as well as a decrease with cerebellum. It is worth noting that the same circuit has also been advocated also in normal (nonhuman) primates²⁵² and healthy humans²⁵³. However, our findings involve anatomical clusters, which are not part of the previously described tremor network. All the statistically significant functional connections between the target (left VLV) and right visual association cortex and left fusiform gyrus are most probably related to polysynaptic connections, which can relate regions that are structurally segregated. Right BA 19, related to ADL drop, is encompassing here visual areas V2 and V3. The main functions are: visuo-spatial information processing²¹², face-name association²⁵⁴, multimodal integration functions and

differentiation points of the main two visual streams (“what” and “where”). Left fusiform gyrus (BA 37) is involved in face recognition²⁵⁵, visual motion processing²⁵⁶ or face-name association²⁵⁷. In a recent study, Ignacio Seranno et al.²⁵⁸ have depicted differences in cortical thickness of right fusiform gyrus between 2 groups of ET patients. The authors concluded that these structural differences might account for a different clinical subtyping.

Concerning the FC alterations between pretherapeutic ET versus HC, several aspects warrant further consideration. At cortical level, some of the representative regions have already been reported by previous studies. This includes *primary somatosensory/somatomotor cortex*²⁵⁹, responsible for integration of somatic sensation, visual stimuli, and movement planning²⁶⁰ or BA 32, involved in “Stroop” task²⁶¹, with relevance in ET. We further report newly discovered FC alterations of left VLV with left posterior parietal BA 7 and left visual association cortex BA 19. The BA 7 is involved in locating objects in the space and represents a point of convergence between vision and proprioception; its presence suggests a functional alteration of sensorial networks in ET. The left BA 19 presence is somewhat surprising, most probably by polysynaptic connections, and would express currently underestimated alterations of visual networks in ET. Interestingly, we also report altered FC between the left VLV with the PPN, an anatomical structure responsible for modulation of gait (initiation, maintenance, modulation and other stereotyped motor behaviors). The PPN has been classically explored in DBS for Parkinson’s disease patients with axial symptoms, less responsive to subthalamic nucleus stimulation and is considered highly inter-connected with the pallido-thalamo-cortical circuit²⁶². In the context of ET patients, alterations in FC between this structure and the motor thalamus are most probably related to other neurological features, already acknowledged, mainly deficits on both balance (the ability to maintain the body within its base of support) and gait²⁶³. An additional argument in favor of this statement is the found correlation between pretherapeutic ADL and FC with this structure, being know that ADL is global score including also aspects related to gate and posture.

An added value of this particular part of our research project is the display of longitudinal changes in FC, 1 year after Vim GKR. For dorsal attention and salience network, FC exhibited a decrease from positive median values to ones close to zero after Vim GKR. This would support the fact that pretherapeutic global increase in FC, described by other authors in these networks²⁴⁸, is an adaptive change during ET disease course. In this sense, Vim GKR generates a progressive functional reorganization of these systems, with further decrease of an originally probably adaptive and compensatory hyperactivity, thought to balance tremor appearance and disease progression. The same type of changes described in the previous networks is applicable to left VLV FC with anterior insula, involved in salience and warrants further attention. It is well acknowledged that insula is the bottom-up

detection of salient events, allowing switching between other large-scale networks to facilitate access to attention and working memory resources, when a salient event is detected. Moreover and of high relevance, anterior insula has a strong additional functional coupling with anterior cingulate cortex, facilitating rapid access to the motor system²⁶⁴. It would so act as an integral hub in the generation of appropriate behavioral responses to salient stimuli²⁶⁴. Sridharan et al.²⁶⁵. revealed that right anterior insula plays a critical and causal role in interchanging between two other major networks (central attention and default-mode network), known to demonstrate competitive interactions during cognitive information processing. Across stimulus modalities, this structure would play a critical and causal role in activating the central attention and deactivating the default-mode network²⁶⁵. These entire features would give the insula a balance capacity between salience and motor networks. We additionally report FC changes with the right SMA, which has multiple roles, including postural stability during stance or walking, bimanual coordination or initiation of internally generated as opposed to stimulus driven movement²⁶⁶.

5.5.3. Methodological perspectives: connectivity activation patterns

5.5.3.1. General concept

Spatial patterns of spontaneous activity might involve different subregions of a network at different times, possibly reflecting functionally relevant relationships that cannot be captured by conventional data analysis²⁶⁷. Seed region-based linear correlation analysis is a reliable measurement of co-activation of two regions, but provides little valuable information of co-activation of more than two regions²⁶⁷. Here, we used BOLD fMRI during resting-state, to characterize dynamic interactions of the extrastriate cortex.

In fact, we examined a subpart of the right extrastriate cortex (Brodmann area 19, including V3, V4 and V5) as a unique ROI. It was been chosen from our previously published data^{71, 223}, given its interconnection with the cerebellum lobule VI, bilateral motor cortex and FEF. We applied co-activation patterns (CAP) methodology, to extract whole brain spatial patterns of brain activity that occur dynamically over time. We hypothesized, based upon previous findings^{71-73, 268}, that the extrastriate cortex in ET presents adaptive changes, in synchrony with the cerebello-thalamo-cortical axis, as a part of a multi-component oscillatory system. Lastly, we examined whether this oscillatory system responds to interventional studies, such as Vim GKR, and further correlated the BOLD response signal not only 1 year after such intervention, but also in a HC group.

5.5.3.2. Materials and methods

5.5.3.2.1. Subjects

Here, we included 42 participants: 12 HC (group 1; age and gender matched), 15 patients with ET (group 2; right-sided, drug-resistant) before Vim GKR and the same 15 (group 3) one year after left unilateral Vim GKR. In fact, 30 patients (with pre- and posttherapeutic data, $n=60$) entered the initial analysis. As there was still residual movement in the results with a threshold of 0.5 mm for the Power index, we decided to lower it to a more conservative value of 0.4 mm, so as to avoid any movement artifacts. Finally, after rigorous scrubbing procedure, only 15 remained for subsequent functional connectivity analysis and are reported in the frame of this part of the research project. For those, only the remaining frames were further considered. At baseline, the mean number of remaining frames was 251 out of 300 (median 269, range [202,283]) and at 1 year after Vim GKR it was also 251 (median 259, range [179,294]).

Mean baseline ADL ($n=15$) was 28 (range [13,49]) and mean drop after Vim GKR was -23.6 (range [2,-48]). Mean baseline TSTH ($n=15$) was 19 (range [8,30]) and mean drop after Vim GKR was -13 (range [-4,-22]). The mean time to clinical response was 133 days (median 120, range [15,300]), which is in accordance with the delayed and well-known clinical and radiological response of RS²³⁵ taking up to one year after the procedure.

5.5.3.2.2. Co-activation pattern mapping: brief description

Co-activation patterns (CAPs)^{267, 269} were generated using an in-house toolbox, created as part of our interest in dynamic connectivity²⁷⁰. CAP analysis is a frame-wise dynamic functional connectivity tool, which allows the identification of spatially distinct networks co-activating with a chosen ROI region at given time points. They can then be further analyzed in terms of spatial and temporal features. The whole-brain co-activation patterns with the right extrastriate cortex seed were computed, by retaining fMRI volumes for which the seed signal exceeded a z-scored value of $T_{seed}=0.5$ and subsequently separating them through K-means clustering (spatial correlation used as distance measure, 100 iterations, 20 repetitions, random data points for initialization); similarly to previous CAP studies^{267, 269}, only the 15% most active and 5% most deactive voxels in each fMRI volume were considered for the clustering step, also discarding all remaining non-null clusters with less than 6 neighboring elements. A CAP was defined as the average of all frames attributed to a cluster.

For each CAP, we computed a dynamically informative subject-specific metric: the *count number or number of occurrences* (i.e., the number of times entering the assessed state). Thus, larger count values reflect a more frequent occurrence of a given co-activation pattern

during moments of seed activity. Here, we report a part the results obtained with K=3 CAPS, number chosen after careful analysis. The CAP were generated on 27 subjects (12 HC plus 15 pretherapeutic ET); furthermore, they were assigned to the 15 ET cases, 1 year after Vim GKR.

One-way MANOVA analysis with repeated measures (STATA version 11 (STATA Corp LLC, College Stations, TX, USA)) was considered appropriate, as there were no multivariate outliers seen by boxplot and Mahalanobis distance ($p > .001$), no multicollinearity ($r < .65$), and homogeneity of variance-covariance matrices (Box's M test, $p > .001$).

The normalized counts that significantly differed between groups were used to determine the relation with the clinical tremor scores and time to tremor arrest (see *Methods* section). A p-value lower than 0.05 (Spearman's rank correlation coefficient) was considered statistically significant. Data is presented as median \pm standard error of the mean, unless otherwise stated.

5.5.3.2.3. Results

Co-activation patterns

The retained frames (described in details below) were attributed to the following co-activation regions, equally occurring in a group including both the HC (n=12) and ET patients (n=15)(total, n=27): cerebello-visuo-motor (CAP1, 38.6%), thalamo-visuo-motor (CAP2, 32.6%) and basal ganglia and extrastriate cortex (CAP3, 28.8%).

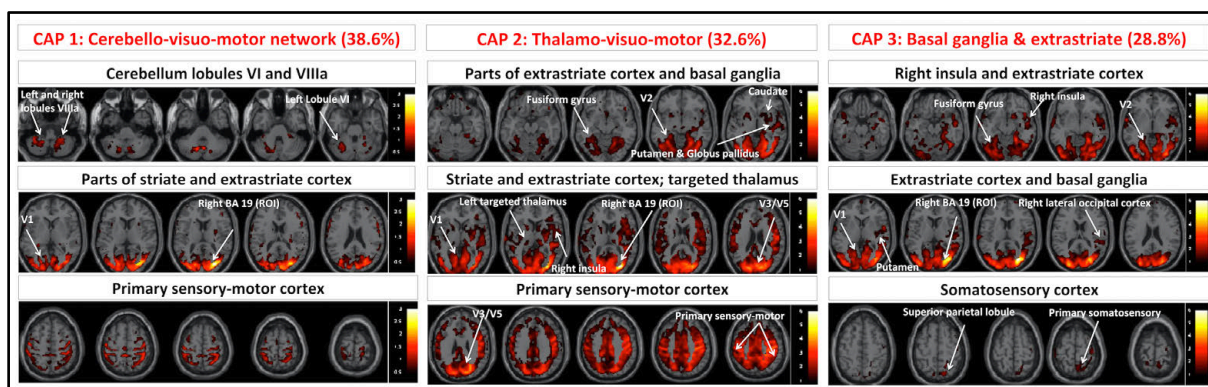


Figure 43: Illustration of connectivity activation patterns in our population, from 1 to 3 (left to right)

CAP 1: Cerebello-visuo-motor

This CAP illustrates the cerebellum lobules VI and VIIIa, bilaterally, the fusiform gyrus, visual areas V1, V2, V3 and V5, as well as with the primary sensory-motor cortex (Figure 43, left).

CAP 2: Thalamo-visuo-motor, including targeted thalamus

This CAP displays the left cerebellum lobule VI, fusiform gyrus, V1, V2 and V5 areas and the bilateral primary sensory-motor cortex (Figure 43, center). Moreover, one can

visualize here the left targeted thalamus, as well as parts of the basal ganglia circuitry, such as the caudate, putamen and globus pallidus.

The count metric (Figure 44, a, for illustration) was increased in pretherapeutic ET (median 25, range [10,44]) as compared to HC (median 17, range [4,43]; $p=0.02$), and further decreased to similar values as the HC at 1 year after thalamotomy (median 19, range [2,26]; $p_{HC,postET}=0.96$; $p_{preET,postET}=0.003$; $p_{ANOVA}<0.001$). There were statistically significant negative correlations between pretherapeutic CAP2 count numbers and ADL (Figure 44, b, Spearman's rank correlation coefficients of 0.02).

CAP 3: Basal ganglia and extrastriate cortex

This CAP includes the left and right cerebellum lobule VIIIa, parts of the extrastriate cortex (fusiform gyrus, left V2, right V3, V5), the bilateral primary visual cortex V1, the right superior parietal lobule and the right primary somatosensory cortex, the right insula and parts of the basal ganglia, such as the right putamen (Figure 43, right).

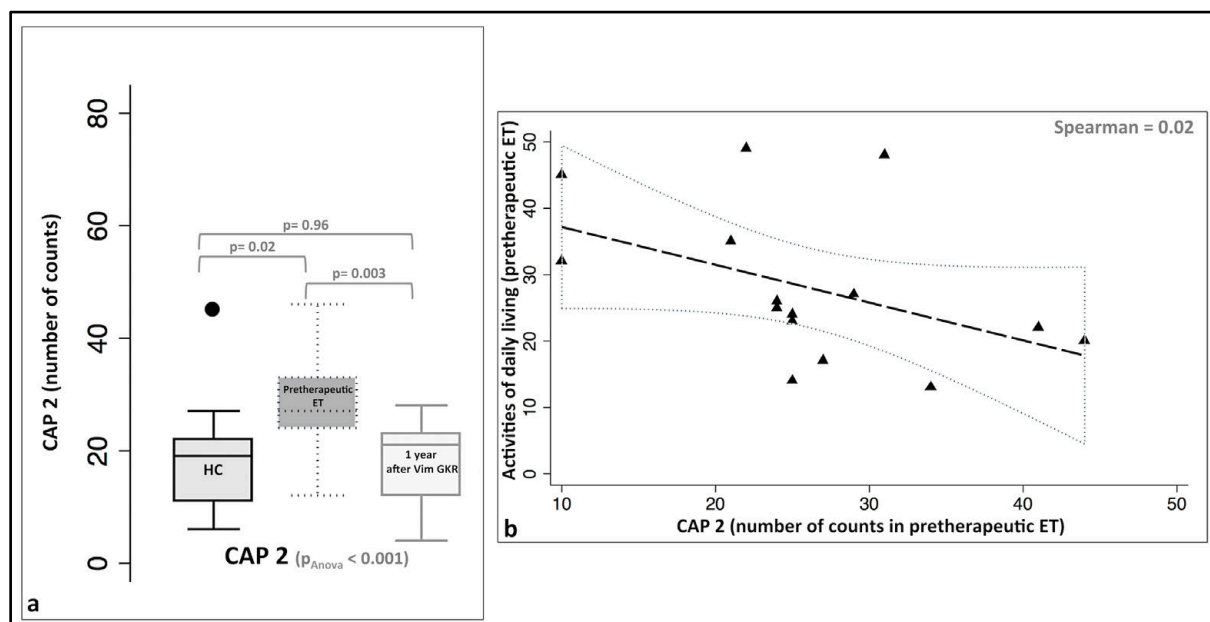


Figure 44: a-illustration of the number of counts, as boxplots, for CAP 2, in ET, HC and post-Vim GKR states, with associated p-values; b-correlation between pretherapeutic ADL and the number of counts for CAP2

In conclusion, multiple regression analysis showed that pretherapeutic standard tremor scores negatively correlated with the increase occurrence of the thalamo-visuo-motor network, suggesting a rather compensatory pathophysiological trait. The clinical improvement after thalamotomy was related to changes of occurrences of the basal ganglia and extrastriate cortex circuitry, which came back to HC values after the intervention, which suggests a role of dynamics of the extrastriate cortex in tremor intervention. This also suggests a broader implication of the visual system in tremor generation, and not only through visual feedback, given its connections on the dorsal-stream visual pathway, and the cerebello-thalamo-cortical circuitry, with which its dynamic balance seems to be crucial for reduced tremor.

5.5.4. General discussion of radiobiology of Vim GKR in ET

There is an emerging literature concerning the potential role of the visual system in tremor, as well as of a visually sensitive structural and functional network in tremor in general and ET in particular. The candidate, using multiple computational approaches, has also shed new light on this novel and interesting pathophysiological aspect.

It has been previously advocated that vision is critical for the performance of basic motor tasks, particularly those tasks which require a degree of fine motor control and dexterity⁷⁷. Furthermore, reports of the tremor-vision association have provided subjects with an amplified view of their tremor, which has already been acknowledged⁷⁸. The hypothesis of such studies was that in neurologically intact subjects, a potential tremor presence at the level of the distal segment is so small that subtle changes in tremor amplitude cannot be detected by the visual system⁷⁹. One might think that by amplifying the tremor image (but not tremor itself), the visual system might be better capable to perceive the small amplitude tremor inherent to each limb segment. Furthermore, this type of reaction could potentially allow for greater control of the limb segment in question. This has not been conclusively demonstrated, in the sense that augmented visual feedback would minimize finger tremor⁷⁸. However, this amplification approach is broadly adopted in microsurgery, so as to maximize accuracy and precision⁸⁰. Most probably, while visual feedback plays a role, other factors might be involved in tremor influence, such as the goal of the task, the number of the involved segments, the dexterity, etc.

Moreover, in ET, Gironell *et al.*⁷⁰ analyzed 19 patients, while recording neurophysiologic tremor with a tri-axial accelerometer transducer attached to the dorsal surface of the index finger of the most affected hand. One recording was made with visual feedback (eyes opened) and the other without visual feedback (eyes closed) and the order of the two recordings was randomized. The authors concluded that tremor significantly improved in the absence of a visual feedback. Possible hypotheses remained a visual component of tremor, but also that visual feedback might increase patient anxiety, increasing also in turn muscle activity and therefore tremor⁷⁰.

Additional evidence came from structural studies, evaluating pretherapeutic gray matter density (GMD), but also its changes after thalamotomy for ET, as related to clinical effect. We have postulated that a widespread visually-sensitive structural network in ET is affected by Vim GKR^{72, 211}. Additional reports using DTI²⁷¹ revealed visuospatial function correlation with the right parieto-occipital lobe. Furthermore, functional studies have brought new evidence of a visually sensitive network in essential tremor. In an observational study, Archer *et al.*²⁷² used task-based fMRI and suggested the involvement of the extrastriate areas V3 and V5, as related to tremor severity in patients with essential tremor (ET). The authors

obtained right hand force measurements during functional MRI of a grip force task while they manipulated visual feedback. The conclusion was that the severity of tremor is exacerbated by increased visual feedback, suggesting that designers of new computing technologies should consider using lower visual feedback to reduce tremor in ET. This aspect is in perfect concordance with previous observations in a randomized trial in ET, which concluded that tremor significantly improved in the absence of a visual feedback⁷⁰. We implemented an interventional study, and investigated ET patients using resting-state fMRI²⁴¹, acquired before and 1 year after Vim GKR. The results have been already underlined and prompt towards a visually sensitive functional network in ET, which responds to Vim GKR^{71, 223, 250}. Other functional studies, including one recent resting-state (18F)-FDG PET/CT, considered the brain glucose metabolism in 10 patients with ET²⁷³, and reported an unexpected hypermetabolism in primary and association visual cortices.

The thalamus versus the cerebellum could be seen as a calibrator of the relationship between the “tremor ax” and the visual system. It is now well acknowledged that the cerebello-thalamo-cortical loops play a major role in the emergence of pathological tremor and voluntary rhythmic movements²⁷⁴. Recent evidence has even suggested that there are specific fingerprints between essential, Parkinsonian’s and mimicked tremors²⁷⁴. However, despite the subtle differences in cerebellar source topography, the authors found no evidence that the cerebellum is the source of oscillation in essential tremor, or that the cortico-bulbo-cerebello-thalamo-cortical loop plays different tremorogenic roles in ET²⁷⁴. Other studies revealed, by coherent source activity, parts of the “tremor axis”, including the cerebellum, the thalamus, or the motor and premotor cortex²⁷⁵. Moreover, some authors considered the cerebellar source in ET as being the motor cerebellum²⁷⁶.

In metabolic studies, magnetic resonance spectroscopy has suggested decreased levels of N-acetylaspartate in the cerebellum. This particular finding would be related to a loss or dysfunction of neurons²⁷⁷. It has been further advocated that cerebellar metabolism is high at rest, increases with arm extension²⁷⁸, and decreases with ethanol administration (which is known to suppress ET)²⁷⁹. Pathological studies²⁸⁰, although not all of them²⁸¹, have shown a Purkinje’s cell loss in the cerebellum. Increased gamma-aminobutyric acid (GABA) has also been reported in the cerebellum of people with ET²⁸².

We postulated that a cerebello-thalamo-visuo-motor network is responsible for tremor arrest after thalamotomy by GKR²²³. We advocated that this pathophysiological feature is explanatory for a more prominent role, rather than a simple, individual, adaptive trait. We suggested that interconnectivity between the cerebellum lobule VI and bilateral motor cortex would have a prone role in sensory guidance of movements of hands and fingers, and further in movement control²⁴¹, placing the cerebellum as a “calibrator” between the visual and motor systems. We thus hypothesized that the input from the visual to the contralateral motor

network could be regulated by the cerebellum, which was also based upon previously published data²¹⁰. Furthermore, other authors have suggested a similar circuitry, based on task-based fMRI findings²⁸³. In our work in perspective, using CAP, we found that resting-state functional connectivity of the extrastriate cortex reveals different dynamic co-activation patterns. Moreover, these patterns are equally distributed between a “cerebello-visuo-motor”, a “thalamo-visuo-motor” and a “basal ganglia and extrastriate” network. In this research project, a clinical improvement after Vim GKR is more related to changes within the basal ganglia and extrastriate cortex circuitry. All these networks aligned ET patients to HC at 1 year after Vim GKR, suggesting a role of the extrastriate cortex and its dynamic connectivity in tremor generation and further arrest after interventional procedures. This opens the discussion for a potential new target for tremor, as we previously advocated in earlier studies, aiming at the extrastriate cortex^{71, 72, 211, 223}. Whether the changes in the circuitry of the extrastriate cortex are adaptive to tremor, or rather relate to tremor generation itself, remains to be discussed and confirmed by further studies.

5.5.5. Strengths and limitations

The strengths of our rs-fMRI studies are several. One is the minimal patient compliance and the extraction of rich information, using powerful computational approaches. The second is related to the absence of prior hypothesis (for the ICA studies), showing new and interesting findings (e.g. the cerebello-thalamo-visuo-motor network), which could improve the current understanding of ET’s pathophysiology, but also the radiobiology of Vim GKR at large. Concerning this former aspect, one might think that in the future, using a particular functional connectivity profile, we could better select patients for Vim GKR, improving the efficacy, while decreasing the toxicity of this procedure. This aspect is not, however, the only important one. A genetic sampling, individual patient’s other disease etc could contribute to the current heterogeneity of the results.

Our study has a number of limitations. One is the still relatively small number of subjects. Another one, related to study design, is the use of resting-state data, which might not be directly related to motor performance; however, we aimed at studying network changes in the absence of a task. Furthermore, the neurological evaluation was not blinded. Thalamic clustering procedure, although robust and reproducible has the same limitations as all clustering procedures from diffusion data. Furthermore, by employing multiple registration steps, we could have introduced errors; however, we meticulously confirmed registration accuracy at each step to alleviate the impact of this issue. Additionally, we did not extract for subsequent analysis the exact MR signature; however, we were interested in an automated

definition method and, furthermore, the average observed effect of the VLV FC was independent on the MR signature volume.

Conclusion and perspectives

6.1. Summary of MD-PHD thesis contribution

The first major contribution of this thesis is the image analysis developed to explore the advantages and pitfalls of the 7 T MRI, in the context of its potential usefulness in functional neurosurgery. The candidate was able to evaluate if SWI at 7 T is valuable to improve Vim GKR targeting, a crucial step of this procedure. In a pilot study using multi-modal imaging, both at 3 and 7 T, the candidate individually contoured the visually distinguishable Vim on 7 T SWI. Moreover, he performed the targeting using the quadrilateral of Guiot, alike in a real clinical realm. Working in binome with Elena Najdenovska, in the frame of her PhD thesis, she performed an automated thalamus segmentation using 3 T DWI, but also an automated segmentation using atlases on the same cases. The targeting points (e.g. by Guiot), showed confined localization inside the manually delineated Vim, which was contained by the VLV cluster from diffusion data. This preliminary work and its proof of concept could help minimally invasive techniques, such as Vim GKR or HIFU, to pass from an indirect targeting towards a direct one. This could be of major help for this step of the procedure, as Vim GKR relies only on neuroimaging for targeting and follow-up. This work has been extended to other types of thalamic nuclei and their respective direct visualization at 7 T, with further comparison with diffusion-based segmentation data. The candidate concluded that while 7 T is of potential benefit, several disadvantages exist and data should be validated in a larger cohort. Image processing techniques should be further used to improve the intrathalamic contrast in the SWI sequence and further gain in visibility with regards to different nuclei and their delineation, especially in elderly subjects, where this contrast at 7 T is different as compared with the younger ones.

The second major contribution is a better understand of the Vim GKR radiobiology in ET. Several findings of our analysis have prompted out toward a basal ganglia network. This aspect was, however, not astonishing, and has a pathophysiological relevance, already acknowledged by other authors. Moreover, pretherapeutic inferior olivary nucleus interconnectivity with motor areas has been illustrated as predictive for tremor improvement one year after Vim GKR. More important was the discovery of a visually sensitive structural and functional network, which is involved in tremor generation and further arrest after Vim GKR. This aspect has been underlined by several, different, convergent computational approaches, in the frame of the present thesis, using both VBM and rs-fMRI

analysis. Some of the statistical methods did not use any prior hypothesis, while others were based on the assumption of the motor thalamus as a core of the cerebello-thalamo-cortical network. This visual network might be, in fact, an integrated part of what the candidate named the “cerebello-thalamo-visuo-motor” network, calibrated either by the thalamus itself, or by the cerebellum. Another aspect was the eventual balance between the salience networks and the motor ones, interconnected with visual association areas, and with opposite pretherapeutic interconnectivity tendencies, which could predict the degree of tremor alleviation 1 year after Vim GKR. We there concluded that those patients having this visual network more integrated pretherapeutically had better chances of clinical improvement after radiosurgery for tremor. This visual network comprises mainly parts of the extrastriate cortex, with different roles, already underlined during the respective section. The eye-hand coordination in ET looks to be an appealing pathophysiological theory and should be further validated by other studies.

A third contribution is related to an overall evaluation of longitudinal structural and functional changes after Vim GKR, beside the one involving the visual system.

Dorsal attention and salience networks have been described by other authors as presenting an increase in FC in ET patients as compared with HC, as a probable compensatory mechanism. We were able to demonstrate that Vim GKR brings FC in these networks close to zero, one year after the intervention. Other relevant changes involved the anterior insula, which we proposed as a hub between salience and motor networks or the supplementary motor area (SMA). Moreover, were described FC modifications within language related areas (BA 47), meaning and phonology (BA 40), or selective response suppression in go/no-go tasks and hand movements (BA 44).

A fourth contribution was related to the illustration of abnormal functional connectivity of other anatomical structures, than the ones already described in the literature, in ET. As an example, the PPN had already an advocated role in PD with axial symptoms, as a target for DBS, as these patients are considered less responsive to STN DBS. The PPN is involved in modulation of gait. The candidate was able to illustrate, for the first time, that pretherapeutic FC of the motor thalamus with this brainstem structure correlated with baseline tremor scores. This aspect opens the nice perspective of a more in depth study in cases with ET and axial symptoms, as a correlation between FC with balance scores and their eventual improvement after radiosurgery.

A fifth contribution was the study of some particular phenotypes of ET, including those with head tremor²²². Though not detailed in the present thesis, the candidate was able to show, using a methodology implying no prior hypothesis, that an abnormal resting-state connectivity between the supplementary motor area and the limbic system predicts head tremor arrest after Vim GKR. Using computational approaches with prior hypothesis, it has

been suggested in the frame of this project that abnormal connectivity between the motor thalamus and fusiform gyrus would be related to the appearance of head tremor and further arrest after Vim GKR. An adaptive mechanism was suggested for the former, as Vim GKR brought FC values close to the HC one year after the intervention.

A sixth contribution was the proposal of new therapeutic targets in ET. This proposal was mainly related to parts of the right extrastriate cortex and should be investigated by other studies, ideally in larger and randomized cohorts.

6.2. Overall limitations

A limitation of the SWI at 7 T was the unstandardized contrast variation among different subjects, especially noticeable between the young and elderly population. In addition, random appearance of blood vessels inside the thalamic region might also alter the provided information. In this sense, efforts should be made in optimizing the SWI contrast and further provide clearer discrimination between the different borders of directly visible thalamic nuclei. Moreover, it could be further employed in automated segmentation approaches, such as the coupled level set functions as already used for exploring the diffusion information.

A limitation of the radiobiological part was the relatively small number of subjects. However, despite the previous, the results presented were strongly statistically significant. To overwhelm this limitation we currently acquire, with the help of Professor Régis in Marseille, a larger cohort. The candidate explores the rs-fMRI data using a different and recent perspective, while testing a beta version of a software developed in MipLab (Professor Van de Ville, Thomas Bolton). This is related to connectivity activation patterns, previously briefly described.

6.3. General perspectives

Ventro-intermediates nucleus radiosurgery for intractable tremor is gaining interest and acceptance. As an alternative to open surgical procedures, its role as a first choice indication is becoming more prominent. Because of incomplete understanding of its radiobiological effects, progress needs to be made to open new avenues towards disrupting borders for the use of radiosurgery. Imaging techniques become more user-friendly and develop quickly (e.g. 7 Tesla acquisitions with special sequences such as SWI, but also fMRI, PET, SPECT) and the software and computer technology develop quickly as well. This allows progress to be made concerning radiosurgical planning parameters, with high conformity and high selectivity planning (rapid dose fall-off). Also, expensive multicentric trials are

conducted worldwide to confirm the applicability of radiosurgery as a first-line treatment.

Considered to be a disruptive innovation by one of its pioneers ⁷, GKR has to make a step forward towards the understanding of its intimate mechanisms in the 21-st century. The lack of radiobiological knowledge is not only limited to the case of the Vim RS. Another interesting example comes from the GKR treatment of arterio-venous malformations (AVM) presenting with epilepsy. Interestingly, seizure cessation in these patients frequently occurs before the AVM occlusion or even sometimes despite a failure of occlusion of the nidus ²⁸⁴. Moreover, in AVM located in functional areas such as the motor cortex, there is no neurological deficit after GKR, while epilepsy resolves and AVM occludes. This illustrates that the biological changes affect some processes (e.g. the seizures) while sparing others (e.g. normal brain function), together with achieving the desire effect (AVM occlusion). Another issue is related to the possible genetics involved in human variability of response to radiosurgery.

Radiosurgery and particularly GKR will gradually overtake and overwhelm the existing invasive neurosurgical approaches. Radiosurgical planning will be made according to a desire radiobiological effects in close relationship with biologically effective doses (BED), directly connected to physical dose but also to some indirect parameters, such as target volume, tissue consistence and radiation dose rate. With that respect, we hope that our research project will contribute to better define these parameters.

In this research project, we have decided to focus on Vim GKR, as we believe that it represents a “pure model” of to study GKS for several reasons. First, there is no underlying lesion to be treated (such as tumor, AVM, ...) which may have accounted for variability on a case by case basis. Second, the targeting is set on similar fixed MRI stereotactic coordinates, aiming at exactly the same target, using a unique shot of 4 mm, and a similar dose prescription in all patients, which guarantee the technical reproducibility of the procedure. Thus, we believe that this “model” represents the best approach to study tissue reactions and clinical effects, and their variability. Improving understanding of its effects both in targeting and radiobiology, it opens further directions of comprehension and application of radiosurgery to other pathologies- not only for functional disorders- such as epilepsy (MTLE, hypothalamic hamatroma), trigeminal neuralgia, but it may also improve the application of radiosurgery for other conditions such as brain tumors and vascular disorders. Thus, our research project has tentatively a wider application range...

We hope that our findings might lead, in the future, to eventual safer, less expensive and more effective methods of neuro-enhancement and further turn decades of hard work into real-life benefits.

Figure Legends:

Figure 4: artistic representation of: **a-** how the gantry of the Cobalt-60 machine is focusing Gamma radiation on the targeted region, while minimizing the amount of radiation that passes through the nearby regions; in the illustrated case, the patient has attached to the head a stereotactic frame; **b-** Gamma Knife machine (adapted from <http://philschatz.com/chemistry-book/contents/m51203.html>)

Figure 5: Overall vision of the anatomical location of the thalamus in humans, on sagittal (lateral, upper part) view; simplified view of the internal structure (lower part), as adapted, with permission from Doctor Jerry L- Prince, from “A novel contrast for DTI visualization for thalamus delineation”, Fan et al.²⁷, Fan X., Thompson M., Bogovic A., Bazin P.-L., Prince J., DOI: 10.117/12.844473, SPIE Medical Imaging 2010, San Diego, California, United States, Proc SPIE 762533

Figure 6: Illustration of parcellation of the thalamus, in axial plane, as depicted in: **a-** the Schaltenbrand’s³¹ or **b-** Morel’s atlas³⁰; while both are based on histological delineation, different subdivision patterns can be seen

Figure 4: activities of daily living impaired by tremor: eating and drinking, dressing, writing (with permission from *Jama Neurology*, Muth et al.⁵¹, American Medical Association, DOI: 10.1001/jama.2016.16376)

Figure 5: reproduced with permission from Haubenberger and Hallett⁵⁴ (*New England Journal of Medicine*, Copyright Massachusetts Medical Society): artistic representation of presumed pathways involved in the pathophysiology of ET: the cortico-ponto-cerebello-thalamo-cortical loop and the dentate nucleus-red nucleus-inferior olivary nucleus-dentate nucleus; are illustrated also the Vim, the zona incerta and the prelemniscal radiation, as areas successfully targeted in drug-resistant tremor

Figure 6: Surgical interventions for drug-resistant essential tremor: upper part, invasive procedures, with electrode implantation inside the brain: electrical stimulation (left), radiofrequency thalamotomy (right); lower part, minimally invasive procedures: radiosurgery (left), high-focused ultrasound (right), adapted from doi.org/10.1093/brain/awy096

Figure 7: The thalamus appearance on T1 weighted imaging (right panel), with corresponding axial slice from the Schaltenbrand’s atlas (left)³¹, modified and adapted from Abosch et al.³⁴; one can see the absence of intrinsic contrast for distinguishing different thalamic subparts, as the former appear like an homogenous region

Figure 8: targeting of the ventro-intermediate nucleus of the thalamus by radiosurgery: a, use of non-stereotactic DTI, to visualize the internal capsule and limit the irradiation doses towards this structure; b, the quadrilatere of Guiot; c, the placement of a unique 4-mm shot, with the isodoses of 90 and 15 Gy colored in green

Figure 9: a, minimal MR signature; b, the classical “cocade” aspect; c, larger MR signature

Figure 10: **a**, adapted from Steiner et al.¹³¹, first human autopsies after thalamotomy for pain; reproduced with permission from Springer Nature **b**, adapted from Kondziolka et al.¹⁴², 6 months after baboon irradiation, with 100 Gy, ventral thalamus (main image: hematoxylin and eosin stain, showing thalamic tissue within the radiosurgical target, with vascular hyalinization and wall thickening typical of radiation vasculopathy being prominent; secondary image, MRI of the irradiated zone); reproduced with permission from Karger Publishers

Figure 11: **a**, image extracted from Abosch et al.³⁴, showing SWI acquisition thalamic level (axial slice, right side); **b**, image acquired on a healthy subject at Center of Biomedical Imaging (CIBM), Lausanne, Switzerland, showing different thalamic subparts, including the Vim (courtesy and draw by E. Najdenovska)

Figure 12: Preprocessing steps for VBM analysis: **a**, initial T1 weighted image; **b**, normalized images; **c**, gray matter extraction; **d**, smoothed image; **e**, final cluster (data from patients treated in CHU Timone, Marseille)

Figure 13: Artistic illustration of how we can pass from the neuronal activity to fMRI BOLD response (Courtesy of the USC Laboratory of Neuroimaging and Athinoula A. Martinos Center for Biomedical Imaging, Consortium of the Human Connectome Project-www.humanconnectomeproject.org)

Figure 14: Illustration of an FA map, with the internal capsule, the Vim RS isocenter and the RAPRL location, in a patient treated in Marseille (CHU Timone), France

Figure 15: Schematic overview of the methods used to define the Vim in the present thesis¹⁸⁷ (*functional definition refers to its validation in functional neurosurgery)

Figure 16: Schematic overview of the registrations applied for transforming into the common image space¹⁸⁷

Figure 17: Illustration of the visible structures corresponding to the thalamic area in axial view on the SWI acquired at 7T, based upon the illustration from the pioneering work of Abosch et al.³⁴. In panel A the SWI features are compared with the Schalterbrand atlas (plate 53 Hd +3.5) superimposed on the right thalamus. The arrows and the respective color contours indicate the nuclei: Vim, Pulvinar (Pu), ventro-caudalus (Vc), ventro-odalis (Vo), the medio-dorsal group (MD) and the internal capsule (ic). The shown SWI image is part of the dataset used in this study. Panel B gives a corresponding axial plate of the Morel's atlas where the (same) color (shade) matches appropriate regions of the Shalterbrand's atlas, while keeping the same nomenclature used in each one of them. In fact, considering the Morel's atlas³⁰ nomenclature, Vim is part of the Ventro-Lateral-posterior nuclei, which furthermore, together with ventro-lateral anterior and ventro-posterior nuclei form the VLV cluster¹⁸⁷

Figure 18: Schematic representation of the ROIs separation in 8 regions, in 2D and 3D view (middle). The labeling of the subparts is done according to the hemispheres to which the ROI belongs¹⁸⁷.

Figure 19: Boxplot showing the difference between the six targeting points obtained by the quadrilateres of Guiot for each subject respectively (in the healthy subjects, YS1 to YS5)¹⁸⁷

Figure 20: Illustration of the difficulties encountered for the manual delineation of the Vim regarding the image contrast on SWI acquired at 7T and the presence of blood vessels in the targeted area. We can observe that the contrast varies between subjects, but also between the two groups, young (here YS1 and YS2) versus the elderly (ES2 and ES3). The arrow for Subject YS1, illustrates the relatively big blood vessel passing through the left targeted thalamic region that prevented manual discrimination of the Vim. The presence of small vessels surrounding the Vim can be observed in each panel¹⁸⁷

Figure 21: Visual representation of the comparison between the methods. Panel A give the results in axial view of each young subject respectively (YS1-YS5), while panel B shows a 3D view of the Subject YS2's outlined Vim, as well as its localization inside the VLV cluster and within the thalamus. Among the shown findings, the Guiot points are given in magenta, the manual Vim delineation in yellow and the automatically segmented VLV cluster in red. The remaining automatically delineated clusters shown in panel A are: Pulvinar (Pu), medio-dorsal (MD) and the anterior (A) group of nuclei as well as the cluster enclosing the centro-lateral and the lateral posterior nuclei along with the medial part of the Pulvinar (CL-LP-PuM). It can be seen that for all the subjects the Guiot points are always inside and/or on the border of the manual delineation, which furthermore is observed in the anterior-lateral part of the VLV cluster close to its lateral bord¹⁸⁷.

Figure 22: Visual comparison between the manual delineation and the multi-atlas outline of the Vim. The Dice coefficient estimates the overlap between the two outlines.

Figure 23: Superimposed dosimetry with the 90 Gy isodose line (green) to the therapeutic images (a), 3T (b) and 7T (c) 3 months follow-up MRI (d) and 3T 6 months follow-up MRI; please note that 7T already shows a visible MR signature corresponding to the targeted area, while at 3T nothing was yet visible

Figure 24: global overview of GMD at baseline and 1 year for left temporal pole and visual association area, depending on clinical response ($\leq 50\%$ TSTH improvement, versus $>50\%$ TSTH improvement; it is of interest that for both clusters (temporal and occipital), for a TSTH improvement $\leq 50\%$, the baseline values are lower as compared with the ones for TSTH improvement $>50\%$; at 1 year, the NR patients achieve a median value comparable to that of R at baseline, while the former remain stable;

Figure 25: correlations between TSTH improvement and differences in GMD (Spearman $\rho = 0.01$ for both clusters); left- temporal cluster, right-occipital cluster

Figure 26: left, correlation between pretherapeutic GMD (left temporal cluster) and 1 year TSTH improvement (Spearman $\rho = 0.004$); right, illustration of GMD increase (for the NR) and respectively no change (for R), as structural differences between R and NR during time, before and after Vim GKR, presented by clusters (1=left temporal and 2=left occipital, with a sagittal illustration for each one of them)

Figure 27: higher pretherapeutic GMD predicts better 1-year TSTH improvement

Figure 28: two pre-processing pipelines developed in LTS-5, Swiss Federal Institute of Technology

Figure 29: Illustrative example of 3 networks generated by the ICA approach²²⁰

Figure 30: Interconnectivity within network 12, between bilateral motor cortex and FEF with ION, reproduced with permission from doi.org/10.1111/ane.12891

Figure 31: Interconnectivity within network 13, between bilateral thalamus with left cerebellar lobule V, reproduced with permission from doi.org/10.1111/ane.12891

Figure 32: Interconnectivity within network 14, between DMN and salience with BA 10, reproduced with permission from doi.org/10.1111/ane.12891

Figure 33: Main component 9 (IC with MNI -30 8 0), from left to right: anatomical images, boxplots and corresponding values by group, as well as difference in IC 1 year after Vim GKR, allowing a clear separation between groups, reproduced with permission from doi.org/10.1007/s00701-017-3456-x

Figure 34: Main component 13 (IC with MNI 32 -80 10), from left to right: anatomical images, boxplots and corresponding values by group, as well as difference in IC 1 year after Vim GKR, allowing separation between groups, reproduced with permission from doi.org/10.1007/s00701-017-3456-x

Figure 35: Adapted from Brain²²³, with permission: right, main effect of time: upper part, interconnectivity between the main network, including remnant salience network with right fusiform gyrus (including V5); middle part, boxplot illustration of overall interconnectivity values in pre- and posttherapeutic states; lower part, boxplot illustration with regard to the group clinical effect (with less or equal and more than 50% improvement); left, interaction between clinical effect and time: upper part, interconnectivity between the main network, including left cerebellum lobule VI, frontal eye fields and bilateral motor cortex with right visual association area (Brodmann area 19, including V3, V4 and V5); middle part, pretherapeutic interconnectivity predicts tremor score on the treated hand improvement 1 year after Vim RS (Spearman rank correlation coefficient 0.001); lower part, boxplot illustration with regard to the group clinical effect (with less or equal and more than 50% improvement).

Figure 36: a- region-of-interest extraction by Dr Najdenovska, using a methodology, which has already been published; b- brief and artistical overview of the seed-to-voxel approach, with the 1-year MR signature volume always contained inside the VLV cluster (permission for reproducing this figure is not required, but the journal article need to be cited²²¹)

Figure 37: a- illustration of left VLV seed-to-voxel FC maps (with right visual association area), which predicts 1 year ADL's improvement; b- boxplots with the FC values for HC, baseline ET and

ET 1 year after SRS-T; **c-** the illustration of mean, median, standard deviation and range for each of the groups (permission for reproducing this figure is not required, but the journal article need to be cited²⁵⁰)

Figure 38: a- illustration of left VLV seed-to-voxel FC maps (with left fusiform gyrus), which predicts 1 year head tremor improvement (n=11, for pretherapeutic head tremor score ≥ 1); ; b- boxplots with the FC values for HC, baseline ET and ET 1 year after Vim GKR; c- the illustration of mean, median, standard deviation and range for each of the groups (permission for reproducing this figure is not required, but the journal article need to be cited²⁵⁰)

Figure 39: Difference in FC between HC and ET in (from left to right): left primary somatosensory area, pedunculo pontine nucleus, and dorsal anterior cingulate (permission for reproducing this figure is not required, but the journal article need to be cited²²¹)

Figure 40: decreased pretherapeutic FC of left VLV with pedunculo pontine nucleus as compared with HC (Spearman= 0.01) correlates with baseline ADL (permission for reproducing this figure is not required, but the journal article need to be cited²²¹)

Figure 41: ET patients, as compared with HC, showed increased left FC with left visual association cortex (BA19, $p_{FWE-corr}=0.005$) and left superior parietal regions (BA 7, $p_{FWE-corr}=0.014$) (permission for reproducing this figure is not required, but the journal article need to be cited²²¹)

Figure 42: Illustration of differences of left VLV seed-to-voxel FC values for the statistically significant clusters in pretherapeutic – 1 year after Vim GKR: right insular and orbito-frontal (**a**), posterior parietal cortex (**b**), left anterior insular cortex (**c**), right inferior frontal gyrus and frontal-eye fields (**d**) (permission for reproducing this figure is not required, but the journal article need to be cited²²¹)

Figure 43: Illustration of connectivity activation patterns in our population, from 1 to 3 (left to right)

Figure 44: a-illustration of the number of counts, as boxplots, for CAP 2, in ET, HC and post-Vim GKR states, with associated p-values; b-correlation between pretherapeutic ADL and the number of counts for CAP2

References

1. Leksell L. The stereotaxic method and radiosurgery of the brain. *Acta chirurgica Scandinavica*. 1951 Dec 13;102(4):316-9.
2. Leksell L. Cerebral radiosurgery. I. Gammathalanotomy in two cases of intractable pain. *Acta Chir Scand*. 1968;134(8):585-95.
3. Larsson B. The high-energy proton beam as a neurosurgical tool. *Nature*. 1958;182(4644):1222-3.
4. Leksell L, Larsson B, Andersson B, Rexed B, Sourander P, Mair W. Lesions in the depth of the brain produced by a beam of high energy protons. *Acta radiologica*. 1960 Oct;54:251-64.
5. Tuleasca C, Leroy HA, Regis J, Levivier M. Gamma Knife radiosurgery for cervical spine lesions: expanding the indications in the new era of Icon. *Acta neurochirurgica*. 2016 Nov;158(11):2235-6.
6. Hamilton T, Dade Lunsford L. Worldwide variance in the potential utilization of Gamma Knife radiosurgery. *Journal of neurosurgery*. 2016 Dec;125(Suppl 1):160-5.
7. Niranjana A, Madhavan R, Gerszten PC, Lunsford LD. Intracranial radiosurgery: an effective and disruptive innovation in neurosurgery. *Stereotactic and functional neurosurgery*. 2012;90(1):1-7.
8. Szeifert GT, Atteberry DS, Kondziolka D, Levivier M, Lunsford LD. Cerebral metastases pathology after radiosurgery: a multicenter study. *Cancer*. 2006 Jun 15;106(12):2672-81.
9. Szeifert GT, Kondziolka D, Atteberry DS, et al. Radiosurgical pathology of brain tumors: metastases, schwannomas, meningiomas, astrocytomas, hemangioblastomas. *Prog Neurol Surg*. 2007;20:91-105.
10. Szeifert GT, Kondziolka D, Levivier M, Lunsford LD. Histopathology of brain metastases after radiosurgery. *Prog Neurol Surg*. 2012;25:30-8.
11. Szeifert GT, Major O, Kemeny AA. Ultrastructural changes in arteriovenous malformations after gamma knife surgery: an electron microscopic study. *J Neurosurg*. 2005 Jan;102 Suppl:289-92.
12. Szeifert GT, Salmon I, Baleriaux D, Brotchi J, Levivier M. Immunohistochemical analysis of a cerebral arteriovenous malformation obliterated by radiosurgery and presenting with re-bleeding. Case report. *Neurol Res*. 2003 Oct;25(7):718-21.
13. Szeifert GT, Timperley WR, Forster DM, Kemeny AA. Histopathological changes in cerebral arteriovenous malformations following Gamma Knife radiosurgery. *Prog Neurol Surg*. 2007;20:212-9.
14. Tuleasca C, Pralong E, Najdenovska E, et al. Deep brain stimulation after previous gamma knife thalamotomy of the Vim for essential tremor is feasible! Clinical, electrophysiological and radiological findings. *Acta neurochirurgica*. 2017 Jul;159(7):1371-3.
15. Witjas T, Carron R, Krack P, et al. A prospective single-blind study of Gamma Knife thalamotomy for tremor. *Neurology*. 2015 Nov 3;85(18):1562-8.

16. Kondziolka D, Flickinger JC, Hudak R. Results following gamma knife radiosurgical anterior capsulotomies for obsessive compulsive disorder. *Neurosurgery*. 2011 Jan;68(1):28-32; discussion 23-3.
17. Kondziolka D, Zorro O, Lobato-Polo J, et al. Gamma Knife stereotactic radiosurgery for idiopathic trigeminal neuralgia. *Journal of neurosurgery*. 2010 Apr;112(4):758-65.
18. Massager N, Lorenzoni J, Devriendt D, Desmedt F, Brotchi J, Levivier M. Gamma knife surgery for idiopathic trigeminal neuralgia performed using a far-anterior cisternal target and a high dose of radiation. *Journal of neurosurgery*. 2004 Apr;100(4):597-605.
19. Regis J, Metellus P, Hayashi M, Roussel P, Donnet A, Bille-Turc F. Prospective controlled trial of gamma knife surgery for essential trigeminal neuralgia. *Journal of neurosurgery*. 2006 Jun;104(6):913-24.
20. Bartolomei F, Hayashi M, Tamura M, et al. Long-term efficacy of gamma knife radiosurgery in mesial temporal lobe epilepsy. *Neurology*. 2008 May 06;70(19):1658-63.
21. Regis J, Carron R, Park M. Is radiosurgery a neuromodulation therapy? : A 2009 Fabrikant award lecture. *Journal of neuro-oncology*. 2010 Jun;98(2):155-62.
22. Haber SN. The primate basal ganglia: parallel and integrative networks. *Journal of chemical neuroanatomy*. 2003 Dec;26(4):317-30.
23. Lambert C, Simon H, Colman J, Barrick TR. Defining thalamic nuclei and topographic connectivity gradients in vivo. *NeuroImage*. 2017 Sep;158:466-79.
24. Fan Y, Nickerson LD, Li H, et al. Functional Connectivity-Based Parcellation of the Thalamus: An Unsupervised Clustering Method and Its Validity Investigation. *Brain connectivity*. 2015 Dec;5(10):620-30.
25. Ji B, Li Z, Li K, et al. Dynamic thalamus parcellation from resting-state fMRI data. *Human brain mapping*. 2016 Mar;37(3):954-67.
26. Hanbery J, Ajmone-Marsan C, Dilworth M. Pathways of non-specific thalamo-cortical projection system. *Electroencephalography and clinical neurophysiology*. 1954 Feb;6(1):103-18.
27. Fan X, Thompson M, Bogovic JA, Bazin PL, Prince JL. A Novel Contrast for DTI Visualization for Thalamus Delineation. *Proceedings of SPIE--the International Society for Optical Engineering*. 2010 Feb 13;7625.
28. Herrero MT, Barcia C, Navarro JM. Functional anatomy of thalamus and basal ganglia. *Child's nervous system : ChNS : official journal of the International Society for Pediatric Neurosurgery*. 2002 Aug;18(8):386-404.
29. Guillery RW. Anatomical evidence concerning the role of the thalamus in corticocortical communication: a brief review. *Journal of anatomy*. 1995 Dec;187 (Pt 3):583-92.
30. Morel A, Magnin M, Jeanmonod D. Multiarchitectonic and stereotactic atlas of the human thalamus. *The Journal of comparative neurology*. 1997 Nov 03;387(4):588-630.
31. Schaltenbrand G, Wahren W, Hassler H. Atlas for Stereotaxy of the Human Brain. Thieme, editor1977.

32. Wiegell MR, Tuch DS, Larsson HB, Wedeen VJ. Automatic segmentation of thalamic nuclei from diffusion tensor magnetic resonance imaging. *NeuroImage*. 2003 Jun;19(2 Pt 1):391-401.
33. Battistella G, Najdenovska E, Maeder P, et al. Robust thalamic nuclei segmentation method based on local diffusion magnetic resonance properties. *Brain structure & function*. 2016 Nov 25.
34. Abosch A, Yacoub E, Ugurbil K, Harel N. An assessment of current brain targets for deep brain stimulation surgery with susceptibility-weighted imaging at 7 tesla. *Neurosurgery*. 2010 Dec;67(6):1745-56; discussion 56.
35. Massion J. The thalamus in the motor system. *Appl Neurophysiol*. 1976;39(3-4):222-38.
36. Bosch-Bouju C, Hyland BI, Parr-Brownlie LC. Motor thalamus integration of cortical, cerebellar and basal ganglia information: implications for normal and parkinsonian conditions. *Frontiers in computational neuroscience*. 2013;7:163.
37. Guiot G, Hardy J, Albe-Fessard D. [Precise delimitation of the subcortical structures and identification of thalamic nuclei in man by stereotactic electrophysiology]. *Neurochirurgia (Stuttg)*. 1962 Apr;5:1-18.
38. Tuite PJ, Dagher A. *Magnetic resonance imaging in movement disorders : a guide for clinicians and scientists*. Cambridge: Cambridge University Press; 2013.
39. Louis ED. Essential tremor. *The Lancet Neurology*. 2005 Feb;4(2):100-10.
40. Louis ED. Clinical practice. Essential tremor. *The New England journal of medicine*. 2001 Sep 20;345(12):887-91.
41. Louis ED. Essential tremor. *Archives of neurology*. 2000 Oct;57(10):1522-4.
42. Brennan KC, Jurewicz EC, Ford B, Pullman SL, Louis ED. Is essential tremor predominantly a kinetic or a postural tremor? A clinical and electrophysiological study. *Movement disorders : official journal of the Movement Disorder Society*. 2002 Mar;17(2):313-6.
43. Critchley M. Observations on essential (heredofamial) tremor. *Brain : a journal of neurology*. 1949 Jun;72(Pt. 2):113-39.
44. Louis ED. Essential Tremor with Head Tremor: Trait or State? *The Canadian journal of neurological sciences Le journal canadien des sciences neurologiques*. 2016 May;43(3):443-4.
45. Robakis D, Louis ED. Head tremor in essential tremor: "Yes-yes", "no-no", or "round and round"? *Parkinsonism & related disorders*. 2016 Jan;22:98-101.
46. Jimenez-Jimenez FJ, Rubio L, Alonso-Navarro H, et al. Impairment of rapid repetitive finger movements and visual reaction time in patients with essential tremor. *European journal of neurology*. 2010 Jan;17(1):152-9.
47. Benito-Leon J, Louis ED, Bermejo-Pareja F, Neurological Disorders in Central Spain Study G. Reported hearing impairment in essential tremor: a population-based case-control study. *Neuroepidemiology*. 2007;29(3-4):213-7.

48. Benito-Leon J, Louis ED, Bermejo-Pareja F, Neurological Disorders in Central Spain Study G. Population-based case-control study of cognitive function in essential tremor. *Neurology*. 2006 Jan 10;66(1):69-74.
49. Louis ED, Benito-Leon J, Bermejo-Pareja F, Neurological Disorders in Central Spain Study G. Self-reported depression and anti-depressant medication use in essential tremor: cross-sectional and prospective analyses in a population-based study. *European journal of neurology*. 2007 Oct;14(10):1138-46.
50. Louis ED. Essential tremors: a family of neurodegenerative disorders? *Archives of neurology*. 2009 Oct;66(10):1202-8.
51. Muth CC. Essential Tremor. *Jama*. 2016 Nov 22;316(20):2162.
52. Bain PG, Findley LJ, Atchison P, et al. Assessing tremor severity. *Journal of neurology, neurosurgery, and psychiatry*. 1993 Aug;56(8):868-73.
53. Fahn S, Tolosa E, Marin C. Clinical rating scale for tremor. *Parkinson's Disease and Movement Disorders*: Baltimore: Urban and Schwarzenberg; 1988. p. 225–34.
54. Haubenberger D, Hallett M. Essential Tremor. *The New England journal of medicine*. 2018 May 10;378(19):1802-10.
55. Buijink AW, van der Stouwe AM, Broersma M, et al. Motor network disruption in essential tremor: a functional and effective connectivity study. *Brain : a journal of neurology*. 2015 Oct;138(Pt 10):2934-47.
56. Fang W, Chen H, Wang H, et al. Essential tremor is associated with disruption of functional connectivity in the ventral intermediate Nucleus--Motor Cortex--Cerebellum circuit. *Human brain mapping*. 2016 Jan;37(1):165-78.
57. Hua SE, Lenz FA. Posture-related oscillations in human cerebellar thalamus in essential tremor are enabled by voluntary motor circuits. *Journal of neurophysiology*. 2005 Jan;93(1):117-27.
58. Hua SE, Lenz FA, Zirh TA, Reich SG, Dougherty PM. Thalamic neuronal activity correlated with essential tremor. *Journal of neurology, neurosurgery, and psychiatry*. 1998 Feb;64(2):273-6.
59. Yamamoto T, Wagner A, Hassler R, Sasaki K. Studies on the cerebellocerebral and thalamocortical projections in squirrel monkeys (*Saimiri sciureus*). *Experimental neurology*. 1983 Jan;79(1):27-37.
60. Benabid AL, Pollak P, Gao D, et al. Chronic electrical stimulation of the ventralis intermedialis nucleus of the thalamus as a treatment of movement disorders. *Journal of neurosurgery*. 1996 Feb;84(2):203-14.
61. Goldman MS, Ahlskog JE, Kelly PJ. The symptomatic and functional outcome of stereotactic thalamotomy for medically intractable essential tremor. *Journal of neurosurgery*. 1992 Jun;76(6):924-8.
62. Elble RJ. Tremor disorders. *Current opinion in neurology*. 2013 Aug;26(4):413-9.
63. Llinas R, Yarom Y. Electrophysiology of mammalian inferior olivary neurones in vitro. Different types of voltage-dependent ionic conductances. *The Journal of physiology*.

1981 Jun;315:549-67.

64. Lamarre Y, Mercier LA. Neurophysiological studies of harmaline-induced tremor in the cat. *Canadian journal of physiology and pharmacology*. 1971 Dec;49(12):1049-58.
65. Louis ED, Babij R, Cortes E, Vonsattel JP, Faust PL. The inferior olivary nucleus: a postmortem study of essential tremor cases versus controls. *Movement disorders : official journal of the Movement Disorder Society*. 2013 Jun;28(6):779-86.
66. Wills AJ, Jenkins IH, Thompson PD, Findley LJ, Brooks DJ. Red nuclear and cerebellar but no olivary activation associated with essential tremor: a positron emission tomographic study. *Annals of neurology*. 1994 Oct;36(4):636-42.
67. Hesselmann V, Maarouf M, Hunsche S, et al. Functional MRI for immediate monitoring stereotactic thalamotomy in a patient with essential tremor. *European radiology*. 2006 Oct;16(10):2229-33.
68. Gironell A, Figueiras FP, Pagonabarraga J, et al. Gaba and serotonin molecular neuroimaging in essential tremor: a clinical correlation study. *Parkinsonism & related disorders*. 2012 Aug;18(7):876-80.
69. Sharifi S, Nederveen AJ, Booij J, van Rootselaar AF. Neuroimaging essentials in essential tremor: a systematic review. *NeuroImage Clinical*. 2014;5:217-31.
70. Gironell A, Ribosa-Nogue R, Pagonabarraga J. Withdrawal of visual feedback in essential tremor. *Parkinsonism & related disorders*. 2012 May;18(4):402-3; author reply 4.
71. Tuleasca C, Najdenovska E, Regis J, et al. Clinical response to Vim's thalamic stereotactic radiosurgery for essential tremor is associated with distinctive functional connectivity patterns. *Acta neurochirurgica*. 2018 Jan 15.
72. Tuleasca C, Witjas T, Najdenovska E, et al. Assessing the clinical outcome of Vim radiosurgery with voxel-based morphometry: visual areas are linked with tremor arrest! *Acta neurochirurgica*. 2017 Sep 23.
73. Archer DB, Coombes SA, Chu WT, et al. A widespread visually-sensitive functional network relates to symptoms in essential tremor. *Brain : a journal of neurology*. 2017 Dec 22.
74. Coltz JD, Johnson MT, Ebner TJ. Cerebellar Purkinje cell simple spike discharge encodes movement velocity in primates during visuomotor arm tracking. *The Journal of neuroscience : the official journal of the Society for Neuroscience*. 1999 Mar 1;19(5):1782-803.
75. Carrie G. Finger tremor with an amplified visual display of position and following eye closure. *Journal of the neurological sciences*. 1966;3(4):329-39.
76. Carrie JR. Visual effects on finger tremor in normal subjects and anxious patients. *The British journal of psychiatry : the journal of mental science*. 1965 Dec;111(481):1181-4.
77. Cesari P, Newell KM. The scaling of human grip configurations. *Journal of experimental psychology Human perception and performance*. 1999 Aug;25(4):927-35.
78. Vasilakos K, Glass L, Beuter A. Interaction of tremor and magnification in a motor performance task with visual feedback. *Journal of motor behavior*. 1998 Jun;30(2):158-68.

79. Scobey RP, Johnson CA. Displacement thresholds for unidirectional and oscillatory movement. *Vision research*. 1981;21(8):1297-302.
80. Meola A, Cutolo F, Carbone M, Cagnazzo F, Ferrari M, Ferrari V. Augmented reality in neurosurgery: a systematic review. *Neurosurgical review*. 2017 Oct;40(4):537-48.
81. Keogh J, Morrison S, Barrett R. Augmented visual feedback increases finger tremor during postural pointing. *Experimental brain research*. 2004 Dec;159(4):467-77.
82. Feys P, Helsen W, Buekers M, et al. The effect of changed visual feedback on intention tremor in multiple sclerosis. *Neuroscience letters*. 2006 Feb 6;394(1):17-21.
83. Liu X, Miall C, Aziz TZ, Palace JA, Haggard PN, Stein JF. Analysis of action tremor and impaired control of movement velocity in multiple sclerosis during visually guided wrist-tracking tasks. *Movement disorders : official journal of the Movement Disorder Society*. 1997 Nov;12(6):992-9.
84. Thompson R, Bachman M. Zona incerta: A link between the visual cortical sensory system and the brainstem motor system. *Physiological Psychology*. 1979;7(3):251-3.
85. Power BD, Leamey CA, Mitrofanis J. Evidence for a visual subsector within the zona incerta. *Visual neuroscience*. 2001 Mar-Apr;18(2):179-86.
86. Zesiewicz TA, Elble RJ, Louis ED, et al. Evidence-based guideline update: treatment of essential tremor: report of the Quality Standards subcommittee of the American Academy of Neurology. *Neurology*. 2011 Nov 8;77(19):1752-5.
87. Louis ED. Treatment of Medically Refractory Essential Tremor. *The New England journal of medicine*. 2016 Aug 25;375(8):792-3.
88. Koller WC, Vetere-Overfield B. Acute and chronic effects of propranolol and primidone in essential tremor. *Neurology*. 1989 Dec;39(12):1587-8.
89. Lipsman N, Schwartz ML, Huang Y, et al. MR-guided focused ultrasound thalamotomy for essential tremor: a proof-of-concept study. *The Lancet Neurology*. 2013 May;12(5):462-8.
90. BUCY AC, CASE JT. PHYSIOLOGIC MECHANISM AND ABOLITION BY SURGICAL MEANS. *Arch NeurPsych* 1939 41(4):721-46.
91. Putnam TJ. The operative treatment of diseases characterized by involuntary movements (tremor, athetosis). *Res Publ Assoc Res Nerv Ment Dis* 1940;21:666-96.
92. WALKER AE. RELIEF OF PAIN BY MESENCEPHALIC TRACTOTOMY. *Arch NeurPsych*. 1942:865-83.
93. Spiegel EA, Wycis HT. Mesencephalotomy in treatment of intractable facial pain. *AMA Arch Neurol Psychiatry*. 1953 Jan;69(1):1-13.
94. Talairach J, Hécaen H, David M. Lobotomie préfrontale limitée par électrocoagulation des fibres thalamo-frontales à leur émergence du bras antérieur de la capsule interne. *Rev Neurol* 1949;83:59.
95. Voris HC, Baldwin B. Stereotaxic apparatus for operations on the human brain. *International journal of neurology*. 1965;5(1):109-13.

96. Spiegel EA, Wycis HT, Thur C. The stereoencephalotome (model III of our stereotaxic apparatus for operations on the human brain). *Journal of neurosurgery*. 1951 Jul;8(4):452-3.
97. Spiegel EA, Wycis HT, Marks M, Lee AJ. Stereotaxic Apparatus for Operations on the Human Brain. *Science*. 1947 Oct 10;106(2754):349-50.
98. Cooper IS. The neurosurgical alleviation of parkinsonism. In: Thomas CC, editor. Springfield, USA1956.
99. Hassler R, Riechert T. [Indications and localization of stereotactic brain operations]. *Der Nervenarzt*. 1954 Nov 20;25(11):441-7.
100. Velasco FC, Molina-Negro P, Bertrand C, Hardy J. Further definition of the subthalamic target for arrest of tremor. *Journal of neurosurgery*. 1972 Feb;36(2):184-91.
101. Nagaseki Y, Shibasaki T, Hirai T, et al. Long-term follow-up results of selective VIM-thalamotomy. *Journal of neurosurgery*. 1986 Sep;65(3):296-302.
102. Ohye C, Miyazaki M, Hirai T, Shibasaki T, Nagaseki Y. Stereotactic selective thalamotomy for the treatment of tremor type cerebral palsy in adolescence. *Child's brain*. 1983;10(3):157-67.
103. Benabid AL, Pollak P, Louveau A, Henry S, de Rougemont J. Combined (thalamotomy and stimulation) stereotactic surgery of the VIM thalamic nucleus for bilateral Parkinson disease. *Appl Neurophysiol*. 1987;50(1-6):344-6.
104. Holslag JAH, Neef N, Beudel M, et al. Deep Brain Stimulation for Essential Tremor: A Comparison of Targets. *World neurosurgery*. 2018 Feb;110:e580-e4.
105. Murata J, Kitagawa M, Uesugi H, et al. Electrical stimulation of the posterior subthalamic area for the treatment of intractable proximal tremor. *Journal of neurosurgery*. 2003 Oct;99(4):708-15.
106. Narabayashi H. Stereotaxic Vim thalamotomy for treatment of tremor. *European neurology*. 1989;29 Suppl 1:29-32.
107. Schuurman PR, Bosch DA, Bossuyt PM, et al. A comparison of continuous thalamic stimulation and thalamotomy for suppression of severe tremor. *The New England journal of medicine*. 2000 Feb 17;342(7):461-8.
108. Jankovic J, Cardoso F, Grossman RG, Hamilton WJ. Outcome after stereotactic thalamotomy for parkinsonian, essential, and other types of tremor. *Neurosurgery*. 1995 Oct;37(4):680-6; discussion 6-7.
109. Gildenberg PL. Evolution of neuromodulation. *Stereotact Funct Neurosurg*. 2005;83(2-3):71-9.
110. Herrington TM, Cheng JJ, Eskandar EN. Mechanisms of deep brain stimulation. *Journal of neurophysiology*. 2016 Jan 1;115(1):19-38.
111. Espay AJ, Lang AE, Erro R, et al. Essential pitfalls in "essential" tremor. *Movement disorders : official journal of the Movement Disorder Society*. 2017 Mar;32(3):325-31.
112. Bekar L, Libionka W, Tian GF, et al. Adenosine is crucial for deep brain stimulation-

mediated attenuation of tremor. *Nat Med*. 2008 Jan;14(1):75-80.

113. Alesch F, Pinter MM, Hellscher RJ, Fertl L, Benabid AL, Koos WT. Stimulation of the ventral intermediate thalamic nucleus in tremor dominated Parkinson's disease and essential tremor. *Acta Neurochir (Wien)*. 1995;136(1-2):75-81.

114. Benabid AL, Pollak P, Gervason C, et al. Long-term suppression of tremor by chronic stimulation of the ventral intermediate thalamic nucleus. *Lancet*. 1991 Feb 16;337(8738):403-6.

115. Blond S, Caparros-Lefebvre D, Parker F, et al. Control of tremor and involuntary movement disorders by chronic stereotactic stimulation of the ventral intermediate thalamic nucleus. *J Neurosurg*. 1992 Jul;77(1):62-8.

116. Diederich NJ, Verhagen Metman L, Bakay RA, Alesch F. Ventral intermediate thalamic stimulation in complex tremor syndromes. *Stereotact Funct Neurosurg*. 2008;86(3):167-72.

117. Koller W, Pahwa R, Busenbark K, et al. High-frequency unilateral thalamic stimulation in the treatment of essential and parkinsonian tremor. *Ann Neurol*. 1997 Sep;42(3):292-9.

118. Siegfried J, Lippitz B. Chronic electrical stimulation of the VL-VPL complex and of the pallidum in the treatment of movement disorders: personal experience since 1982. *Stereotact Funct Neurosurg*. 1994;62(1-4):71-5.

119. Burn DJ, Troster AI. Neuropsychiatric complications of medical and surgical therapies for Parkinson's disease. *J Geriatr Psychiatry Neurol*. 2004 Sep;17(3):172-80.

120. Duma CM, Jacques DB, Kopyov OV, Mark RJ, Copcutt B, Farokhi HK. Gamma knife radiosurgery for thalamotomy in parkinsonian tremor: a five-year experience. *J Neurosurg*. 1998 Jun;88(6):1044-9.

121. Friehs GM, Park MC, Goldman MA, Zerris VA, Noren G, Sampath P. Stereotactic radiosurgery for functional disorders. *Neurosurg Focus*. 2007;23(6):E3.

122. Kondziolka D, Ong JG, Lee JY, Moore RY, Flickinger JC, Lunsford LD. Gamma Knife thalamotomy for essential tremor. *Journal of neurosurgery*. 2008 Jan;108(1):111-7.

123. Young RF, Li F, Vermeulen S, Meier R. Gamma Knife thalamotomy for treatment of essential tremor: long-term results. *J Neurosurg*. 2010 Jun;112(6):1311-7.

124. Ohye C, Higuchi Y, Shibasaki T, et al. Gammaknife thalamotomy for Parkinson's disease and essential tremor: A prospective multicenter study. *Neurosurgery*. 2011 Sep 12.

125. Carron R, Witjas T, Lee JK, Park MC, Azulay J-P, Regis J. Gammaknife VIM thalamotomy for tremor. Outcome in a series of 61 consecutive patients. *Journal of Radiosurgery and SRBT (Stereotactic Body Radiation Therapy)*. 2011;1, Supplement 1:59-60.

126. Martinez-Moreno NE, Sahgal A, De Salles A, et al. Stereotactic radiosurgery for tremor: systematic review. *Journal of neurosurgery*. 2018 Feb 23:1-12.

127. Niranjana A, Raju SS, Kooshkabadi A, Monaco E, 3rd, Flickinger JC, Lunsford LD. Stereotactic radiosurgery for essential tremor: Retrospective analysis of a 19-year experience. *Movement disorders : official journal of the Movement Disorder Society*. 2017

May;32(5):769-77.

128. Elias WJ, Lipsman N, Ondo WG, et al. A Randomized Trial of Focused Ultrasound Thalamotomy for Essential Tremor. *The New England journal of medicine*. 2016 Aug 25;375(8):730-9.
129. Schreglmann SR, Krauss JK, Chang JW, Bhatia KP, Kagi G. Functional lesional neurosurgery for tremor: a systematic review and meta-analysis. *Journal of neurology, neurosurgery, and psychiatry*. 2018 Jan 11.
130. Lindquist C, Steiner L, T. H. Gamma knife thalamotomy for tremor. Report of two cases. . New York, NY: Raven Press; 1992.
131. Steiner L, Forster D, Leksell L, Meyerson BA, Boethius J. Gammathalamotomy in intractable pain. *Acta neurochirurgica*. 1980;52(3-4):173-84.
132. Rand RW, Jacques DB, Melbye RW, Copcutt BG, Fisher MR, Levenick MN. Gamma Knife thalamotomy and pallidotomy in patients with movement disorders: preliminary results. *Stereotact Funct Neurosurg*. 1993;61 Suppl 1:65-92.
133. Carron R, Witjas T, Tancu C, Spatola G, Régis J, editors. Correlations between the clinical results and the MR characteristics of the thalamic lesion in Vim Gammaknife radiosurgery for tremor. *Journal of radiosurgery and SBRT*; 2017.
134. Guiot G, Arfel G, Derome P, Kahn A. [Neurophysiologic control procedures for stereotaxic thalamotomy]. *Neuro-Chirurgie*. 1968 May;14(4):553-66.
135. Ohye C. From selective thalamotomy with microrecording to gamma thalamotomy for movement disorders. *Stereotactic and functional neurosurgery*. 2006;84(4):155-61.
136. Brierley JB, Beck E. The significance in human stereotactic brain surgery of individual variation in the diencephalon and globus pallidus. *J Neurol Neurosurg Psychiatry*. 1959 Nov;22:287-98.
137. Tasker RR, Organ LW, Hawrylyshyn P. The thalamus and midbrain in man. In: RH W, editor. *A physiological Atlas Using Electrical Stimulation A Monograph in the Bannerstone Division of American Lectrues in Neurosurgery*: Springfield; 1982. p. 376-401.
138. Ohye C, Shibazaki T, Sato S. Gamma knife thalamotomy for movement disorders: evaluation of the thalamic lesion and clinical results. *J Neurosurg*. 2005 Jan;102 Suppl:234-40.
139. Friehs GM, Noren G, Ohye C, et al. Lesion size following Gamma Knife treatment for functional disorders. *Stereotact Funct Neurosurg*. 1996;66 Suppl 1:320-8.
140. Ohye C, Shibazaki T, Ishihara J, Zhang J. Evaluation of gamma thalamotomy for parkinsonian and other tremors: survival of neurons adjacent to the thalamic lesion after gamma thalamotomy. *J Neurosurg*. 2000 Dec;93 Suppl 3:120-7.
141. Kondziolka D, Somaza S, Martinez AJ, et al. Radioprotective effects of the 21-aminosteroid U-74389G for stereotactic radiosurgery. *Neurosurgery*. 1997 Jul;41(1):203-8.
142. Kondziolka D, Couce M, Niranjana A, Maesawa S, Fellows W. Histology of the 100-Gy Thalamotomy in the Baboon. In: Kondziolka D, editor. *Radiosurgery*: Karger; 2002. p. 279-84.

143. Lemaire JJ, Sakka L, Ouchchane L, Caire F, Gabrillargues J, Bonny JM. Anatomy of the human thalamus based on spontaneous contrast and microscopic voxels in high-field magnetic resonance imaging. *Neurosurgery*. 2010 Mar;66(3 Suppl Operative):161-72.
144. Haacke EM, Mittal S, Wu Z, Neelavalli J, Cheng YC. Susceptibility-weighted imaging: technical aspects and clinical applications, part 1. *AJNR American journal of neuroradiology*. 2009 Jan;30(1):19-30.
145. Tsui YK, Tsai FY, Hasso AN, Greensite F, Nguyen BV. Susceptibility-weighted imaging for differential diagnosis of cerebral vascular pathology: a pictorial review. *Journal of the neurological sciences*. 2009 Dec 15;287(1-2):7-16.
146. Duyn J. MR susceptibility imaging. *Journal of magnetic resonance*. 2013 Apr;229:198-207.
147. Deistung A, Schafer A, Schweser F, Biedermann U, Turner R, Reichenbach JR. Toward in vivo histology: a comparison of quantitative susceptibility mapping (QSM) with magnitude-, phase-, and R2*-imaging at ultra-high magnetic field strength. *Neuroimage*. 2013 Jan 15;65:299-314.
148. Tourdias T, Saranathan M, Levesque IR, Su J, Rutt BK. Visualization of intra-thalamic nuclei with optimized white-matter-nulled MPRAGE at 7T. *Neuroimage*. 2014 Jan 1;84:534-45.
149. Haacke EM, Xu Y, Cheng YC, Reichenbach JR. Susceptibility weighted imaging (SWI). *Magn Reson Med*. 2004 Sep;52(3):612-8.
150. F. Schweser, A. Deistung, B.W. Lehr, Reichenbach JR. Quantitative imaging of intrinsic magnetic tissue properties using MRI signal phase: An approach to in vivo brain iron metabolism? *NeuroImage*. 2011;54(4):2789-280.
151. Moenninghoff C, Maderwald S, Theysohn JM, et al. Imaging of adult astrocytic brain tumours with 7 T MRI: preliminary results. *Eur Radiol*. 2010 Mar;20(3):704-13.
152. Tallantyre EC, Brookes MJ, Dixon JE, Morgan PS, Evangelou N, Morris PG. Demonstrating the perivascular distribution of MS lesions in vivo with 7-Tesla MRI. *Neurology*. 2008 May 27;70(22):2076-8.
153. Tallantyre EC, Morgan PS, Dixon JE, et al. 3 Tesla and 7 Tesla MRI of multiple sclerosis cortical lesions. *J Magn Reson Imaging*. 2010 Oct;32(4):971-7.
154. van der Kolk AG, Hendrikse J, Zwanenburg JJ, Visser F, Luijten PR. Clinical applications of 7 T MRI in the brain. *Eur J Radiol*. 2013 May;82(5):708-18.
155. Wardlaw JM. Blood-brain barrier and cerebral small vessel disease. *J Neurol Sci*. 2010 Dec 15;299(1-2):66-71.
156. Cho ZH, Min HK, Oh SH, et al. Direct visualization of deep brain stimulation targets in Parkinson disease with the use of 7-tesla magnetic resonance imaging. *J Neurosurg*. 2010 Sep;113(3):639-47.
157. Lotfipour AK, Wharton S, Schwarz ST, et al. High resolution magnetic susceptibility mapping of the substantia nigra in Parkinson's disease. *J Magn Reson Imaging*. 2012 Jan;35(1):48-55.

158. Schaltenbrand G. [Diagnosis and diagnostic measures in neurology]. *Munch Med Wochenschr.* 1959 Mar 6;101(10):401-4.
159. Ashburner J, Friston KJ. Voxel-based morphometry--the methods. *NeuroImage.* 2000 Jun;11(6 Pt 1):805-21.
160. Bagepally BS, Bhatt MD, Chandran V, et al. Decrease in cerebral and cerebellar gray matter in essential tremor: a voxel-based morphometric analysis under 3T MRI. *Journal of neuroimaging : official journal of the American Society of Neuroimaging.* 2012 Jul;22(3):275-8.
161. Benito-Leon J, Alvarez-Linera J, Hernandez-Tamames JA, Alonso-Navarro H, Jimenez-Jimenez FJ, Louis ED. Brain structural changes in essential tremor: voxel-based morphometry at 3-Tesla. *Journal of the neurological sciences.* 2009 Dec 15;287(1-2):138-42.
162. Buijink AW, Broersma M, van der Stouwe AM, et al. Cerebellar Atrophy in Cortical Myoclonic Tremor and Not in Hereditary Essential Tremor-a Voxel-Based Morphometry Study. *Cerebellum.* 2016 Dec;15(6):696-704.
163. Cerasa A, Messina D, Nicoletti G, et al. Cerebellar atrophy in essential tremor using an automated segmentation method. *AJNR American journal of neuroradiology.* 2009 Jun;30(6):1240-3.
164. Daniels C, Peller M, Wolff S, et al. Voxel-based morphometry shows no decreases in cerebellar gray matter volume in essential tremor. *Neurology.* 2006 Oct 24;67(8):1452-6.
165. Daniels JK, Gaebler M, Lamke JP, Walter H. Grey matter alterations in patients with depersonalization disorder: a voxel-based morphometry study. *Journal of psychiatry & neuroscience : JPN.* 2015 Jan;40(1):19-27.
166. Lin CH, Chen CM, Lu MK, et al. VBM Reveals Brain Volume Differences between Parkinson's Disease and Essential Tremor Patients. *Frontiers in human neuroscience.* 2013;7:247.
167. Nicoletti V, Cecchi P, Frosini D, et al. Morphometric and functional MRI changes in essential tremor with and without resting tremor. *Journal of neurology.* 2015 Mar;262(3):719-28.
168. Quattrone A, Cerasa A, Messina D, et al. Essential head tremor is associated with cerebellar vermis atrophy: a volumetric and voxel-based morphometry MR imaging study. *AJNR American journal of neuroradiology.* 2008 Oct;29(9):1692-7.
169. Biswal B, Yetkin FZ, Haughton VM, Hyde JS. Functional connectivity in the motor cortex of resting human brain using echo-planar MRI. *Magnetic resonance in medicine.* 1995 Oct;34(4):537-41.
170. Fox MD, Greicius M. Clinical applications of resting state functional connectivity. *Frontiers in systems neuroscience.* 2010;4:19.
171. Fox MD, Corbetta M, Snyder AZ, Vincent JL, Raichle ME. Spontaneous neuronal activity distinguishes human dorsal and ventral attention systems. *Proceedings of the National Academy of Sciences of the United States of America.* 2006 Jun 27;103(26):10046-51.
172. Dale AM. Optimal experimental design for event-related fMRI. *Hum Brain Mapp.* 1999;8(2-3):109-14.

173. Gallea C, Popa T, Garcia-Lorenzo D, et al. Intrinsic signature of essential tremor in the cerebello-frontal network. *Brain : a journal of neurology*. 2015 Oct;138(Pt 10):2920-33.
174. Lenka A, Bhalsing KS, Panda R, et al. Role of altered cerebello-thalamo-cortical network in the neurobiology of essential tremor. *Neuroradiology*. 2017 Feb;59(2):157-68.
175. Benito-Leon J, Louis ED, Romero JP, et al. Altered Functional Connectivity in Essential Tremor: A Resting-State fMRI Study. *Medicine*. 2015 Dec;94(49):e1936.
176. Damoiseaux JS, Rombouts SA, Barkhof F, et al. Consistent resting-state networks across healthy subjects. *Proceedings of the National Academy of Sciences of the United States of America*. 2006 Sep 12;103(37):13848-53.
177. Fang W, Lv F, Luo T, et al. Abnormal regional homogeneity in patients with essential tremor revealed by resting-state functional MRI. *PloS one*. 2013;8(7):e69199.
178. Yin W, Lin W, Li W, Qian S, Mou X. Resting State fMRI Demonstrates a Disturbance of the Cerebello-Cortical Circuit in Essential Tremor. *Brain topography*. 2016 May;29(3):412-8.
179. Troster AI, Woods SP, Fields JA, et al. Neuropsychological deficits in essential tremor: an expression of cerebello-thalamo-cortical pathophysiology? *European journal of neurology*. 2002 Mar;9(2):143-51.
180. Lefranc M, Carron R, Regis J. Prelemniscal Radiations: A New Reliable Landmark of the Thalamic Nucleus Ventralis Intermedius Location. *Stereotactic and functional neurosurgery*. 2015;93(6):400-6.
181. Sedrak M, Gorgulho A, Frew A, Behnke E, DeSalles A, Pouratian N. Diffusion tensor imaging and colored fractional anisotropy mapping of the ventralis intermedius nucleus of the thalamus. *Neurosurgery*. 2011 Nov;69(5):1124-9; discussion 9-30.
182. Yamada K, Akazawa K, Yuen S, et al. MR imaging of ventral thalamic nuclei. *AJNR American journal of neuroradiology*. 2010 Apr;31(4):732-5.
183. Coenen VA, Allert N, Madler B. A role of diffusion tensor imaging fiber tracking in deep brain stimulation surgery: DBS of the dentato-rubro-thalamic tract (drt) for the treatment of therapy-refractory tremor. *Acta neurochirurgica*. 2011 Aug;153(8):1579-85; discussion 85.
184. Barkhoudarian G, Klochkov T, Sedrak M, et al. A role of diffusion tensor imaging in movement disorder surgery. *Acta neurochirurgica*. 2010 Dec;152(12):2089-95.
185. Carrillo-Ruiz JD, Velasco F, Jimenez F, Velasco AL, Velasco M, Castro G. Neuromodulation of prelemniscal radiations in the treatment of Parkinson's disease. *Acta neurochirurgica Supplement*. 2007;97(Pt 2):185-90.
186. Sedrak M, Gorgulho A, Bari A, et al. Diffusion tensor imaging (DTI) and colored fractional anisotropy (FA) mapping of the subthalamic nucleus (STN) and the globus pallidus interna (GPi). *Acta neurochirurgica*. 2010 Dec;152(12):2079-84.
187. Najdenovska E, Tuleasca C, Jorge J, et al. Imaging of the Ventral Intermediate Thalamic Nucleus at 7T (submitted for publication, under review). *Scientific Reports- Nature*. 2018.
188. Marques JP, Kober T, Krueger G, van der Zwaag W, Van de Moortele PF, Gruetter R.

MP2RAGE, a self bias-field corrected sequence for improved segmentation and T1-mapping at high field. *NeuroImage*. 2010 Jan 15;49(2):1271-81.

189. Fedorov A, Beichel R, Kalpathy-Cramer J, et al. 3D Slicer as an image computing platform for the Quantitative Imaging Network. *Magnetic Resonance Imaging*. 2012 2012/11/01/;30(9):1323-41.

190. Andersson JLR, Jenkinson M, Smith S. Non-linear registration aka Spatial normalization2007.

191. Smith SM, Jenkinson M, Woolrich MW, et al. Advances in functional and structural MR image analysis and implementation as FSL. *NeuroImage*. 2004;23 Suppl 1:S208-19.

192. Johnson H.J., Harris G., K. W. BRAINSFit: Mutual Information Registrations of Whole-Brain 3D Images, Using the Insight Toolkit. *The Insight Journal*. 2007.

193. Fonov VS, Evans AC, McKinsty RC, Almlí CR, Collins DL. Unbiased nonlinear average age-appropriate brain templates from birth to adulthood. *NeuroImage*. 2009 7//;47, Supplement 1:S102.

194. Guiot G, Brion S, Akerman M. [Stereotaxic anatomy of the internal pallidum, of the thalamus and of the internal capsule. Studies of the individual variations. II]. *Ann Chir*. 1961 Jun;15:703-41.

195. Schaltenbrand G, Wahren W. Atlas For Stereotaxy of The Human Brain With Guide to The Atlas For Stereotaxy of The Human Brain. Thieme, editor: Thieme; 1977.

196. Dice LR. Measures of the Amount of Ecologic Association Between Species Ecology. 1945;26(3):297-302.

197. Battistella G, Najdenovska E, Maeder P, et al. Robust thalamic nuclei segmentation method based on local diffusion magnetic resonance properties. *Brain structure & function*. 2017 Jul;222(5):2203-16.

198. Deeley MA, Chen A, Datteri R, et al. Comparison of manual and automatic segmentation methods for brain structures in the presence of space-occupying lesions: a multi-expert study. *Physics in medicine and biology*. 2011 Jul 21;56(14):4557-77.

199. Van de Velde J, Wouters J, Vercauteren T, et al. Optimal number of atlases and label fusion for automatic multi-atlas-based brachial plexus contouring in radiotherapy treatment planning. *Radiation oncology*. 2016 Jan 07;11:1.

200. Wharton S, Bowtell R. Effects of white matter microstructure on phase and susceptibility maps. *Magnetic resonance in medicine : official journal of the Society of Magnetic Resonance in Medicine / Society of Magnetic Resonance in Medicine*. 2015 Mar;73(3):1258-69.

201. Jorge J, Najdenovska E, Tuleasca C, et al. Improved susceptibility-weighted imaging of the thalamic nuclei at 7T with enhanced contrast and venous exclusion. *Annual Meeting and Exhibition of the International Society for Magnetic Resonance in Medicine (ISMRM); Paris, France2018*.

202. Kondziolka D, Lacomis D, Niranjana A, et al. Histological effects of trigeminal nerve radiosurgery in a primate model: implications for trigeminal neuralgia radiosurgery. *Neurosurgery*. 2000 Apr;46(4):971-6; discussion 6-7.

203. Regis J. Gamma knife for functional diseases. *Neurotherapeutics*. 2014 Jul;11(3):583-92.
204. Terao T, Yokochi F, Taniguchi M, et al. Microelectrode findings and topographic reorganisation of kinaesthetic cells after gamma knife thalamotomy. *Acta neurochirurgica*. 2008 Aug;150(8):823-7; discussion 7.
205. Lyons KE, Pahwa R. Pharmacotherapy of essential tremor : an overview of existing and upcoming agents. *CNS drugs*. 2008;22(12):1037-45.
206. Lieberman MD, Cunningham WA. Type I and Type II error concerns in fMRI research: re-balancing the scale. *Social cognitive and affective neuroscience*. 2009 Dec;4(4):423-8.
207. Nakamura K, Kawashima R, Sugiura M, et al. Neural substrates for recognition of familiar voices: a PET study. *Neuropsychologia*. 2001;39(10):1047-54.
208. Roe AW, Chelazzi L, Connor CE, et al. Toward a unified theory of visual area V4. *Neuron*. 2012 Apr 12;74(1):12-29.
209. Zhou H, Desimone R. Feature-based attention in the frontal eye field and area V4 during visual search. *Neuron*. 2011 Jun 23;70(6):1205-17.
210. Glickstein M. How are visual areas of the brain connected to motor areas for the sensory guidance of movement? *Trends in neurosciences*. 2000 Dec;23(12):613-7.
211. Tuleasca C, Witjas T, Van de Ville D, et al. Right Brodmann area 18 predicts tremor arrest after Vim radiosurgery: a voxel-based morphometry study. *Acta neurochirurgica*. 2017 Nov 11.
212. Waberski TD, Gobbele R, Lamberty K, Buchner H, Marshall JC, Fink GR. Timing of visuo-spatial information processing: electrical source imaging related to line bisection judgements. *Neuropsychologia*. 2008 Apr;46(5):1201-10.
213. Larsson J, Landy MS, Heeger DJ. Orientation-selective adaptation to first- and second-order patterns in human visual cortex. *Journal of neurophysiology*. 2006 Feb;95(2):862-81.
214. Carrasco M. Visual attention: the past 25 years. *Vision research*. 2011 Jul 01;51(13):1484-525.
215. Zeki S. The visual association cortex. *Current opinion in neurobiology*. 1993 Apr;3(2):155-9.
216. Zeki S, Watson JD, Lueck CJ, Friston KJ, Kennard C, Frackowiak RS. A direct demonstration of functional specialization in human visual cortex. *The Journal of neuroscience : the official journal of the Society for Neuroscience*. 1991 Mar;11(3):641-9.
217. Tardif E, Richer L, Bergeron A, Lepore F, Guillemot JP. Spatial resolution and contrast sensitivity of single neurons in area 19 of split-chiasm cats: a comparison with primary visual cortex. *The European journal of neuroscience*. 1997 Sep;9(9):1929-39.
218. Power JD, Barnes KA, Snyder AZ, Schlaggar BL, Petersen SE. Spurious but systematic correlations in functional connectivity MRI networks arise from subject motion. *NeuroImage*. 2012 Feb 01;59(3):2142-54.

219. Song XW, Dong ZY, Long XY, et al. REST: a toolkit for resting-state functional magnetic resonance imaging data processing. *PLoS one*. 2011;6(9):e25031.
220. Tuleasca C, Najdenovska E, Regis J, et al. Pretherapeutic functional neuroimaging predicts tremor arrest after thalamotomy. *Acta neurologica Scandinavica*. 2018 Jan 7.
221. Tuleasca C, Najdenovska E, Regis J, et al. Ventrolateral Motor Thalamus Abnormal Connectivity in Essential Tremor Before and After Thalamotomy: A Resting-State Functional Magnetic Resonance Imaging Study. *World neurosurgery*. 2018 Feb 21.
222. Tuleasca C, Regis J, Najdenovska E, et al. Pretherapeutic Functional Imaging Allows Prediction of Head Tremor Arrest After Thalamotomy for Essential Tremor: The Role of Altered Interconnectivity Between Thalamolimbic and Supplementary Motor Circuits. *World neurosurgery*. 2018 Feb 2.
223. Tuleasca C, Regis J, Najdenovska E, et al. Visually-sensitive networks in essential tremor: evidence from structural and functional imaging. *Brain : a journal of neurology*. 2018 Apr 12.
224. Witjas T, Carron R, Azulay JP, Regis J, editors. Gammaknife Thalamotomy For Intractable Tremors: Clinical Outcome And Correlations With Neuroimaging Features. *MDS 17th International Congress of Parkinson's Disease and Movement Disorders*; 2013.
225. Comon P. Independent Component Analysis: a new concept. *Signal Processing*. 1994;36(3):287-314.
226. Lewicki MS. A review of methods for spike sorting: the detection and classification of neural action potentials. *Network*. 1998 Nov;9(4):R53-78.
227. Delorme A, Sejnowski T, Makeig S. Enhanced detection of artifacts in EEG data using higher-order statistics and independent component analysis. *NeuroImage*. 2007;34(4):1443-9.
228. Calhoun VD, Adali T, Pearlson GD, Pekar JJ. A method for making group inferences from functional MRI data using independent component analysis. *Human brain mapping*. 2001 Nov;14(3):140-51.
229. Stone JV. Independent component analysis: an introduction. *Trends in cognitive sciences*. 2002 Feb 01;6(2):59-64.
230. De Zeeuw CI, Simpson JI, Hoogenraad CC, Galjart N, Koekkoek SK, Ruigrok TJ. Microcircuitry and function of the inferior olive. *Trends in neurosciences*. 1998 Sep;21(9):391-400.
231. Marr D. A theory of cerebellar cortex. *The Journal of physiology*. 1969 Jun;202(2):437-70.
232. Welsh JP, Lang EJ, Suglhara I, Llinas R. Dynamic organization of motor control within the olivocerebellar system. *Nature*. 1995 Mar 30;374(6521):453-7.
233. Yarom Y, Cohen D. The olivocerebellar system as a generator of temporal patterns. *Annals of the New York Academy of Sciences*. 2002 Dec;978:122-34.
234. Louis ED, Lenka A. The Olivary Hypothesis of Essential Tremor: Time to Lay this Model to Rest? Tremor and other hyperkinetic movements. 2017;7:473.

235. Campbell AM, Glover J, Chiang VL, Gerrard J, Yu JB. Gamma knife stereotactic radiosurgical thalamotomy for intractable tremor: a systematic review of the literature. *Radiotherapy and oncology : journal of the European Society for Therapeutic Radiology and Oncology*. 2015 Mar;114(3):296-301.
236. Schnitzler A, Munks C, Butz M, Timmermann L, Gross J. Synchronized brain network associated with essential tremor as revealed by magnetoencephalography. *Movement disorders : official journal of the Movement Disorder Society*. 2009 Aug 15;24(11):1629-35.
237. Stoodley CJ, Schmahmann JD. Functional topography in the human cerebellum: a meta-analysis of neuroimaging studies. *NeuroImage*. 2009 Jan 15;44(2):489-501.
238. Semendeferi K, Armstrong E, Schleicher A, Zilles K, Van Hoesen GW. Prefrontal cortex in humans and apes: a comparative study of area 10. *American journal of physical anthropology*. 2001 Mar;114(3):224-41.
239. Ramnani N, Owen AM. Anterior prefrontal cortex: insights into function from anatomy and neuroimaging. *Nature reviews Neuroscience*. 2004 Mar;5(3):184-94.
240. Gilbert SJ, Frith CD, Burgess PW. Involvement of rostral prefrontal cortex in selection between stimulus-oriented and stimulus-independent thought. *The European journal of neuroscience*. 2005 Mar;21(5):1423-31.
241. Tuleasca C, Najdenovska E, Régis J, et al. Clinical response to Vim's thalamic stereotactic radiosurgery for essential tremor is associated with distinctive functional connectivity patterns *Acta neurochirurgica*. 2018.
242. Crick FC, Koch C. What is the function of the claustrum? *Philosophical transactions of the Royal Society of London Series B, Biological sciences*. 2005 Jun 29;360(1458):1271-9.
243. Calvert GA. Crossmodal processing in the human brain: insights from functional neuroimaging studies. *Cerebral cortex*. 2001 Dec;11(12):1110-23.
244. Banati RB, Goerres GW, Tjoa C, Aggleton JP, Grasby P. The functional anatomy of visual-tactile integration in man: a study using positron emission tomography. *Neuropsychologia*. 2000;38(2):115-24.
245. Alexander GE, Crutcher MD. Functional architecture of basal ganglia circuits: neural substrates of parallel processing. *Trends in neurosciences*. 1990 Jul;13(7):266-71.
246. Saint-Cyr JA, Ungerleider LG, Desimone R. Organization of visual cortical inputs to the striatum and subsequent outputs to the pallido-nigral complex in the monkey. *The Journal of comparative neurology*. 1990 Aug 08;298(2):129-56.
247. Deuschl G, Elble R. Essential tremor--neurodegenerative or nondegenerative disease towards a working definition of ET. *Movement disorders : official journal of the Movement Disorder Society*. 2009 Oct 30;24(14):2033-41.
248. Fang W, Chen H, Wang H, et al. Multiple Resting-State Networks Are Associated With Tremors and Cognitive Features in Essential Tremor. *Movement disorders : official journal of the Movement Disorder Society*. 2015 Dec;30(14):1926-36.
249. Najdenovska E, Tuleasca C, Bloch J, et al. Exploring Local Diffusion MRI Properties for Vim Localization: Evaluation in Clinical Cases. *J Neurol Surg A Cent Eur Neurosurg*. 2017:78.

250. Tuleasca C, Najdenovska E, Régis J, et al. Pretherapeutic motor thalamus resting-state functional connectivity with visual areas predicts tremor arrest after thalamotomy for essential tremor: tracing the cerebello-thalamo-visuo-motor network (accepted for publication, in press). *World neurosurgery*. 2018.
251. Hyam JA, Owen SL, Kringelbach ML, et al. Contrasting connectivity of the ventralis intermedius and ventralis oralis posterior nuclei of the motor thalamus demonstrated by probabilistic tractography. *Neurosurgery*. 2012 Jan;70(1):162-9; discussion 9.
252. Asanuma C, Thach WT, Jones EG. Cytoarchitectonic delineation of the ventral lateral thalamic region in the monkey. *Brain research*. 1983 May;286(3):219-35.
253. Behrens TE, Johansen-Berg H, Woolrich MW, et al. Non-invasive mapping of connections between human thalamus and cortex using diffusion imaging. *Nature neuroscience*. 2003 Jul;6(7):750-7.
254. Zahra H, Teh BS, Paulino AC, et al. Stereotactic radiosurgery for trigeminal neuralgia utilizing the BrainLAB Novalis system. *Technology in cancer research & treatment*. 2009 Dec;8(6):407-12.
255. Rossion B, Schiltz C, Crommelinck M. The functionally defined right occipital and fusiform "face areas" discriminate novel from visually familiar faces. *NeuroImage*. 2003 Jul;19(3):877-83.
256. Beer J, Blakemore C, Previc FH, Liotti M. Areas of the human brain activated by ambient visual motion, indicating three kinds of self-movement. *Experimental brain research*. 2002 Mar;143(1):78-88.
257. Herholz K, Ehlen P, Kessler J, Strotmann T, Kalbe E, Markowitsch HJ. Learning face-name associations and the effect of age and performance: a PET activation study. *Neuropsychologia*. 2001;39(6):643-50.
258. Serrano JI, Romero JP, Castillo MDD, Rocon E, Louis ED, Benito-Leon J. A data mining approach using cortical thickness for diagnosis and characterization of essential tremor. *Scientific reports*. 2017 May 19;7(1):2190.
259. Muthuraman M, Heute U, Deuschl G, Raethjen J. The central oscillatory network of essential tremor. *Conference proceedings : Annual International Conference of the IEEE Engineering in Medicine and Biology Society IEEE Engineering in Medicine and Biology Society Annual Conference*. 2010;2010:154-7.
260. Borich MR, Brodie SM, Gray WA, Ionta S, Boyd LA. Understanding the role of the primary somatosensory cortex: Opportunities for rehabilitation. *Neuropsychologia*. 2015 Dec;79(Pt B):246-55.
261. Cerasa A, Passamonti L, Novellino F, et al. Fronto-parietal overactivation in patients with essential tremor during Stroop task. *Neuroreport*. 2010 Jan 27;21(2):148-51.
262. Zhang J, Wang ZI, Baker KB, Vitek JL. Effect of globus pallidus internus stimulation on neuronal activity in the pedunculopontine tegmental nucleus in the primate model of Parkinson's disease. *Experimental neurology*. 2012 Jan;233(1):575-80.
263. Arkadir D, Louis ED. The balance and gait disorder of essential tremor: what does this mean for patients? *Therapeutic advances in neurological disorders*. 2013 Jul;6(4):229-36.

264. Menon V, Uddin LQ. Saliency, switching, attention and control: a network model of insula function. *Brain structure & function*. 2010 Jun;214(5-6):655-67.
265. Sridharan D, Levitin DJ, Menon V. A critical role for the right fronto-insular cortex in switching between central-executive and default-mode networks. *Proceedings of the National Academy of Sciences of the United States of America*. 2008 Aug 26;105(34):12569-74.
266. Roland PE, Larsen B, Lassen NA, Skinhoj E. Supplementary motor area and other cortical areas in organization of voluntary movements in man. *Journal of neurophysiology*. 1980 Jan;43(1):118-36.
267. Liu X, Duyn JH. Time-varying functional network information extracted from brief instances of spontaneous brain activity. *Proceedings of the National Academy of Sciences of the United States of America*. 2013 Mar 12;110(11):4392-7.
268. Neely KA, Kurani AS, Shukla P, et al. Functional Brain Activity Relates to 0-3 and 3-8 Hz Force Oscillations in Essential Tremor. *Cerebral cortex*. 2015 Nov;25(11):4191-202.
269. Liu X, Chang C, Duyn JH. Decomposition of spontaneous brain activity into distinct fMRI co-activation patterns. *Frontiers in systems neuroscience*. 2013;7:101.
270. Preti MG, Bolton TA, Van De Ville D. The dynamic functional connectome: State-of-the-art and perspectives. *NeuroImage*. 2017 Oct 15;160:41-54.
271. Bhalsing KS, Kumar KJ, Saini J, Yadav R, Gupta AK, Pal PK. White matter correlates of cognitive impairment in essential tremor. *AJNR American journal of neuroradiology*. 2015 Mar;36(3):448-53.
272. Archer DB, Coombes SA, Chu WT, et al. A widespread visually-sensitive functional network relates to symptoms in essential tremor. *Brain : a journal of neurology*. 2017.
273. Ivanov B, Kaprelyan A, Bochev P, et al. (18F)-FDG PET/CT IN ESSENTIAL TREMOR: PRELIMINARY RESULT. *Journal of IMAB - Annual Proceeding (Scientific Papers)*. 2015;21(4):914-21.
274. Muthuraman M, Raethjen J, Koirala N, et al. Cerebello-cortical network fingerprints differ between essential, Parkinson's and mimicked tremors. *Brain : a journal of neurology*. 2018 Apr 26.
275. Timmermann L, Gross J, Dirks M, Volkmann J, Freund HJ, Schnitzler A. The cerebral oscillatory network of parkinsonian resting tremor. *Brain : a journal of neurology*. 2003 Jan;126(Pt 1):199-212.
276. Broersma M, van der Stouwe AM, Buijink AW, et al. Bilateral cerebellar activation in unilaterally challenged essential tremor. *NeuroImage Clinical*. 2016;11:1-9.
277. Pagan FL, Butman JA, Dambrosia JM, Hallett M. Evaluation of essential tremor with multi-voxel magnetic resonance spectroscopy. *Neurology*. 2003 Apr 22;60(8):1344-7.
278. Jenkins IH, Bain PG, Colebatch JG, et al. A positron emission tomography study of essential tremor: evidence for overactivity of cerebellar connections. *Annals of neurology*. 1993 Jul;34(1):82-90.
279. Boecker H, Wills AJ, Ceballos-Baumann A, et al. The effect of ethanol on alcohol-responsive essential tremor: a positron emission tomography study. *Annals of neurology*.

1996 May;39(5):650-8.

280. Louis ED, Lee M, Babij R, et al. Reduced Purkinje cell dendritic arborization and loss of dendritic spines in essential tremor. *Brain : a journal of neurology*. 2014 Dec;137(Pt 12):3142-8.

281. Symanski C, Shill HA, Dugger B, et al. Essential tremor is not associated with cerebellar Purkinje cell loss. *Movement disorders : official journal of the Movement Disorder Society*. 2014 Apr;29(4):496-500.

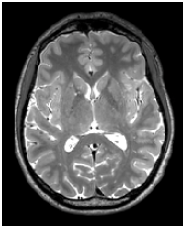
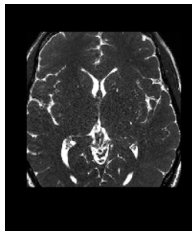
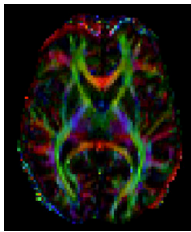
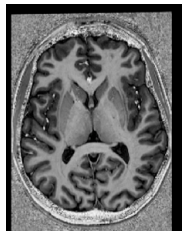
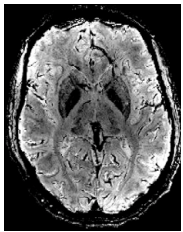
282. Boecker H, Weindl A, Brooks DJ, et al. GABAergic dysfunction in essential tremor: an 11C-flumazenil PET study. *Journal of nuclear medicine : official publication, Society of Nuclear Medicine*. 2010 Jul;51(7):1030-5.

283. Archer DB, Coombes SA, Chu WT, et al. Reply: Visually-sensitive networks in essential tremor: evidence from structural and functional imaging. *Brain : a journal of neurology*. 2018 Apr 12.

284. Kurita H, Kawamoto S, Suzuki I, et al. Control of epilepsy associated with cerebral arteriovenous malformations after radiosurgery. *J Neurol Neurosurg Psychiatry*. 1998 Nov;65(5):648-55.

Supplementary Material

MRI protocol for part 3: The abbreviation YS denotes the parameters used for the acquisitions from the young cohort, while ES from the elderly one, where they differed between them.

Sequence	3T T2-w 	3T T2-w CISS 	3T MPARGE 	3T DWI 	7T MP2RAGE 	7T SWI 
Scanning Machine (Siemens)	YS: Tim Trio ES: Prisma	YS: Tim Trio ES: Prisma	YS: Tim Trio ES: Prisma	YS: Tim Trio ES: Prisma	Medical Solution	Medical Solution
Resolution, mm ³	YS: 0.5x0.5x1.0 ES: 0.7x0.7x2.0	YS: 0.4x0.4x0.4 ES: 0.5x0.5x0.5	1.0x1.0x1.0	2.2x2.2x2.2	0.6x0.6x0.6	0.375x0.375x1.0
Matrix size, mm ²	YS: 512x512 ES: 320x320	YS: 320x320 ES: 512x512	256x256	98x98	320x320	512x512
Slice/partitions, mm	YS: 160 ES: 35	YS: 80 ES: 96	YS: 160 ES: 192	YS: 52 ES: 62	256	72
Repetition time, ms	YS: 3200 ES: 6240	YS: 6.18 ES: 5.98	2300	YS: 6300 ES: 7100	6000	28
Echo time, ms	YS: 402 ES: 86	2.75	YS: 2.98 ES: 2.03	84	YS: 2.64 ES: 2.05	20
Inversion time, ms	/	/	900	/	800/2700	/
Flip angles, degrees	YS: 120 ES: 150	49	9	90	7/5	10
Target	YS: Whole Brain ES: Thalamus	Thalamus	Whole Brain	Whole Brain	Whole Brain	Thalamus

MRI protocol for part 5: resting-state fMRI data acquisition

Imaging was done on head-only 3T magnetic resonance imaging (MRI) scanner, SIEMENS SKYRA (Munich, Germany, 32-channel receive-only phased-array head coil): native (before SRS-T) and Gadolinium contrast-enhanced T1-weighted (T1w, after SRS-T) and resting-state fMRI images. The following parameters were employed: T1w-TR/TE=2300/2.98ms, isotropic voxel of 1mm³, 160 slices; T2*-weighted fast echo planar imaging (BOLD contrast, before the Gadolinium injection)- TR/TE = 3.3s/30 ms/90 degrees), voxel size 4 x 4 x 4 mm³, 300 volumes acquired per subject), 46 interleaved axial slices. The rs-fMRI experiments, acquired with no explicit task, consisted of a 10-min run, in which participant were asked to relax with their eyes closed, without falling asleep or engaging in cognitive or motor tasks. In addition, a field map was acquired to correct for the effect of field inhomogeneity.